Supporting Information

Electron Transfer Reactions in Sub-Porphyrin-Naphthyldiimide Dyads

Betül Küçüköz, [†a] B. Adinarayana, [†b] Atsuhiro Osuka, [b] and Bo Albinsson[*a]

[a] Chemistry and Chemical Engineering, Chalmers University of Technology, Gothenburg, Sweden
[b] Department of Chemistry, Kyoto University, Kyoto, Japan
[†]These authors contributed equally to the study.

1. General Information:

Reagents and materials were purchased from commercial suppliers (reagent grade quality) and were used without further purification unless stated. 1,2-Dichlorobenzene was passed through alumina plug, dried over MS4A, and degassed with nitrogen bubbling. Main precursors N-octyl-1,4,5,8-napthalenetetracarboxylicmonoanhydride **2**[S1] and 5-bromo-10,15-diphenylsubporphyrin **13**[S2] were synthesized according to the reported procedures. The spectroscopic studies were carried out in spectroscopic grade solvents. Silica gel column chromatography was performed on Wakogel C200, C300, and C400 unless otherwise noted. Alumina column chromatography was performed on Sumitomo γ-Alumina KCG-1525W (Blockmann grade II). Thin-layer chromatography (TLC) was carried out on aluminium sheets coated with silica gel 60 F254 (Merck 5554). High-resolution atmospheric-pressure-chemical-ionization time-of-flight mass-spectrometry (HR-APCI-TOF-MS) was recorded on a BRUKER micrOTOF model using positive-ion mode. The NMR solvent $CDCl_3$ was purified by passing through a short pad of aluminium oxide prior to use. ^{1}H, ^{11}B, and ^{13}C NMR spectra were recorded on a JEOL delta-ECA600 spectrometer, and chemical shifts were reported in ppm (δ scale) relative to internal standards $CHCl_3$ (δ = 7.26 ppm for ^{1}H, 77.23 ppm for ^{13}C), and an external standard $BF_3.OEt_2$ in $CDCl_3$ (δ = 0.00 ppm for ^{11}B). UV/Visible absorption spectra were recorded on a Shimadzu UV-3600 spectrometer and a Shimadzu UV-2550 spectrometer. Fluorescence spectra were recorded on a Shimadzu RF-5300PC spectrometer. Absolute fluorescence quantum yields were determined on a HAMAMATSU C9920-02S. Single-crystal diffraction analysis data were collected at –180 °C with a Rigaku XtaLAB P200 by using graphite monochromated Cu-Kα radiation (λ = 1.54187 Å). The structures were solved by direct methods (SHELXS-97) and refined with full-matrix least square technique (SHELXL-2014/7). Redox potentials were measured by the cyclic voltammetry and Differential pulse voltammetry method on an ALS660 electrochemical analyzer model.

2. Synthesis and spectral characterization:

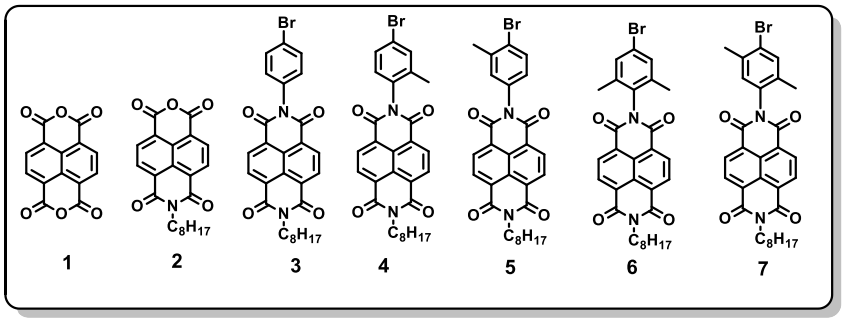

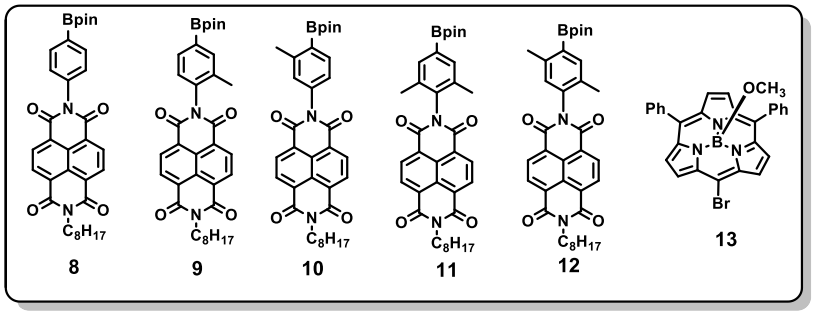

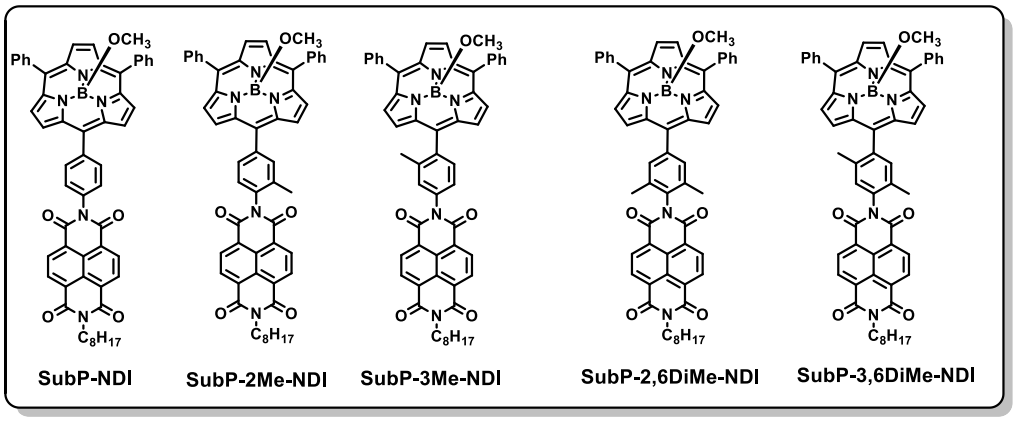

2: This compound was synthesized according to the reported procedure.[S1]

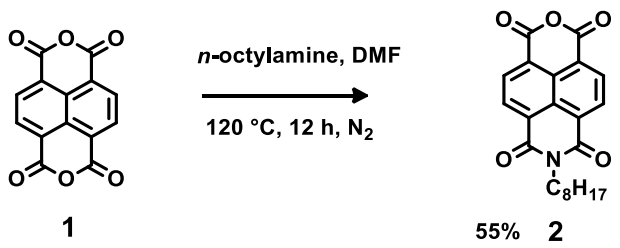

2a. General procedure for the synthesis of 4-bromo-aryl-NDI-derivatives:

A mixture of compound **2** (0.1 mmol, 1 eq), 4-bromo aniline derivatives (0.13 mmol, 1.3 eq) and sodium acetate (0.15 mmol, 1.5 eq) in acetic acid (5 mL) was placed in a 25 mL Schlenk tube. The mixture was refluxed for overnight. After completion of the reaction, the crude

mixture was cooled to room temperature. Addition of water to this reaction mixture caused precipitates, which were washed with saturated sodium hydrogen carbonate and water. The compound was purified by column chromatography using silica gel (C300, in DCM:*n*-hexane:Et_2O = 1:3:1) to afford target molecules in 65-75% yield.

3: This compound was synthesized and purified according to the general procedure.

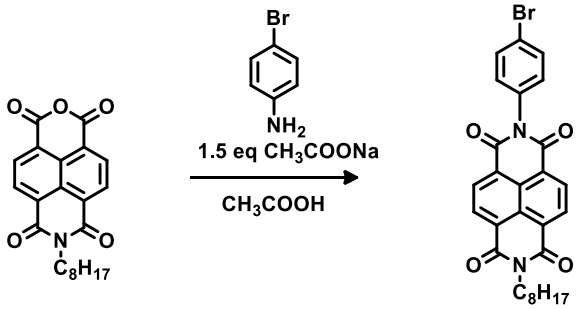

^{1}H NMR (600 MHz, $CDCl_3$); *δ*/ppm = 8.80 (m, 4H, NDI), 7.71 (d, *J* = 8.6 Hz, 2H, Ph), 7.21 (d, *J* = 8.6 Hz, 2H, Ph), 4.24 – 4.17 (m, 2H, alkyl-α-CH_2), 1.76 (dt, *J* = 15, 7.3 Hz, 2H, alkyl-CH_2), 1.44 (dt, *J* = 15, 7.3 Hz, 2H, alkyl-CH_2), 1.40 – 1.34 (m, 2H, alkyl-CH_2), 1.34 – 1.25 (m, 6H, alkyl-CH_2), and 0.88 (t, *J* = 7.0 Hz, 3H, alkyl-CH_3); ^{13}C NMR (151 MHz, $CDCl_3$); *δ*/ppm = 162.99, 162.85, 133.75, 132.99, 131.65, 131.20, 130.44, 127.30, 127.29, 127.21, 127.01, 126.63, 123.49, 41.29, 31.99, 29.47, 29.38, 28.27, 27.29, 22.83, and 14.28; HR-APCI-TOFMS: *m*/*z* calcd for $[C_{28}H_{25}BrN_2O_4]^+$ = 532.0998; found = 533.1033 ($[M+H]^+$).

4: This compound was synthesized and purified according to the general procedure.

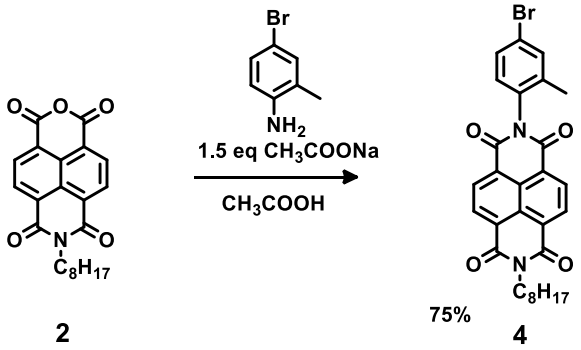

^{1}H NMR (600 MHz, $CDCl_3$); δ = 8.81 (s, 4H), 7.58 (d, *J* = 1.7 Hz, 1H), 7.51 (ddd, *J* = 8.3, 2.2, 0.4 Hz, 1H), 7.09 (d, *J* = 8.3 Hz, 1H), 4.25 – 4.19 (m, 2H), 2.15 (s, 3H), 1.76 (dt, *J* = 15.2, 4.6 Hz, 2H), 1.44 (dt, *J* = 14.6, 6.9 Hz, 2H), 1.37 (ddd, *J* = 14.0, 9.5, 6.7 Hz, 2H), 1.34 – 1.24 (m, 6H), and 0.88 (t, *J* = 7.0 Hz, 3H); ^{13}C NMR (151 MHz, $CDCl_3$); δ = 162.91, 162.67, 131.74, 131.24, 127.44, 127.39, 126.61, 32.01, 29.49, 29.40, 28.31, 27.30, 22.84, 17.73, and 14.29; MS: *m*/*z* calcd for $C_{29}H_{27}BrN_2O_4$ = 546.1154; found = 547.1219 (*M+1*).

5: This compound was synthesized and purified according to the general procedure.

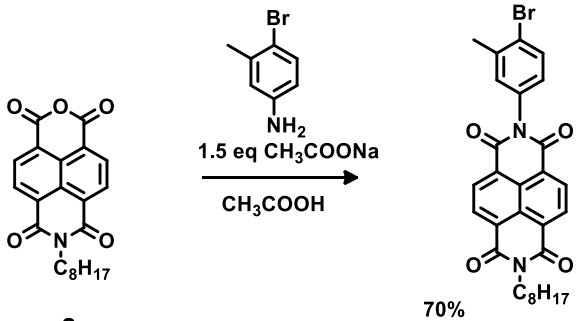

2 5

^{1}H NMR (600 MHz, $CDCl_3$); δ/ppm = 8.79 (m, 4H, NDI), 7.73 (d, J = 8.3 Hz, 1H, Ph), 7.21 (d, J = 2.5 Hz, 1H, Ph), 7.03 (ddd, J = 8.3, 2.5 Hz, 1H, Ph), 4.24 – 4.18 (m, 2H, alkyl-α-CH_2), 2.47 (s, 3H, CH_3), 1.75 (m, 2H, alkyl-CH_2), 1.47 – 1.41 (m, 2H, alkyl-CH_2), 1.40 – 1.34 (m, 2H, alkyl-CH_2), 1.33 – 1.24 (m, 6H, alkyl-CH_2), and 0.88 (t, J = 7.0 Hz, 3H, alkyl-CH_3); ^{13}C NMR (151 MHz, $CDCl_3$); δ/ppm = 163.10, 162.91, 133.82, 133.70, 131.65, 131.23, 130.91, 127.53, 127.31, 127.05, 126.70, 32.01, 29.49, 29.40, 28.30, 27.31, 23.33, 22.84, and 14.29; HR-APCI-TOFMS: m/z calcd for $[C_{29}H_{27}BrN_2O_4]^+$ = 546.1154; found = 547.1218 ($[M+H]^+$).

6: This compound was synthesized and purified according to the general procedure.

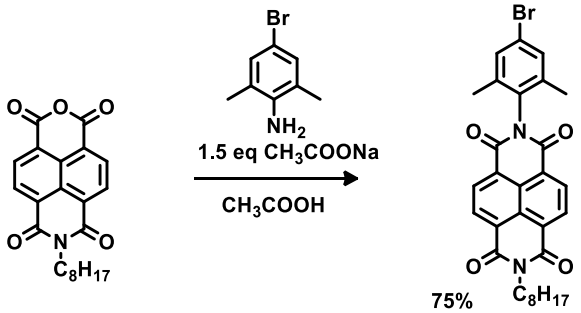

2 6

^{1}H NMR (600 MHz, $CDCl_3$); δ/ppm = 8.82 (s, 4H, NDI), 7.40 (s, 2H, Ph), 4.24 – 4.20 (m, 2H, alkyl-α-CH_2), 2.11 (s, 6H, CH_3), 1.76 (m, 2H, alkyl-CH_2), 1.46 – 1.41 (m, 2H, alkyl-CH_2), 1.40 – 1.34 (m, 2H, alkyl-CH_2), 1.33 – 1.25 (m, 6H, alkyl-CH_2), and 0.88 (m, 3H, alkyl-CH_3); ^{13}C NMR (151 MHz, $CDCl_3$); δ/ppm = 162.90, 162.23, 137.88, 132.56, 131.83, 131.77, 131.23, 127.58, 127.41, 127.15, 126.47, 123.23, 41.27, 32.00, 29.49, 29.39, 28.30, 27.28, 22.83, 17.92, and 14.29; HR-APCI-TOFMS: m/z calcd for $[C_{30}H_{29}BrN_2O_4]^+$ = 560.1311; found = 561.1365 ($[M+H]^+$).

7: This compound was synthesized and purified according to the general procedure.

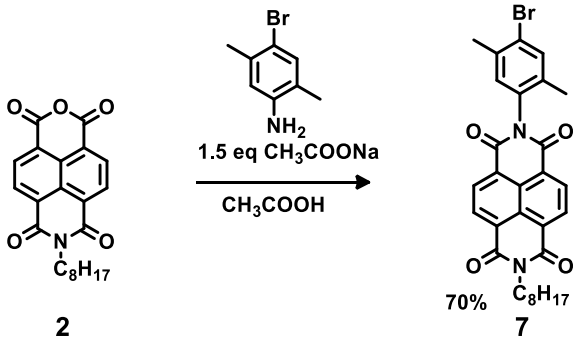

2 7

^{1}H NMR (600 MHz, $CDCl_3$); δ/ppm = 8.82 – 8.79 (m, 4H, NDI), 7.60 (s, 1H, Ph), 7.09 (s, 1H, Ph), 4.26 – 4.19 (m, 2H, alkyl-α-CH_2), 2.41 (s, 3H, CH_3), 2.11 (s, 3H, CH_3), 1.76 (dt, J = 15.1, 7.3 Hz, 2H, alkyl-CH_2), 1.44 (dt, J = 15.1, 7.3 Hz, 2H, alkyl-CH_2), 1.38 (dt, J = 15.1, 6.9 Hz, 2H, alkyl-CH_2), 1.34 – 1.27 (m, 6H, alkyl-CH_2), and 0.88 (t, J = 6.9 Hz, 3H, alkyl-CH_3); ^{13}C NMR (151 MHz, $CDCl_3$); δ/ppm = 162.86, 162.68, 137.19, 135.17, 134.91, 133.08, 131.65, 131.19, 130.61, 127.36, 127.29, 127.05, 126.60, 126.07, 41.25, 31.98, 29.46, 29.37, 28.27, 27.27, 22.81, 22.71, 17.13, and 14.27; HR-APCI-TOFMS: m/z calcd for $[C_{30}H_{29}BrN_2O_4]^+$ = 560.1311; found = 561.1349 ($[M+H]^+$).

2b. General procedure for the synthesis of 4-Bpin-aryl-NDI-derivatives:

A 25 mL Schlenk tube was filled with N_2 and charged with **NDI-Ar-Br (3-7)** (0.1 mmol, 1 eq), bis(pinacolato)diboron (0.2 mmol, 2 eq), KOAc (0.4 mmol, 4 eq), and $PdCl_2$(dppf) (0.02 mmol, 20 mol%). A dry dimethoxyethane (DME) (10 mL) was added via syringe, and the resulting solution was purged with N_2 for 20 min. The reaction mixture was refluxed for overnight. After completion of the reaction, the solution was cooling down to room temperature and the products were extracted with EtOAc. The extract was dried over Na_2SO_4 and concentrated by a rotary evaporator. The compound was purified by column chromatography using silica gel (C300, in DCM:*n*-hexane:Et_2O 1:3:1) to afford target molecules **8**-**12** in 35-60% yield. (Note: The compound was tending to be adsorbed onto silica gel, thus we have done separation by column chromatography quickly and the separated compound was used for the next step without further purification.)

8: This compound was synthesized and purified according to the general procedure.

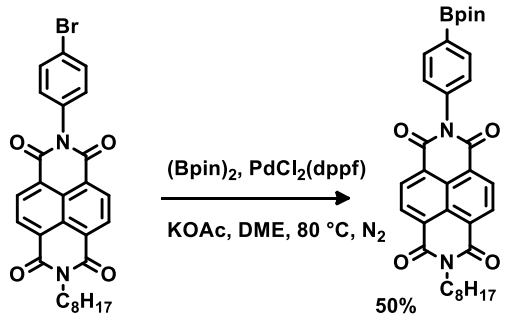

3 8

^{1}H NMR (600 MHz, $CDCl_3$); δ/ppm = 8.80 (m, 4H, NDI), 8.03 (d, J = 8.2 Hz, 2H, Ph), 7.33 (d, J = 8.2 Hz, 2H, Ph), 4.25 – 4.15 (m, 2H, alkyl-α-CH_2), 1.75 (m, 2H, alkyl-CH_2), 1.47 – 1.42 (m, 2H, alkyl-CH_2), 1.30 (m, 8H, alkyl-CH_2), and 0.88 (t, J = 7.0 Hz, 3H, alkyl-CH_3); ^{13}C NMR (151 MHz, $CDCl_3$); δ/ppm = 163.10, 162.99, 136.23, 131.56, 131.22, 127.99, 84.29, 41.28, 32.02, 29.50, 29.40, 28.31, 27.31, 25.09, and 22.85, 14.29; HR-APCI-TOFMS: m/z calcd for $C_{34}H_{37}BN_2O_6$ = 580.2745; found = 580.2797 ([M+H]$^+$).

9: This compound was synthesized and purified according to the general procedure.

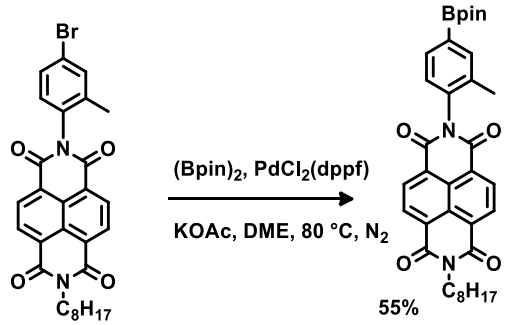

^{1}H NMR (600 MHz, $CDCl_3$); δ/ppm = 8.80 (m, 4H, NDI), 7.88 (s, 1H, Ph), 7.83 (d, J = 7.6 Hz, 1H, Ph), 7.23 (d, J = 7.6 Hz, 1H, Ph), 4.24 – 4.18 (m, 2H, alkyl-α-CH_2), 2.18 (s, 3H, CH_3), 1.76 (m, alkyl-CH_2), 1.44 (m, 2H, alkyl-CH_2), 1.32 – 1.24 (m, 6H, alkyl-CH_2), and 0.88 (t, J = 7.0 Hz, 3H, alkyl-CH_3); ^{13}C NMR (151 MHz, $CDCl_3$); δ/ppm = 162.98, 162.67, 137.89, 135.19, 133.87, 131.58, 131.20, 128.01, 127.45, 127.45, 127.21, 126.83, 84.22, 41.25, 32.00, 29.49, 29.39, 28.30, 27.29, 25.07, 22.83, 17.57, and 14.28; HR-APCI-TOFMS: m/z calcd for [$C_{35}H_{39}BN_2O_6$]$^+$ = 594.2901; found = 595.2985 ([M+H]$^+$).

10: This compound was synthesized and purified according to the general procedure.

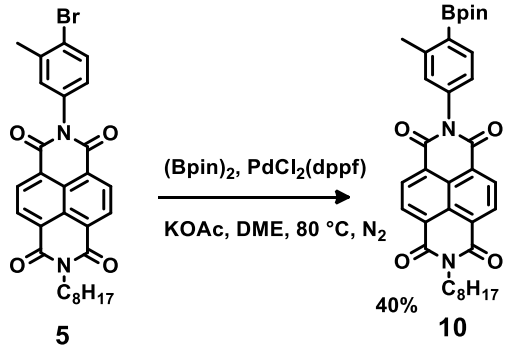

^{1}H NMR (600 MHz, $CDCl_3$); δ/ppm = 8.81 – 8.76 (m, 4H, NDI), 7.99 (d, J = 8.5 Hz, 1H, Ph), 7.14 – 7.10 (m, 2H, Ph), 4.23 – 4.17 (m, 2H, alkyl-α-CH_2), 2.62 (s, 3H, CH_3), 1.75 (m, 2H, alkyl-CH_2), 1.48 – 1.41 (m, 2H, alkyl-CH_2), 1.35 – 1.20 (m, 8H, alkyl-CH_2), and 0.88 (t, J = 6.9 Hz, 3H, alkyl-CH_3); ^{13}C NMR (151 MHz, $CDCl_3$); δ/ppm = 163.12, 163.00, 146.97, 137.54, 137.39, 136.89, 131.51, 131.20, 129.96, 129.47, 127.26, 127.14, 127.04, 124.57, 83.86, 41.26, 32.01, 29.49, 29.39, 28.30, 27.30, 25.20 – 24.96 (m), 22.84, 14.30, and 14.28. HR-APCI-TOFMS: m/z calcd for [$C_{35}H_{39}BN_2O_6$]$^+$ = 594.2901; found = 595.2992 ([M+H]$^+$).

11: This compound was synthesized and purified according to the general procedure.

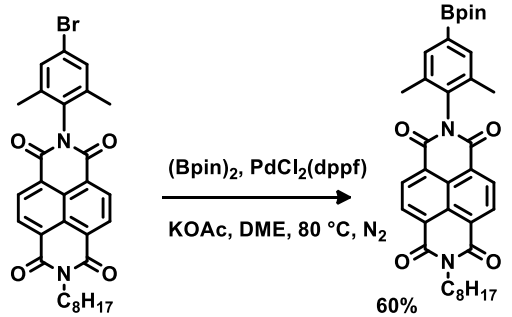

6 11

^{1}H NMR (600 MHz, $CDCl_3$); δ/ppm = 8.81 (m, 4H, NDI), 7.70 (s, 2H, Ph), 4.24 – 4.19 (m, 2H, alkyl-α-CH_2), 2.15 (s, 6H, CH_3), 1.79 – 1.72 (m, 2H, alkyl-CH_2), 1.46 – 1.40 (m, 2H, alkyl-CH_2), 1.29 (m, 8H, alkyl-CH_2), and 0.88 (t, J = 6.9 Hz, 3H, alkyl-CH_3); ^{13}C NMR (151 MHz, $CDCl_3$); δ/ppm= 163.02, 162.26, 136.14, 135.32, 134.93, 131.65, 131.23, 127.63, 127.29, 126.74, 84.18, 77.44, 77.23, 77.02, 41.26, 32.02, 29.51, 29.41, 28.32, 27.30, 25.08, 22.85, 17.85, and 14.30; HR-APCI-TOFMS: m/z calcd for $[C_{36}H_{41}BN_2O_6]^+$ = 608.3058; found = 609.3155 ($[M+H]^+$).

12: This compound was synthesized and purified according to the general procedure.

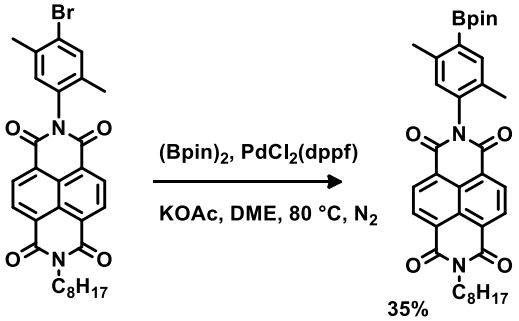

7 12

^{1}H NMR (600 MHz, $CDCl_3$); δ/ppm = 8.80 (m, 4H, NDI), 7.83 (s, 1H, Ph), 7.02 (s, 1H, Ph), 4.24 – 4.19 (m, 2H, alkyl-α-CH_2), 2.56 (s, 3H, CH_3), 2.13 (s, 3H, CH_3), 1.75 (m, 2H, alkyl-CH_2), 1.44 (m, 3H, alkyl-CH_2), 1.29 (m, 8H, alkyl-CH_2), and 0.88 (t, J = 7.0 Hz, 3H, alkyl-CH_3); ^{13}C NMR (151 MHz, $CDCl_3$); δ/ppm = 163.02, 162.73, 144.39, 139.01, 136.12, 131.83, 131.56, 131.21, 129.64, 127.45, 127.45, 127.19, 126.89, 83.81, 41.26, 32.01, 29.50, 29.40, 28.31, 27.30, 25.11, 22.84, 21.97, 17.07, and 14.29; HR-APCI-TOFMS: m/z calcd for $[C_{36}H_{41}BN_2O_6]^+$ = 608.3058; found = 609.3143 ($[M+H]^+$).

13: This compound was synthesized according to the reported procedure.[S2]

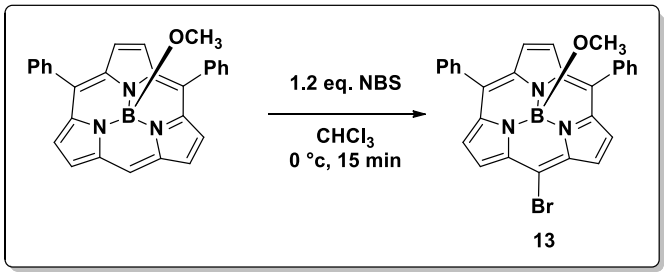

2c. General procedure for the synthesis of SubP-XMe-NDI-derivatives:

A 25 ml Schlenk tube was charged with 5-bromo-10,15-diphenylsubporphyrin **13** (10 mg, 0.020 mmol, 1 eq), **NDI-Ar-Bpin** (**8-12**) (3 eq), $Pd(PPh_3)_2Cl_2$ (10 mol%), and Na_2CO_3 (10 eq) and purged with N_2. A 10 mL mixture of THF/H_2O (8:2) was added via syringe, and the resulting solution was purged with N_2 for 10 min. The reaction mixture was heated at 65 °C for 6 h. After the completion of reaction, the solution was cooling down to room temperature and products were extracted with DCM and the extract was dried over Na_2SO_4 and concentrated by a rotary evaporator. The resulting crude mixture was subjected to the usual axial exchange conditions (DCM/MeOH 50 °C)[S3] followed by removal of the solvent by a rotary evaporator. The crude mixture was partially purified by column chromatography through a silica gel column (DCM:*n*-hexane:Et_2O 1:2:1). The final purification was carried out through recycle GPC by eluting $CHCl_3$ as a solvent and yielding pure target molecules **SubP-XMe-NDI** in 50-60% yield.

SubP-NDI: This compound was synthesized and purified according to the general procedure by using *meso*-bromosubporphyrin **13** (10 mg, 0.020 mmol), **8** (35 mg, 0.060 mmol), $Pd(PPh_3)_2Cl_2$ (1.5 mg, 10 mol%), and Na_2CO_3 (21 mg, 0.20 mmol).

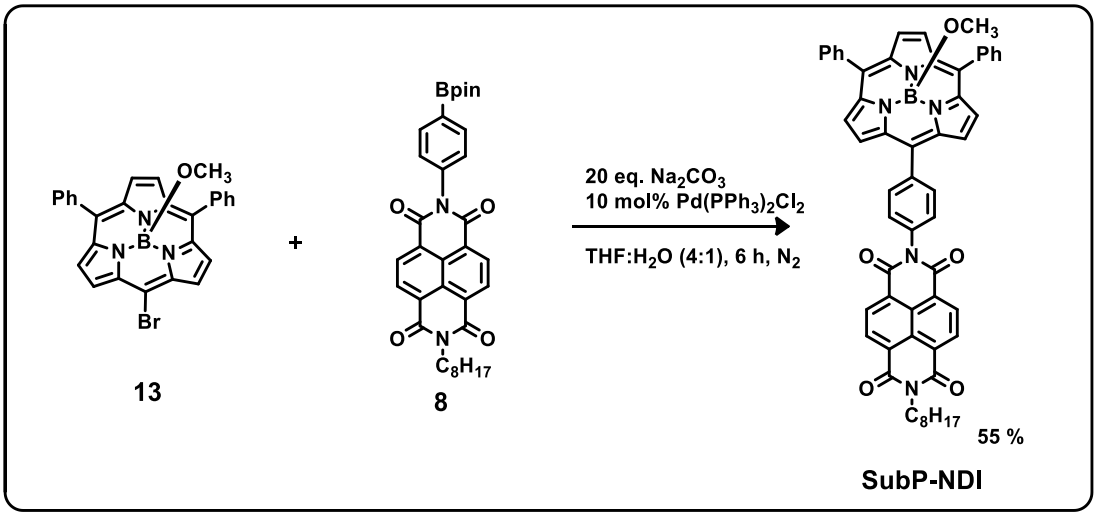

^{1}H NMR (600 MHz, $CDCl_3$); δ/ppm = 8.91 (d, J = 7.5 Hz, 2H, NDI), 8.87 (d, J = 7.5 Hz, 2H, NDI), 8.28 (m, 2H, Ph), 8.25 (m, 2H, β), 8.18 (m, 2H, β), 8.15 (s, 2H, β), 8.11 – 8.07 (m, 4H, Ph), 7.72 (t, J = 7.5 Hz, 4H, Ph), 7.68 (d, J = 8.3 Hz, 2H, Ph), 7.63 (t, J = 7.5 Hz, 2H, Ph), 4.28 – 4.22 (m, 2H, alkyl-α-CH_2), 1.80 (dt, J = 15.4, 7.6 Hz, 2H, alkyl-CH_2), 1.50 – 1.44 (m, 2H, alkyl-CH_2), 1.41 (dd, J = 14.4, 7.4 Hz, 2H, alkyl-CH_2), 1.31 (m, 6H, alkyl-CH_2), 0.90 (t, J =

6.9 Hz, 3H, alkyl-CH_3), and 0.86 (s, 3H, OCH_3); ^{13}C NMR (151 MHz, $CDCl_3$); δ/ppm = 163.43, 162.99, 141.29, 141.18, 140.67, 137.37, 134.24, 133.46, 131.76, 131.34, 129.04, 128.89, 128.86, 128.07, 127.41, 127.37, 126.94, 122.74, 122.55, 122.38, 47.05, 41.35, 32.03, 29.93, 29.52, 29.42, 28.34, 27.34, 22.86, and 14.31; ^{11}B NMR (193 MHz, $CDCl_3$); δ/ppm = –16.15; MALDI-TOFMS: *m*/*z* calcd for $[C_{55}H_{41}BN_5O_4]^+$ = 846.3252 [*M*–OMe]$^+$; found = 846.26 ([*M*–OMe]$^+$); UV–Vis (DCM): λ_{max}/nm (ε/(10^5 M^{-1} cm^{-1})) = 374 (1.68), 460 (0.13), 486 (0.11).

SubP-2Me-NDI: This compound was synthesized and purified according to the general procedure by using *meso*-bromo subporphyrin **13** (10 mg, 0.020 mmol), **9** (36 mg, 0.060 mmol), $Pd(PPh_3)_2Cl_2$ (1.5 mg, 10 mol%), and Na_2CO_3 (21 mg, 0.20 mmol).

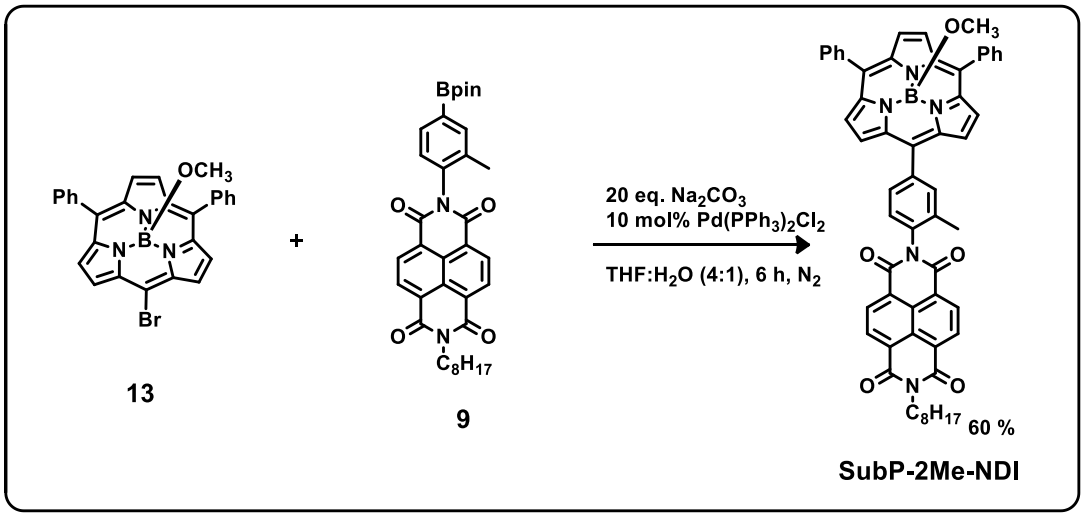

^{1}H NMR (600 MHz, $CDCl_3$); δ/ppm = 8.92 (dd, *J* = 7.5, 1.2 Hz, 2H, NDI), 8.88 (dd, *J* = 7.5, 1.2 Hz, 2H, NDI), 8.25 (dd, *J* = 4.4, 1.5 Hz, 2H, β), 8.19 – 8.16 (m, 3H, β, Ph), 8.14 (d, *J* = 1.5 Hz, 2H, β), 8.09 (d, *J* = 7.8 Hz, 4H, Ph), 8.06 (s, 1H, Ph), 7.72 (t, *J* = 7.5 Hz, 4H, Ph), 7.63 (t, *J* = 7.5 Hz, 2H, Ph), 7.56 (d, *J* = 7.8 Hz, 1H, Ph), 4.27 – 4.22 (m, 2H, alkyl-α-CH_2), 2.42 (s, 3H, CH_3), 1.79 (dd, *J* = 14.4, 7.0 Hz, 2H, alkyl-CH_2), 1.47 (dd, *J* = 14.4, 7.0 Hz, 2H, alkyl-CH_2), 1.44 – 1.37 (m, 2H, alkyl-CH_2), 1.37 – 1.27 (m, 6H, alkyl-CH_2), 0.90 (t, *J* = 6.9 Hz, 3H, alkyl-CH_3), and 0.86 (s, 3H, OCH_3); ^{11}B NMR (193 MHz, $CDCl_3$); δ/ppm = –16.16; ^{13}C NMR (151 MHz, $CDCl_3$); δ/ppm = 163.05, 163.00, 141.27, 141.19, 138.80, 137.42, 136.41, 136.12, 135.95, 133.92, 133.55, 133.38, 132.04, 131.78, 131.34, 128.92, 128.78, 127.58, 127.41, 127.21, 126.88, 122.72, 122.60, 122.53, 121.01, 119.42, 47.07, 47.04, 41.33, 32.03, 29.52, 29.42, 28.34, 27.33, 22.86, 18.33, 18.20, and 14.30; MALDI-TOFMS: *m*/*z* calcd for $[C_{56}H_{43}BN_5O_4]^+$ = 860.3408 *([M*–OMe]$^+$); found = 860.38 ([*M*–OMe]$^+$); UV–Vis (DCM): λ_{max}/nm (ε/(10^5 M^{-1} cm^{-1})) = 374 (2.41), 459 (0.17), 486 (0.13).

SubP-3Me-NDI: This compound was synthesized and purified according to the general procedure by using *meso*-bromo subporphyrin **13** (10 mg, 0.020 mmol), **10** (36 mg, 0.060 mmol), $Pd(PPh_3)_2Cl_2$ (1.5 mg, 10 mol%), and Na_2CO_3 (21 mg, 0.20 mmol).

Note: This compound exists in 4:1 ratio of *exo*:*endo* atropisomers. Which relates to the reported *meso*-aryl-subporphyrin nitro derivative.[S4]

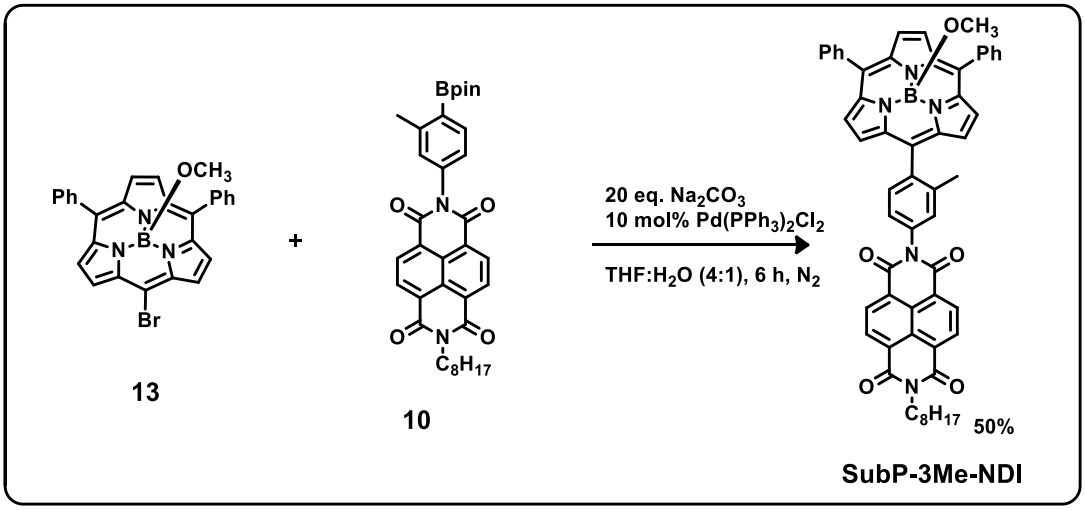

^{1}H NMR (600 MHz, $CDCl_3$); δ/ppm = 8.92 – 8.88 (m, 2H, NDI), 8.86 (m, 2H, NDI), 8.13 (d, *J* = 1.5 Hz, 2H, *β*), 8.08 (t, *J* = 11.5 Hz, 6H, *β*, Ph), 8.02 – 7.97 (m, 2H, *β*), 7.70 (m, 4H, Ph), 7.61 (m, 3H, Ph), 7.30 (s, 2H, Ph), 4.24 (t, *J* = 7.4 Hz, 2H, alkyl-α-CH_2), 2.92 (s, 3H, CH_3), 1.83 – 1.74 (m, 2H, alkyl-CH_2), 1.50 – 1.25 (m, 10H, alkyl-CH_2), 0.94 (s, 3H, OCH_3), 0.89 (t, *J* = 6.1 Hz, 3H, CH_3); ^{11}B NMR (193 MHz, $CDCl_3$); δ/ppm = -15.96; ^{13}C NMR (151 MHz, $CDCl_3$); δ = 163.45, 163.00, 142.48, 141.40, 141.30, 141.15, 137.40, 134.93, 134.71, 134.21, 133.47, 133. 44, 131.69, 131.34, 130.47, 128.85, 128.82, 128.03, 127.40, 127.34, 127.16, 127.00, 125.69, 122.45, 122.40, 121.58, 121.15, 118.28, 47.22, 47.08, 41.34, 32.03, 29.52, 29.42, 28.34, 27.34, 22.86, 22.53, 20.49, 14.31; MALDI-TOF-MS: *m*/*z* calcd for $C_{56}H_{43}BN_5O_4$ = 860.3408 *([M-OMe]*$^{+}$); found = 860.34 ([*M-OMe]*$^{+}$); UV-Vis (DCM): λ_{max}(nm) (ε x 10^5 [$M^{-1}cm^{-1}$]) = 369 (2.00), 457 (0.15), 480 (0.08).

SubP-2,6DiMe-NDI: This compound was synthesized and purified according to the general procedure by using *meso*-bromo subporphyrin **13** (10 mg, 0.020 mmol), **11** (37 mg, 0.060 mmol), $Pd(PPh_3)_2Cl_2$ (1.5 mg, 10 mol%), and Na_2CO_3 (21 mg, 0.20 mmol).

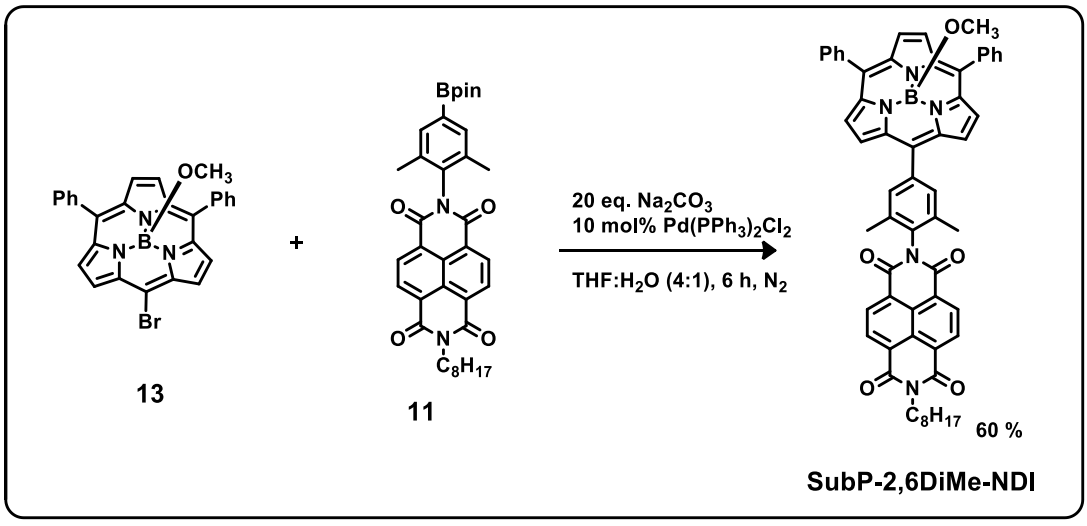

^{1}H NMR (600 MHz, $CDCl_3$); δ/ppm = 8.92 (d, J = 7.5 Hz, 2H, NDI), 8.88 (d, J = 7.5 Hz, 2H, NDI), 8.26 (d, J = 4.5 Hz, 2H, β), 8.17 (d, J = 4.5 Hz, 2H, β), 8.13 (s, 2H, β), 8.11 – 8.07 (m, 4H, Ph), 7.95 (s, 2H, Ph), 7.71 (t, J = 7.7 Hz, 4H, Ph), 7.65 – 7.61 (m, 2H, Ph), 4.29 – 4.23 (m, 2H, alkyl-α-CH_2), 2.37 (s, 6H, CH_3), 1.78 (dd, J = 15.3, 7.8 Hz, 2H, alkyl-CH_2), 1.46 (dd, J = 15.3, 7.8 Hz, 2H, alkyl-CH_2), 1.40 (dd, J = 9.7, 5.7 Hz, 2H, alkyl-CH_2), 1.31 (m, 8H, alkyl-CH_2), 0.90 (t, J = 6.9 Hz, 3H, alkyl-CH_3), and 0.85 (s, 3H, OCH_3); ^{11}B NMR (193 MHz, $CDCl_3$); δ/ppm = –16.15; ^{13}C NMR (151 MHz, $CDCl_3$); δ/ppm = 163.00, 162.62, 141.26, 141.18, 140.63, 138.39, 137.45, 136.06, 133.54, 133.38, 131.82, 131.34, 128.91, 128.76, 128.11, 127.94, 127.72, 127.44, 127.25, 126.77, 122.58, 122.55, 120.91, 120.71, 119.72, 47.06, 47.04, 41.32, 32.03, 29.52, 29.42, 28.34, 27.32, 22.86, 18.55, 18.43, 14.32, and 14.30; MALDI-TOFMS: m/z calcd for $[C_{57}H_{45}BN_5O_4]^+$= 874.3565 ([M–OMe]$^+$); found = 874.31 ([M–OMe]$^+$); UV–Vis (DCM): λ_{max}/nm (ε/(10^5 M^{-1} cm^{-1})) = 374 (2.05), 460 (0.16), 485 (0.13).

SubP-3,6DiMe-NDI**:** This compound was synthesized and purified according to the general procedure by using *meso*-bromo subporphyrin **13** (10 mg, 0.020 mmol), **12** (37 mg, 0.060 mmol), $Pd(PPh_3)_2Cl_2$ (1.5 mg, 10 mol%), and Na_2CO_3 (21 mg, 0.20 mmol).

Note: This compound exists in 4:1 ratio of *exo*:*endo* atropisomers.[S4]

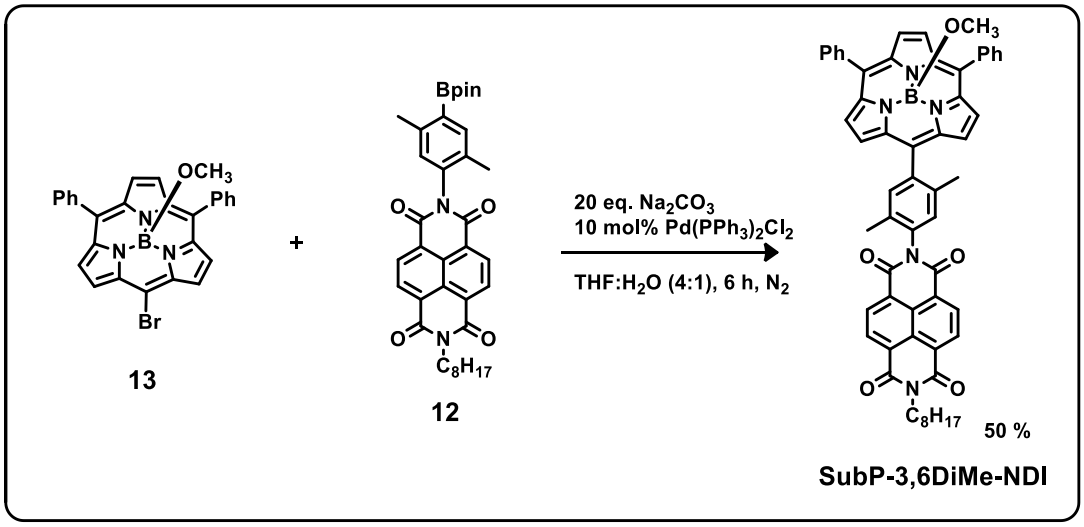

^{1}H NMR (600 MHz, $CDCl_3$); δ/ppm = 8.91 (dd, J = 7.5, 3.8 Hz, 2H, NDI), 8.87 (dd, J = 7.5, 3.8 Hz, 2H, NDI), 8.12 (s, 2H, β), 8.11 – 8.05 (m, 6H, β, Ph), 8.01 (d, J = 4.5 Hz, 2H, β), 7.70 (ddd, J = 9.4, 6.7, 3.7 Hz, 4H, Ph), 7.61 (ddd, J = 7.0, 2.3, 1.2 Hz, 2H, Ph), 7.50 (s, 1H, Ph), 7.14 (s, 1H, Ph), 4.26 – 4.22 (m, 2H, alkyl-α-CH_2), 2.86 (s, 3H, CH_3), 2.16 (s, 3H, CH_3), 1.79 (dt, J = 15.4, 7.6 Hz, 2H, alkyl-CH_2), 1.49 – 1.24 (m, 14H, alkyl-CH_2), 0.93 (s, 3H, OCH_3), and 0.92 – 0.86 (m, 3H, alkyl-CH_3); ^{11}B NMR (193 MHz, $CDCl_3$); δ/ppm = –15.95; ^{13}C NMR (151 MHz, $CDCl_3$); δ/ppm = 163.07, 163.01, 142.48, 141.48, 141. 40, 141.28, 137.45, 133.56, 133.53, 133.36, 132.84, 131.76, 131.72, 131.68, 131.39, 131.35, 128.89, 128.77, 128.74, 128.09, 127.93, 127.37, 126.95, 126.92, 122.47, 122.28, 121.05, 47.23, 47.19, 41.33, 32.03, 29.91, 29.52, 29.42, 28.34, 27.33, 22.86, 17.60, 17.49, 14.32, and 14.30; MALDI-TOFMS: m/z calcd for $[C_{57}H_{45}BN_5O_4]^+$ = 874.3565 ([M–OMe]$^+$); found = 874.44 ([M–OMe]$^+$); UV–Vis (DCM): λ_{max}/nm (ε/(10^5 M^{-1} cm^{-1})) = 369 (2.01), 457 (0.16), 480 (0.10).

3. Mass spectral analysis:

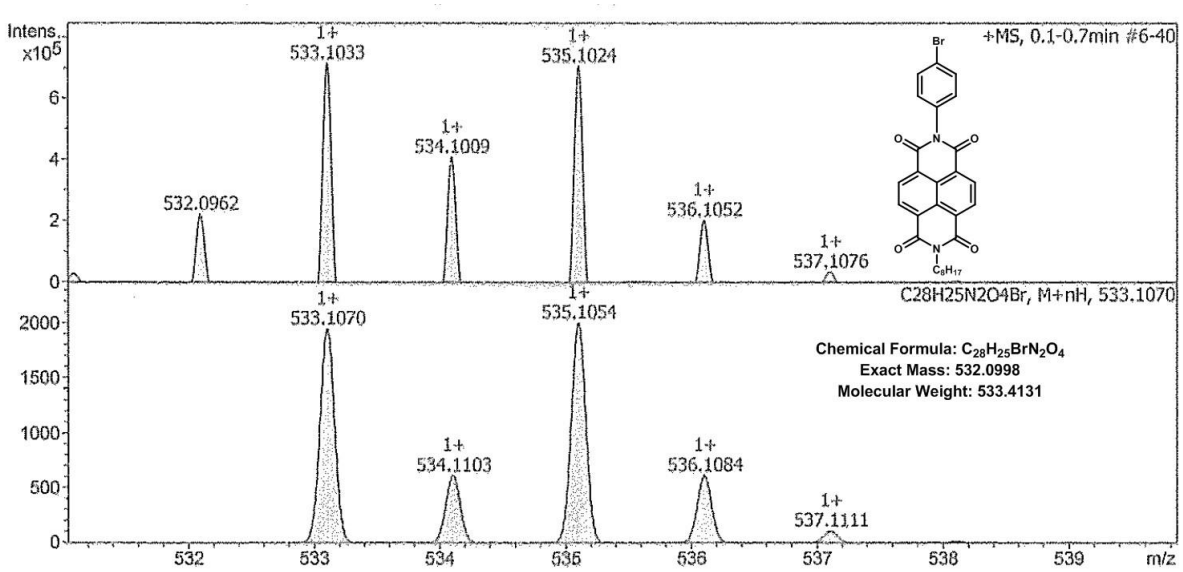

Fig. S1. HR-APCI-TOF-MS of **3** (top: observed, bottom: simulated).

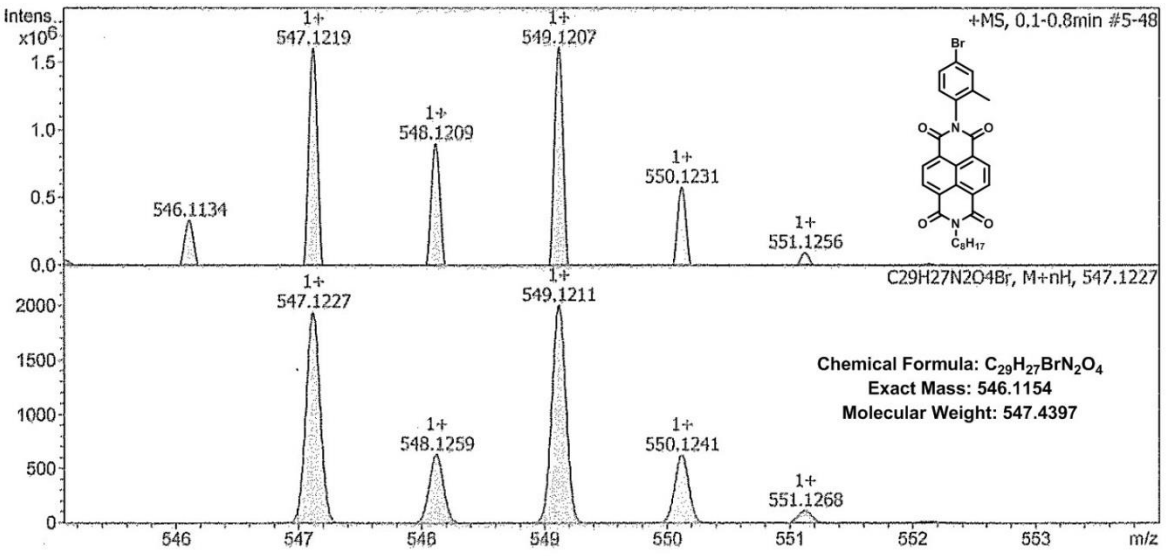

Fig. S2. HR-APCI-TOF-MS of **4** (top: observed, bottom: simulated).

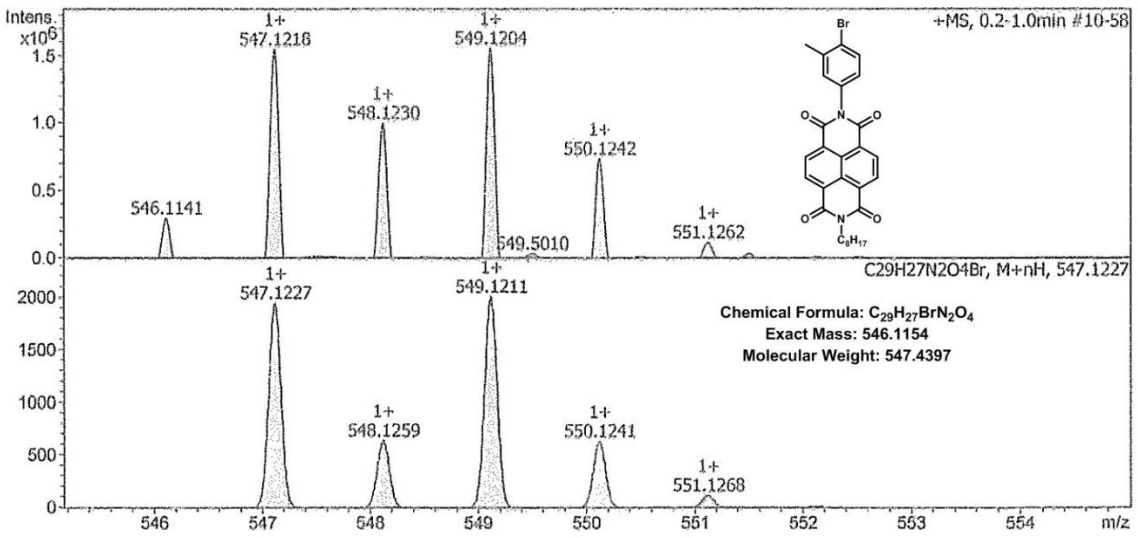

Fig. S3. HR-APCI-TOF-MS of **5** (top: observed, bottom: simulated).

.

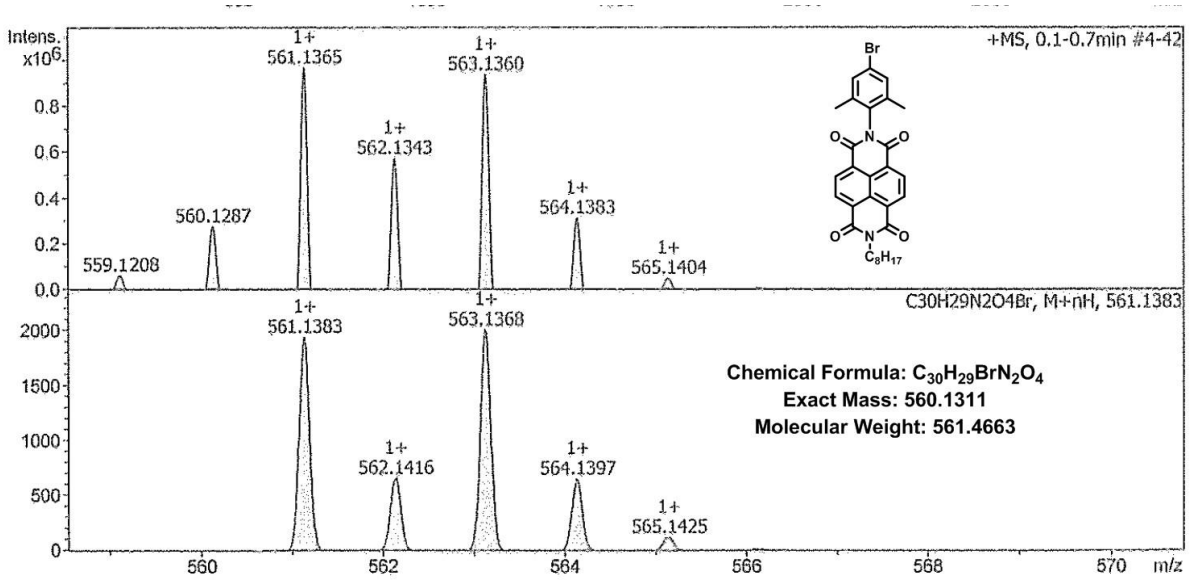

Fig. S4. HR-APCI-TOF-MS of **6** (top: observed, bottom: simulated).

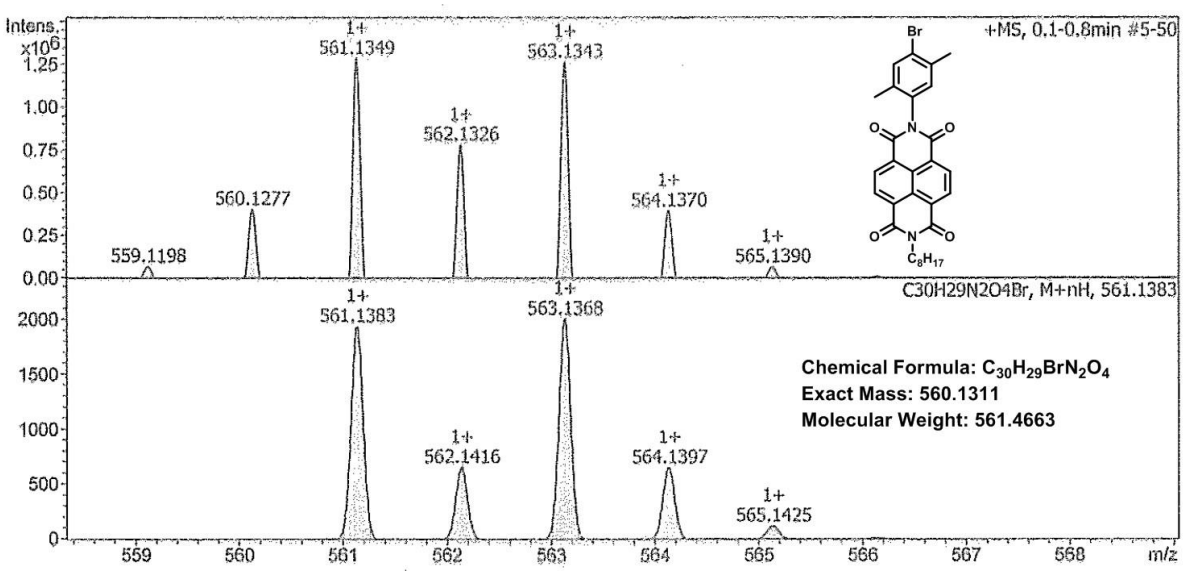

Fig. S5. HR-APCI-TOF-MS of **7** (top: observed, bottom: simulated).

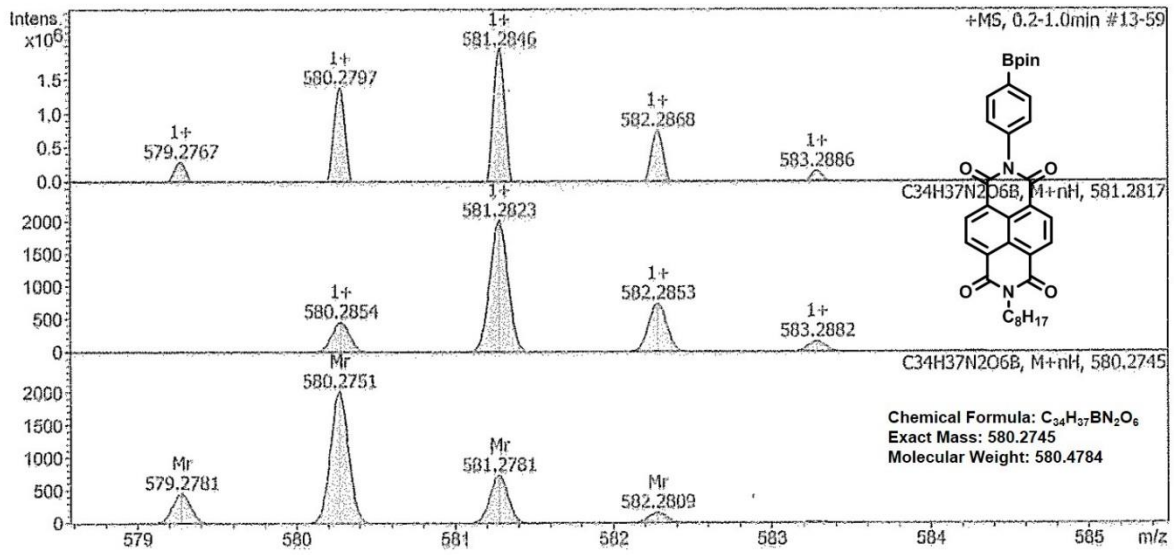

Fig. S6. HR-APCI-TOF-MS of **8** (2nd column indicates the simulated spectrum of protonated species, 3rd column indicates simulated spectrum of neutral species. According to the observed spectral pattern (column 1) we consider that observed spectrum (column 1) is contribution from both the protonated and neutral form).

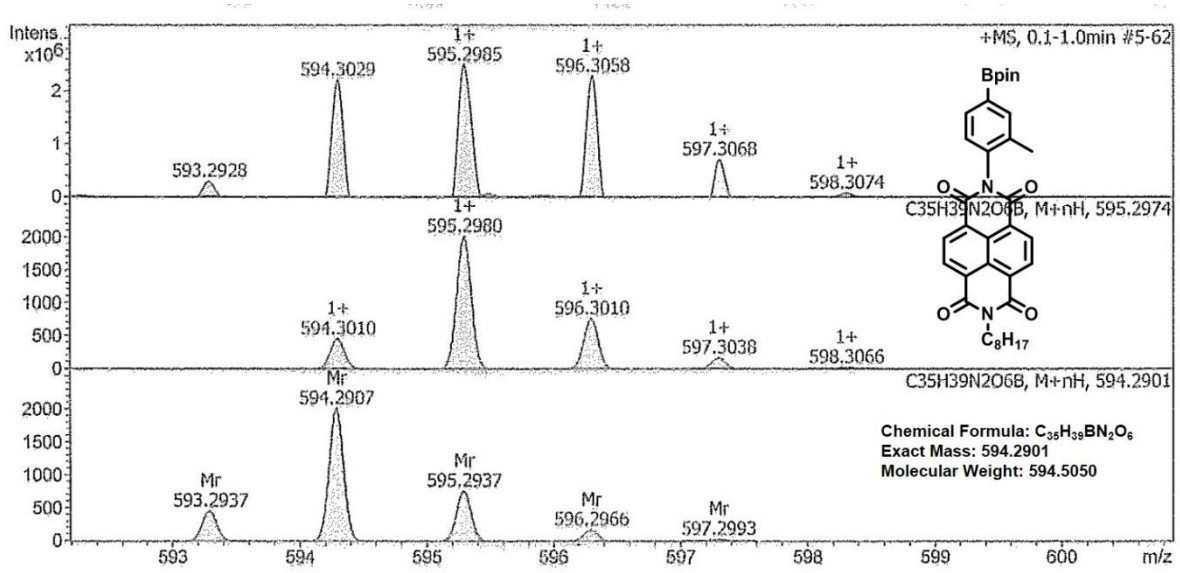

Fig. S7. HR-APCI-TOF-MS of **9** (2nd row indicates the simulated spectrum of protonated species, 3rd row indicates simulated spectrum of neutral species. According to the observed spectral pattern (row 1) we consider that the observed spectrum has contributions from both the protonated and neutral forms).

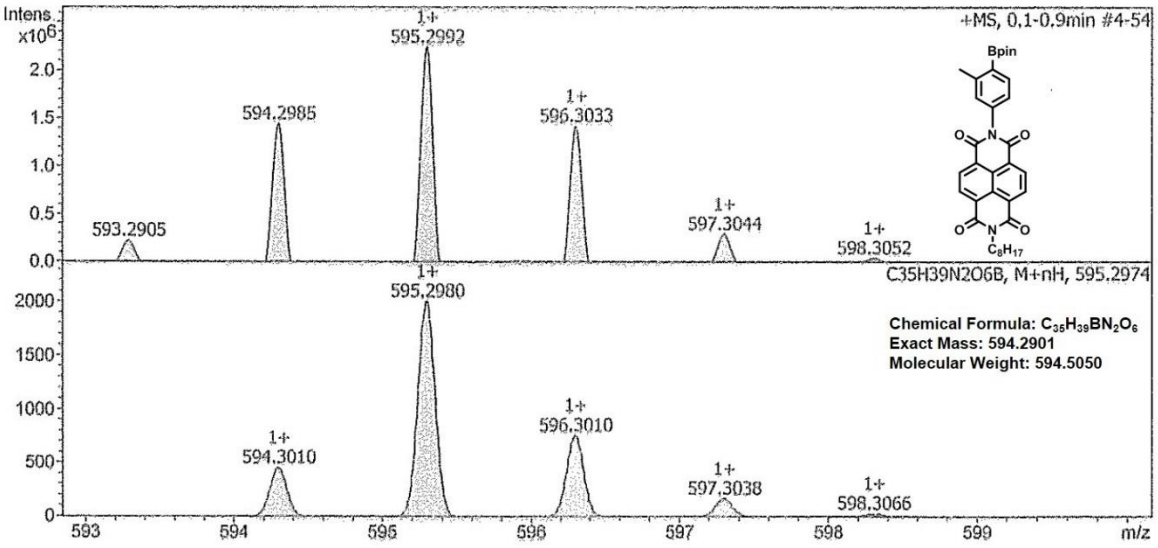

Fig. S8. HR-APCI-TOF-MS of **10** (top: observed, bottom: simulated).

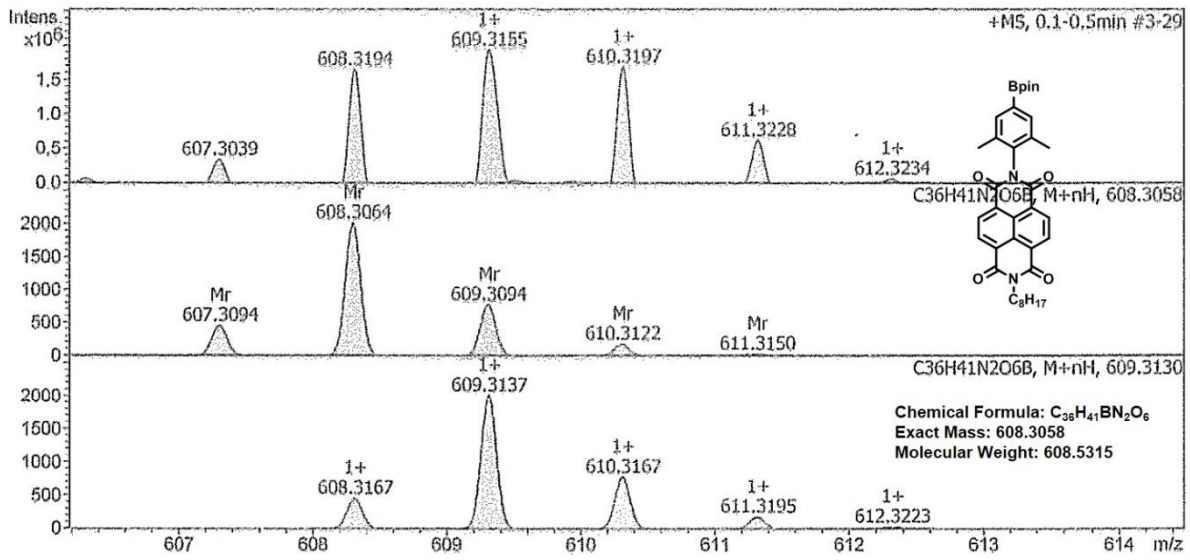

Fig. S9. HR-APCI-TOF-MS of **11** (2nd row indicates the simulated spectrum of protonated species, 3rd row indicates simulated spectrum of neutral species. According to the observed spectral pattern (row 1) we consider the observed spectrum has contributions from both the protonated and neutral forms).

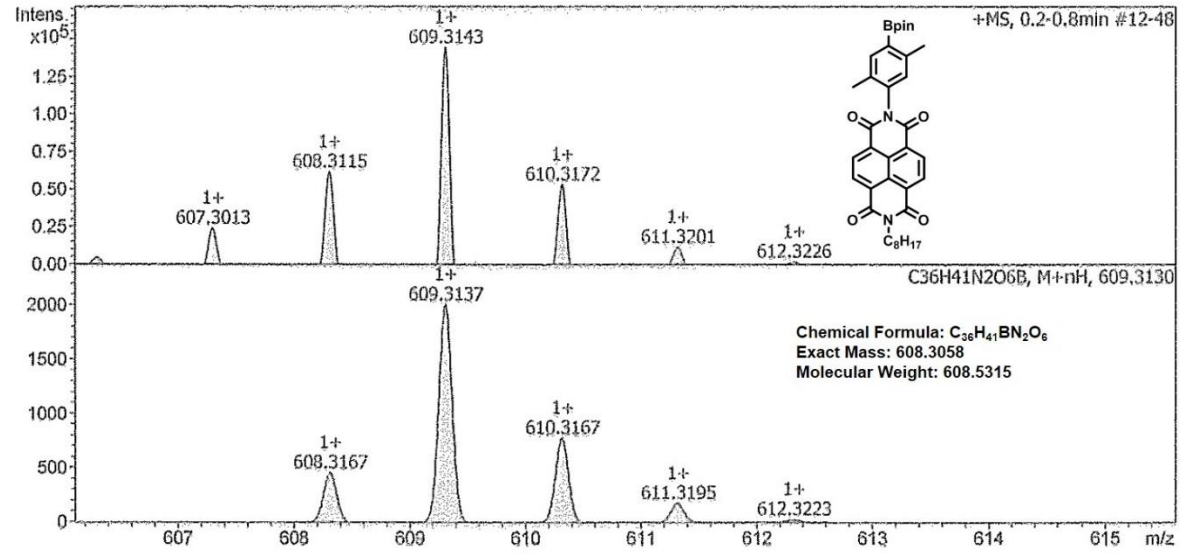

Fig. S10. HR-APCI-TOF-MS of **12** (top: observed, bottom: simulated).

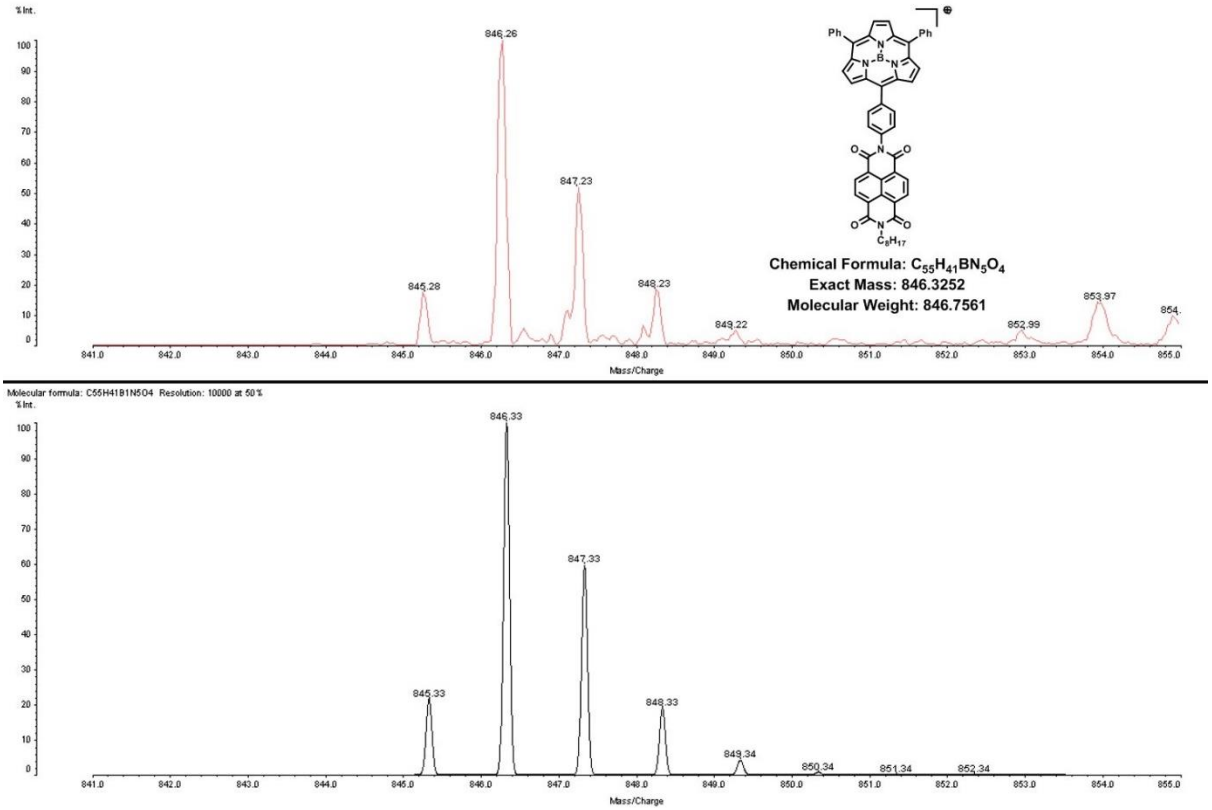

Fig. S11. MALDI-TOF-MS of **SubP-NDI** (top: observed, bottom: simulated).

.

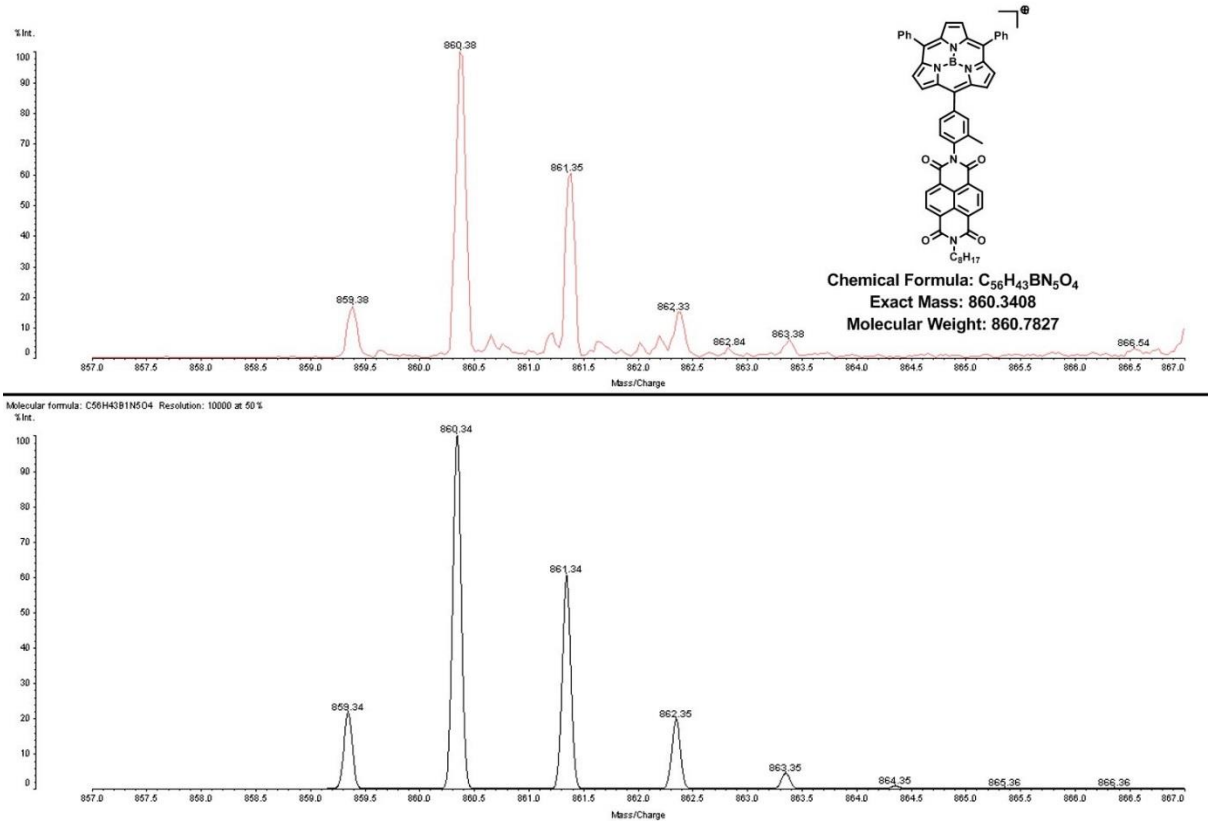

Fig. S12. MALDI-TOF-MS of **SubP-2Me-NDI** (top: observed, bottom: simulated).

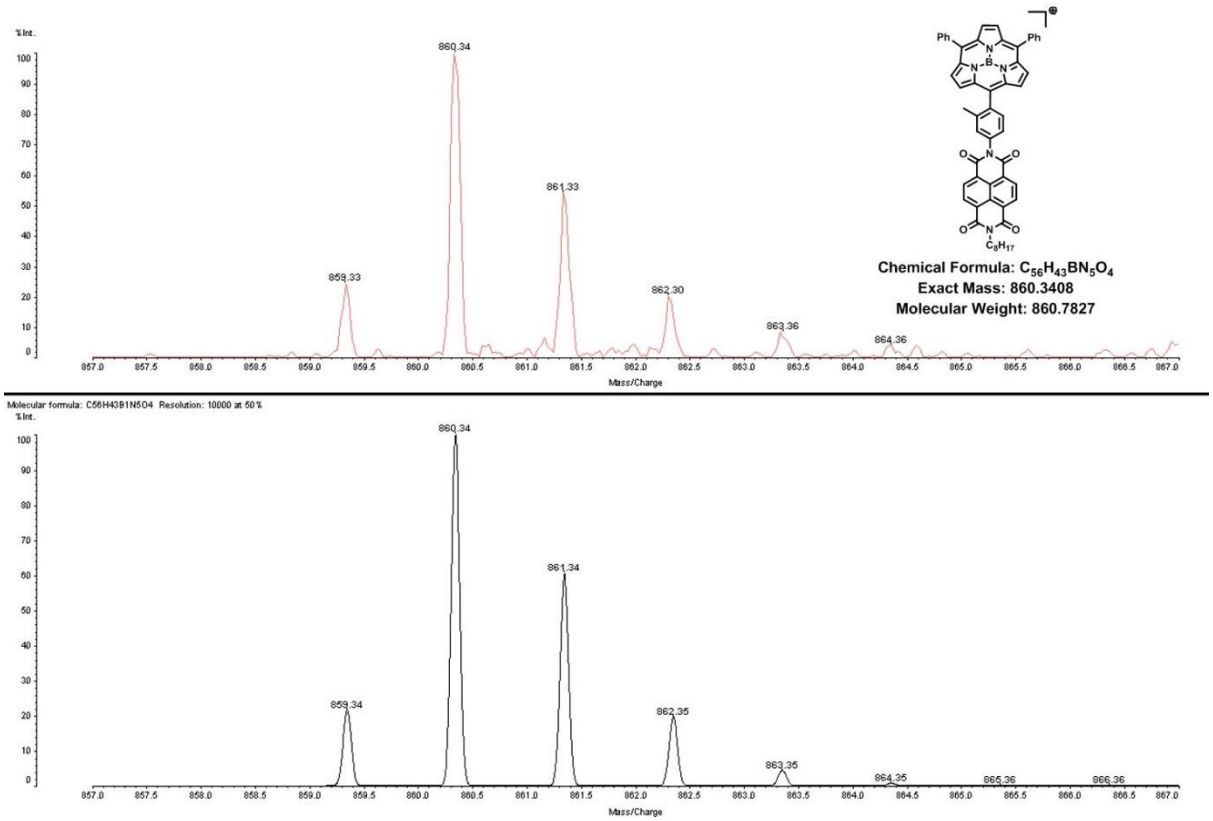

Fig. S13. MALDI-TOF-MS of **SubP-3Me-NDI** (top: observed, bottom: simulated).

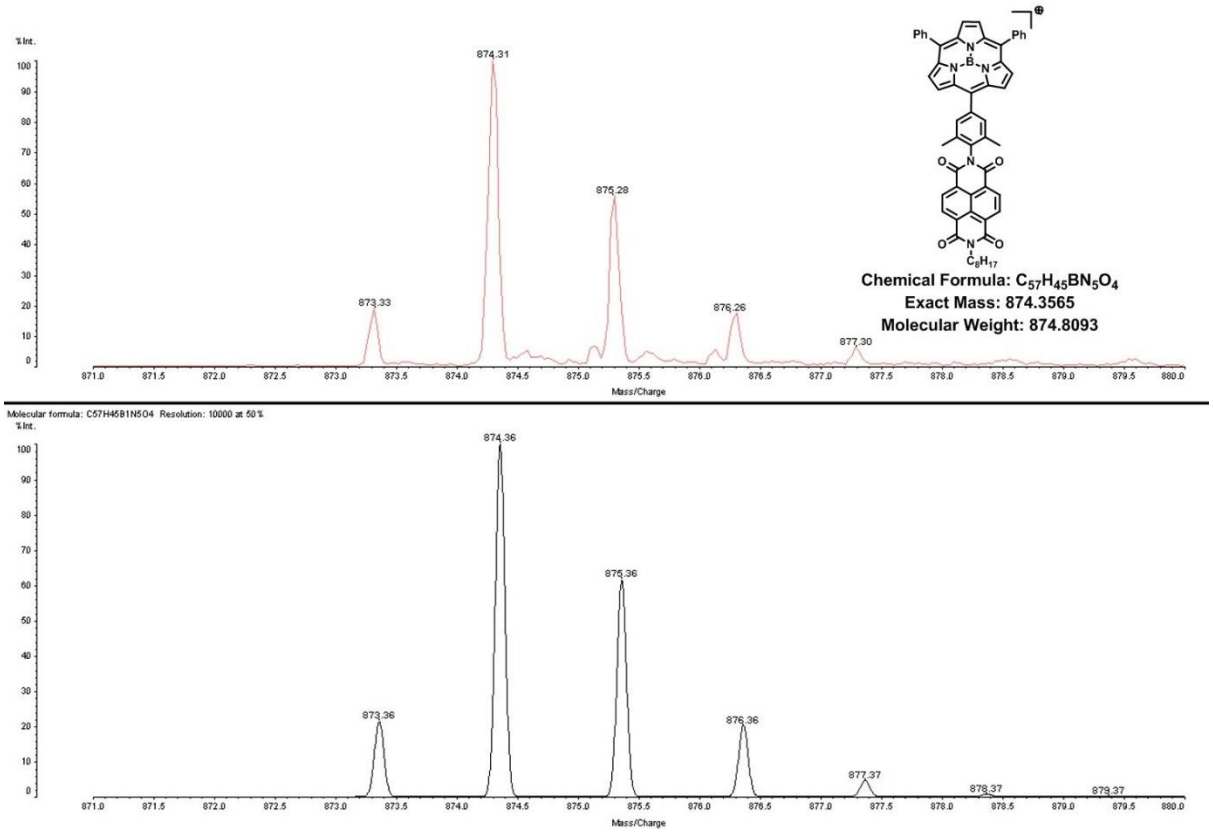

Fig. S14. MALDI-TOF-MS of **SubP-2,6DiMe-NDI** (top: observed, bottom: simulated).

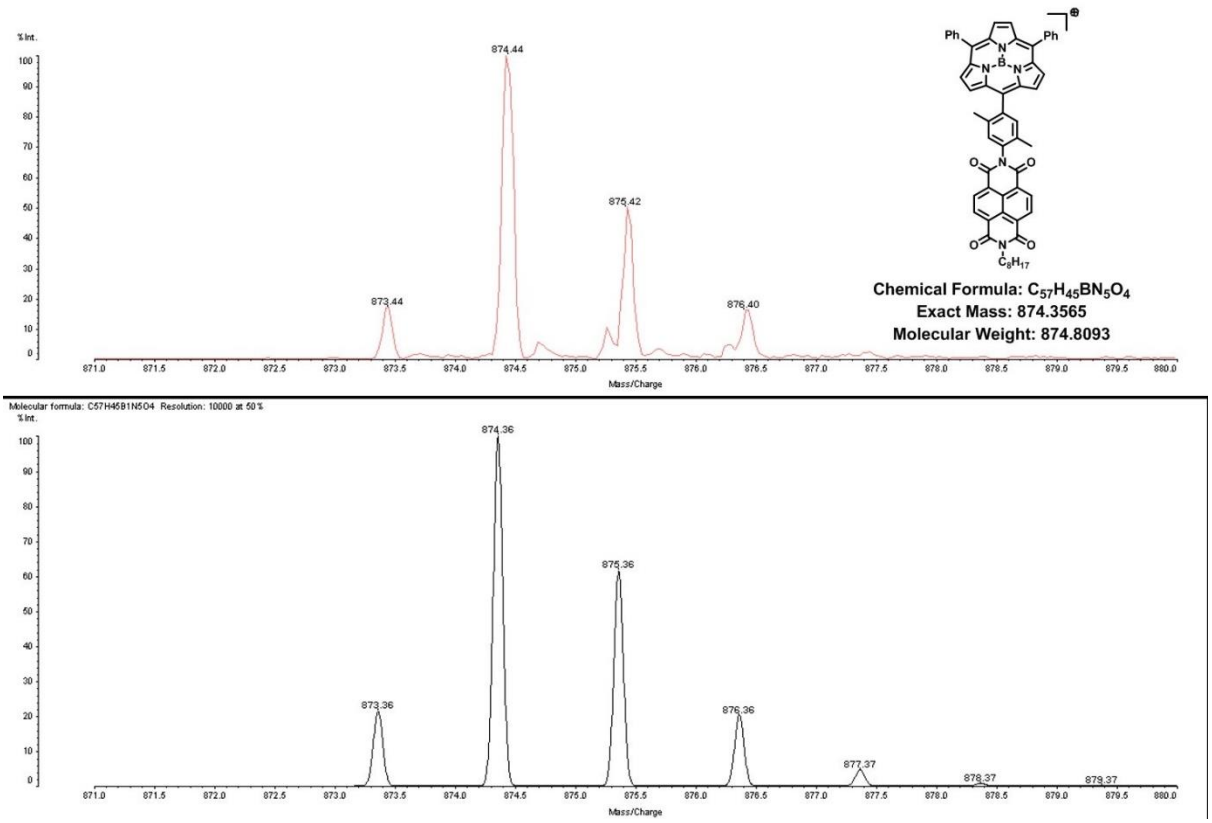

Fig. S15. MALDI-TOF-MS of **SubP-3,6DiMe-NDI** (top: observed, bottom: simulated).

4. NMR spectral analysis:

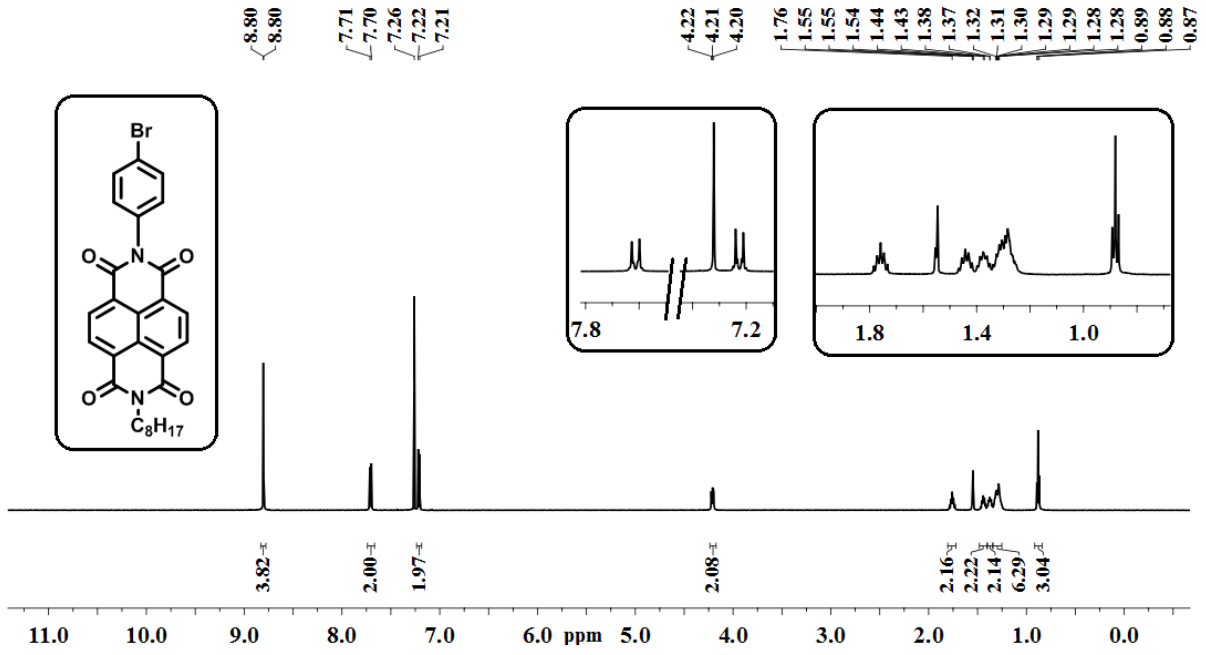

Fig. S16. ^{1}H-NMR spectrum of **3** in $CDCl_3$.

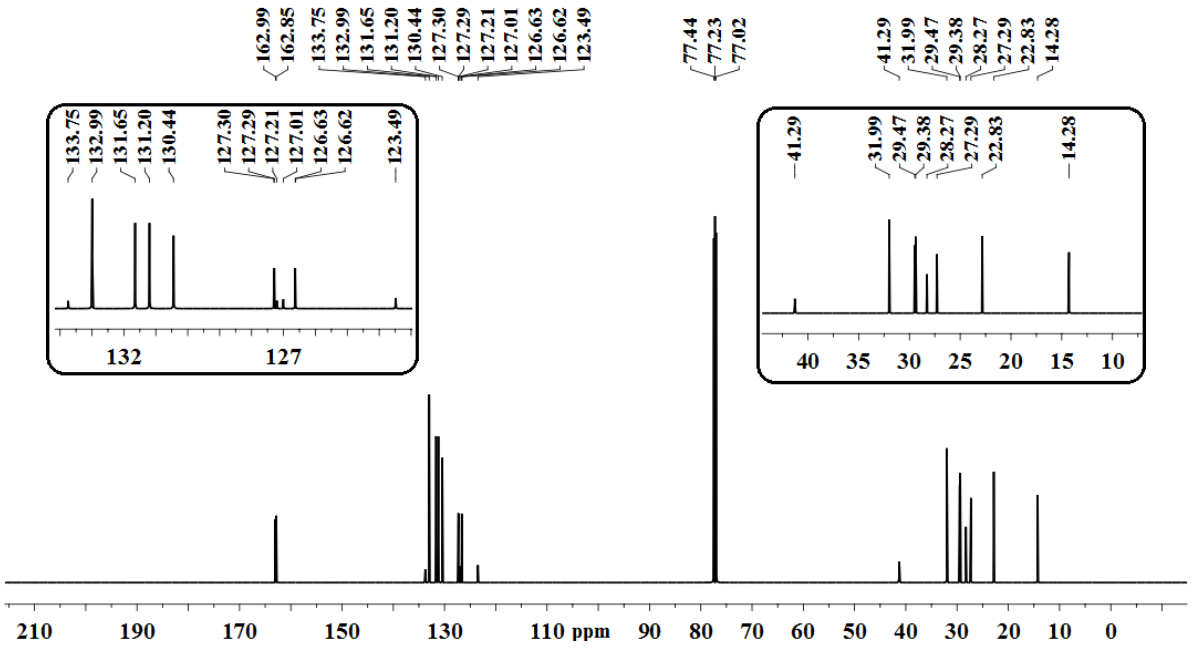

Fig. S17. ^{13}C-NMR spectrum of **3** in $CDCl_3$.

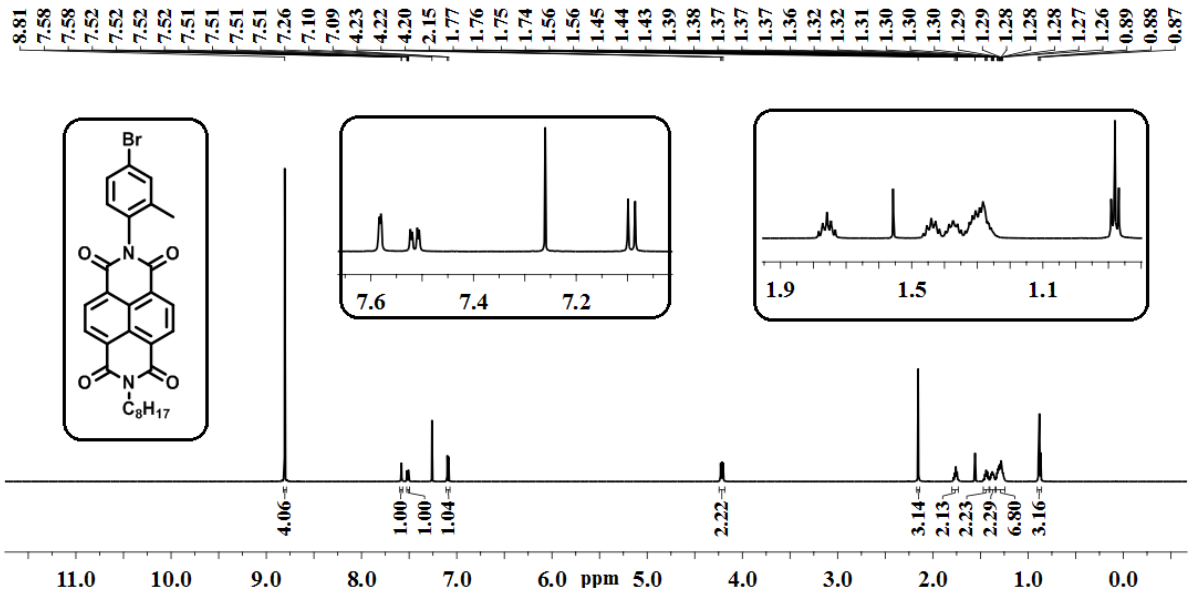

Fig. S18. ^{1}H-NMR spectrum of **4** in $CDCl_3$.

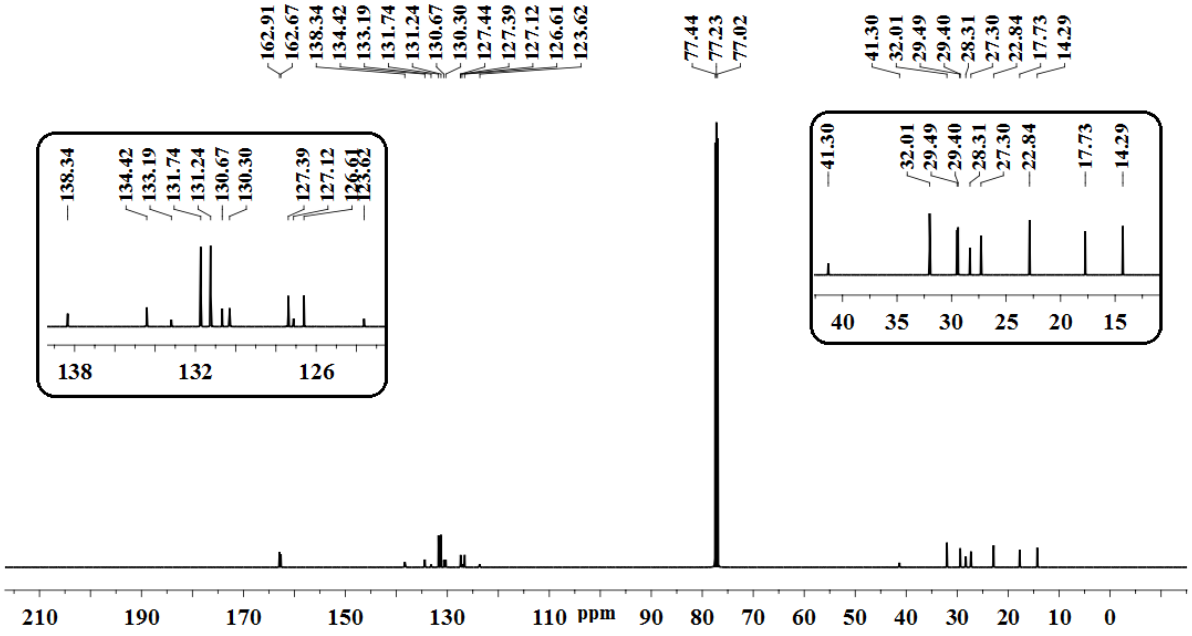

Fig. S19. ^{13}C-NMR spectrum of **4** in $CDCl_3$.

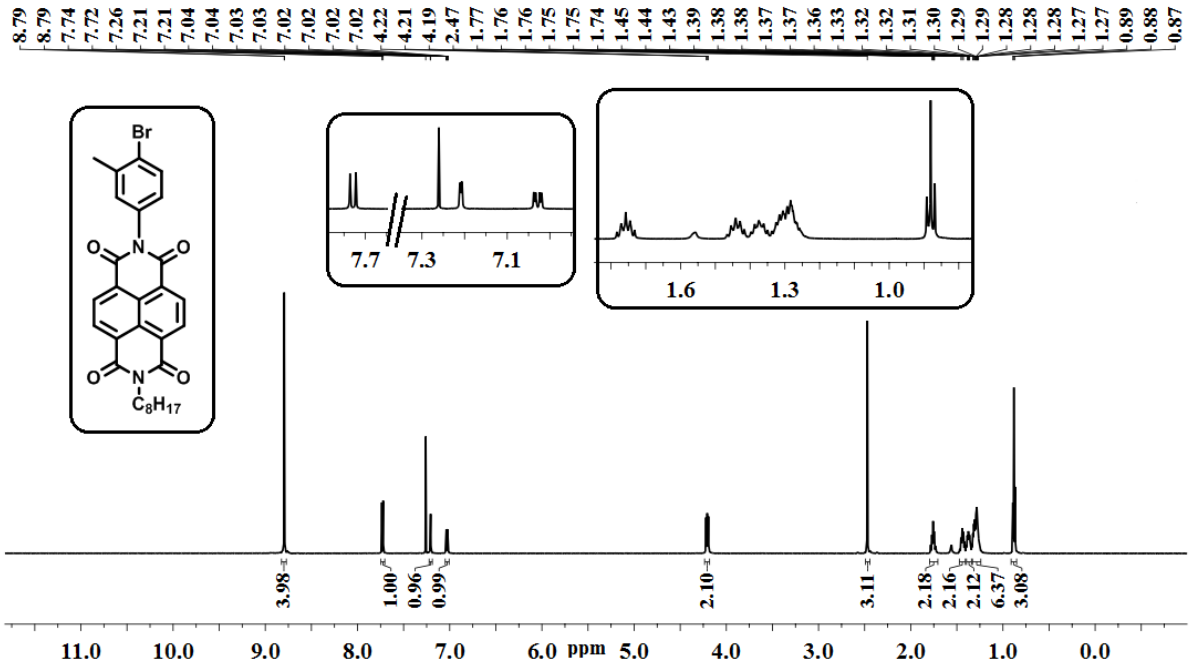

Fig. S20. ^{1}H-NMR spectrum of **5** in $CDCl_3$.

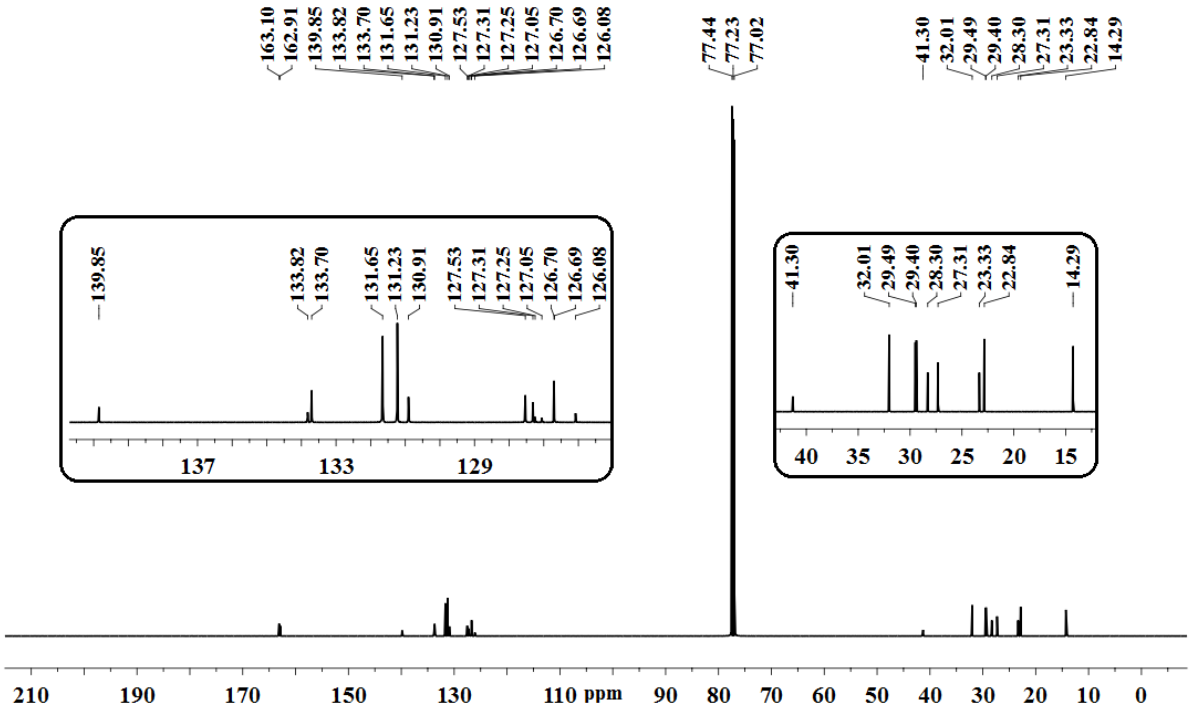

Fig. S21. ^{13}C-NMR spectrum of **5** in $CDCl_3$.

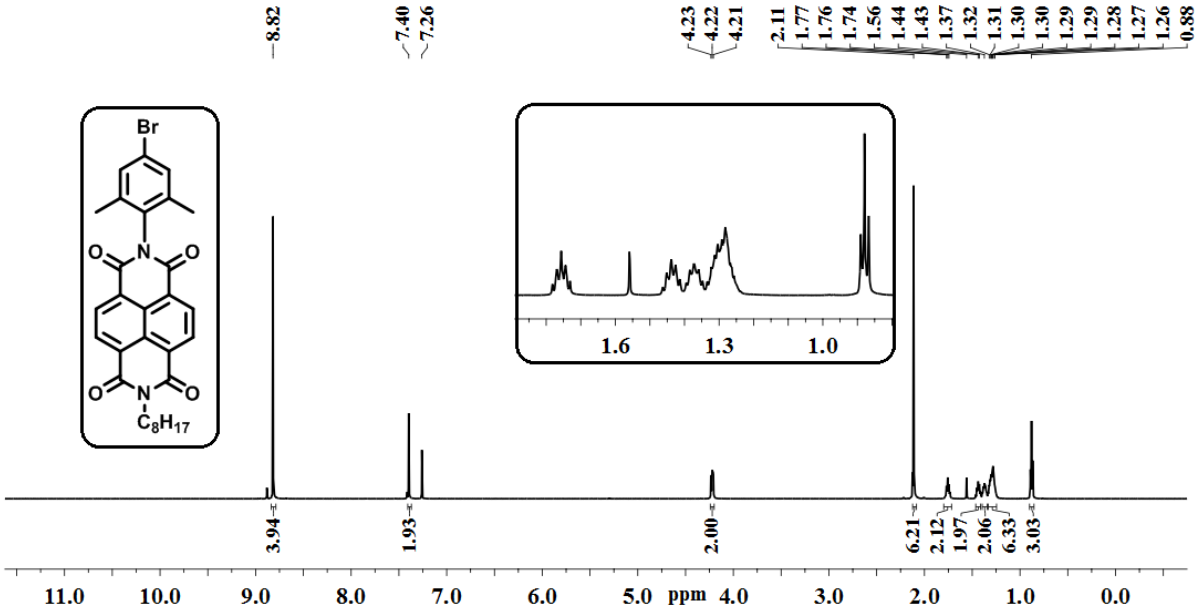

Fig. S22. ^{1}H-NMR spectrum of **6** in $CDCl_3$.

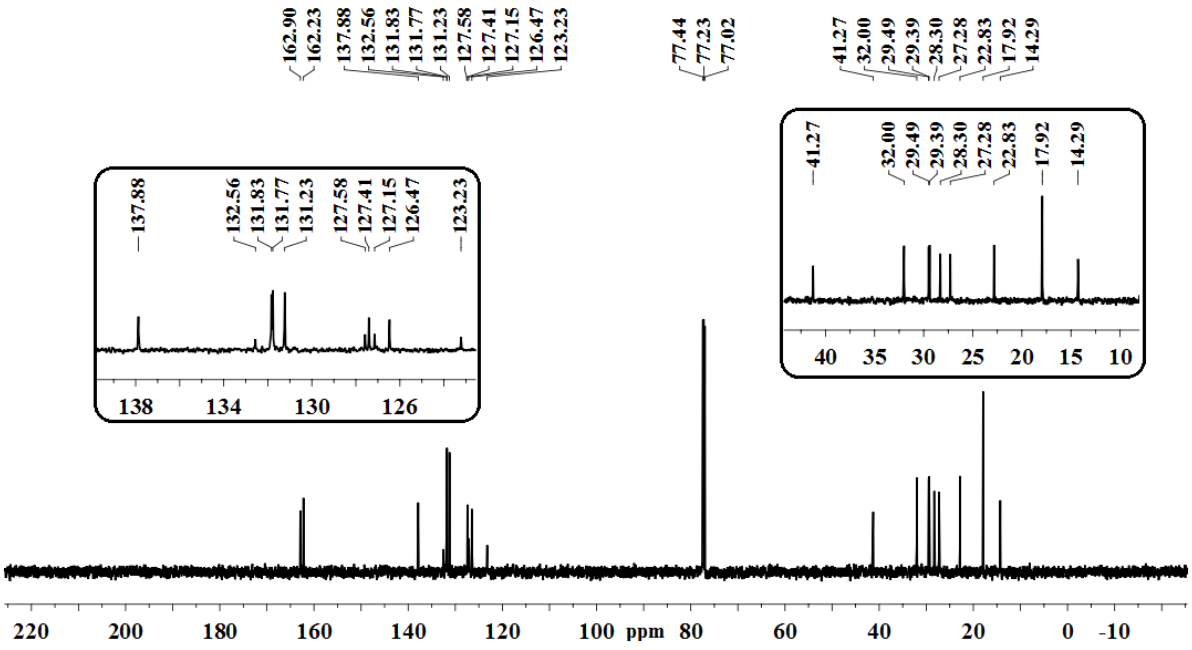

Fig. S23. ^{13}C-NMR spectrum of **6** in $CDCl_3$.

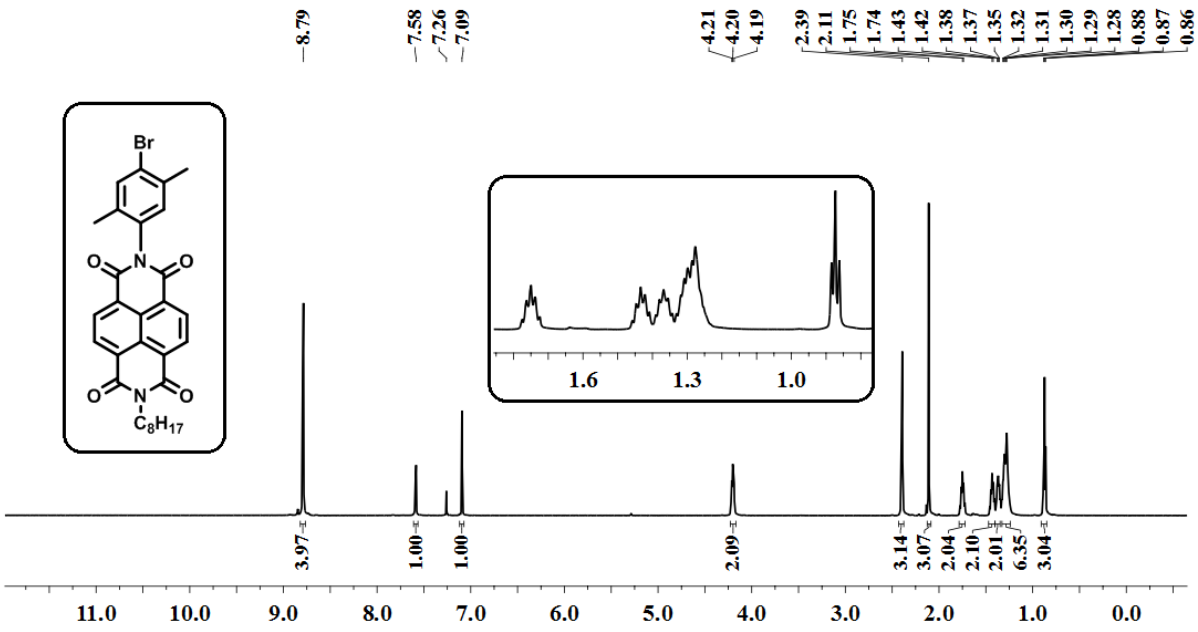

Fig. S24. ^{1}H-NMR spectrum of **7** in $CDCl_3$.

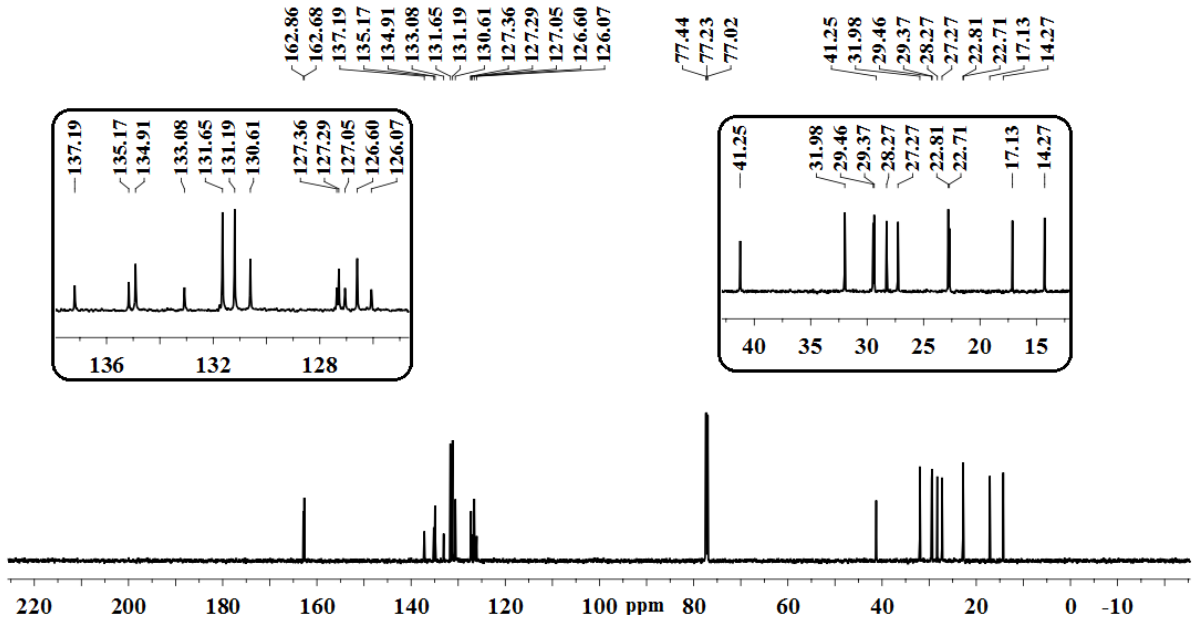

Fig. S25. ^{13}C-NMR spectrum of **7** in $CDCl_3$.

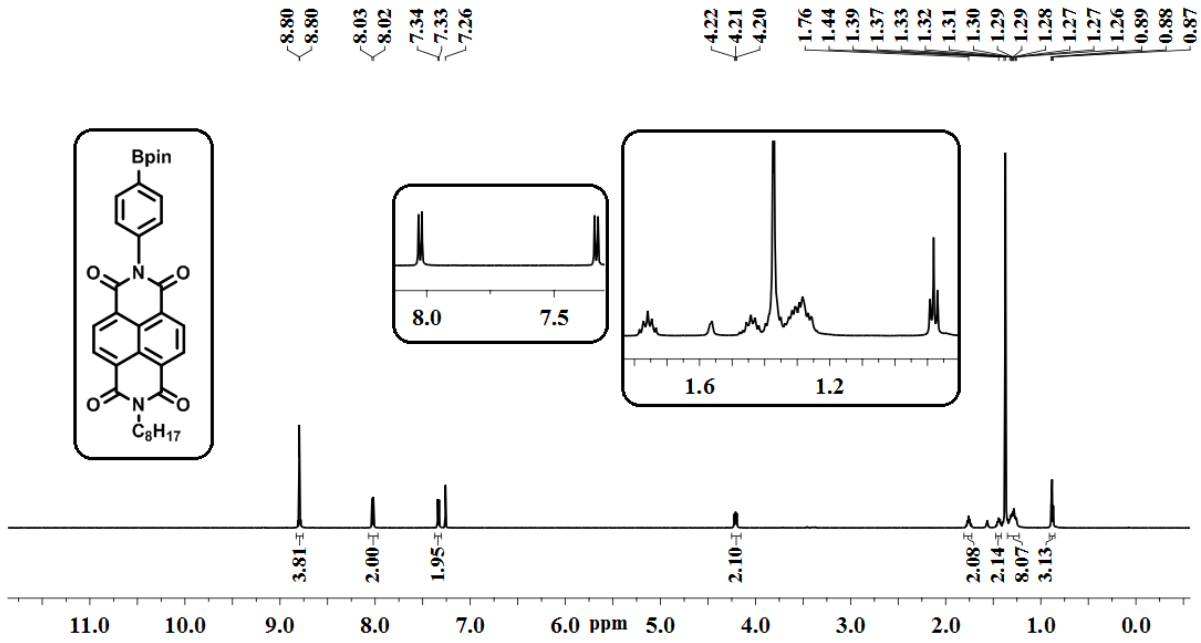

Fig. S26. ^{1}H-NMR spectrum of **8** in $CDCl_3$.

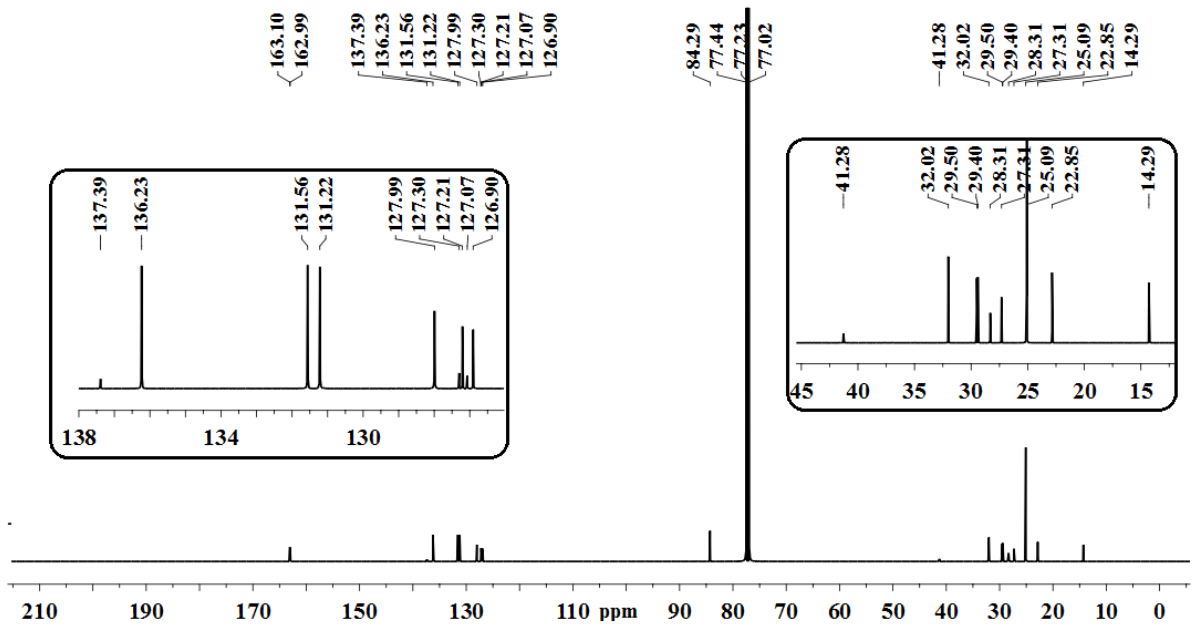

Fig. S27. ^{13}C-NMR spectrum of **8** in $CDCl_3$.

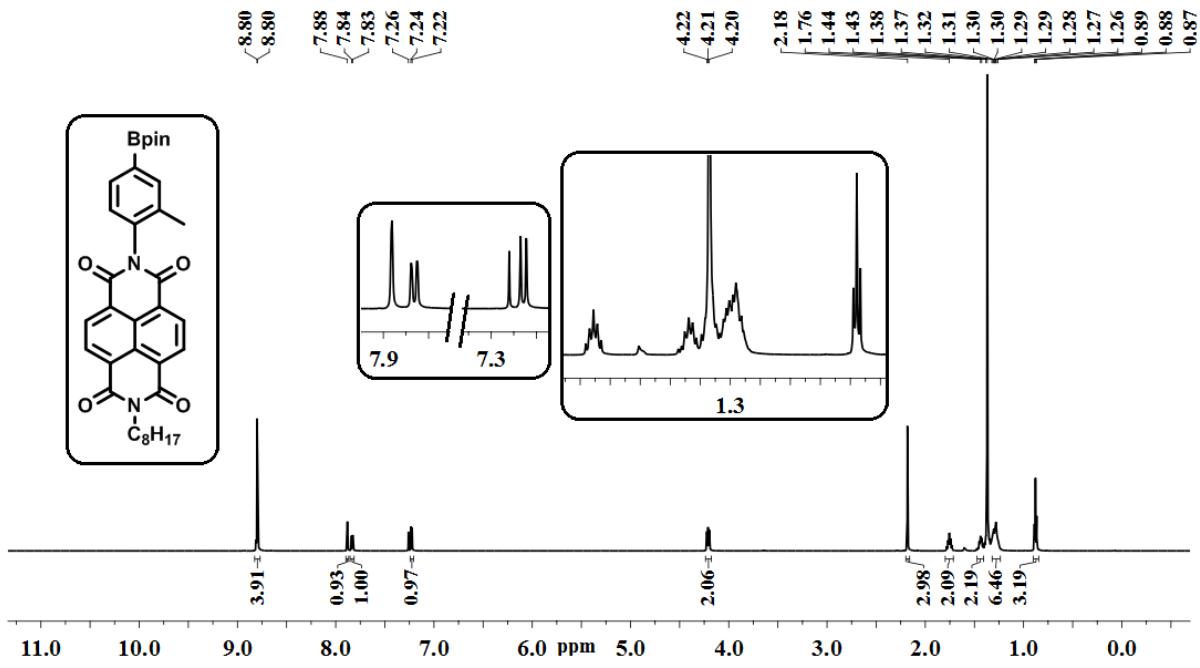

Fig. S28. ^{1}H-NMR spectrum of **9** in $CDCl_3$.

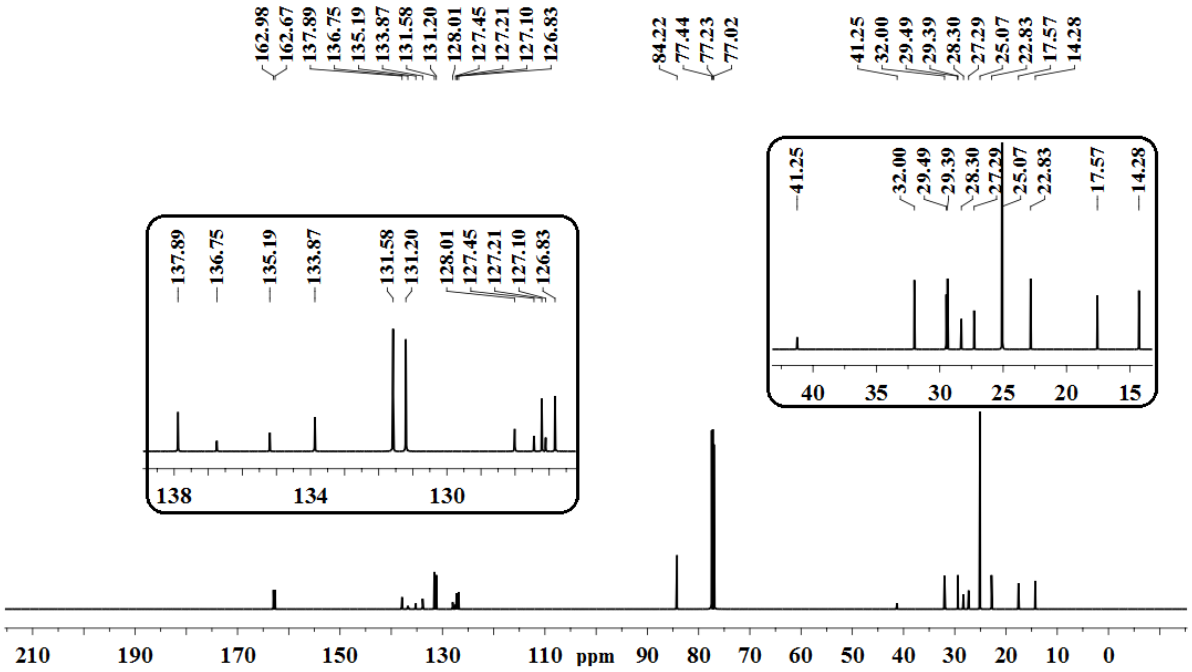

Fig. S29. ^{13}C-NMR spectrum of **9** in $CDCl_3$.

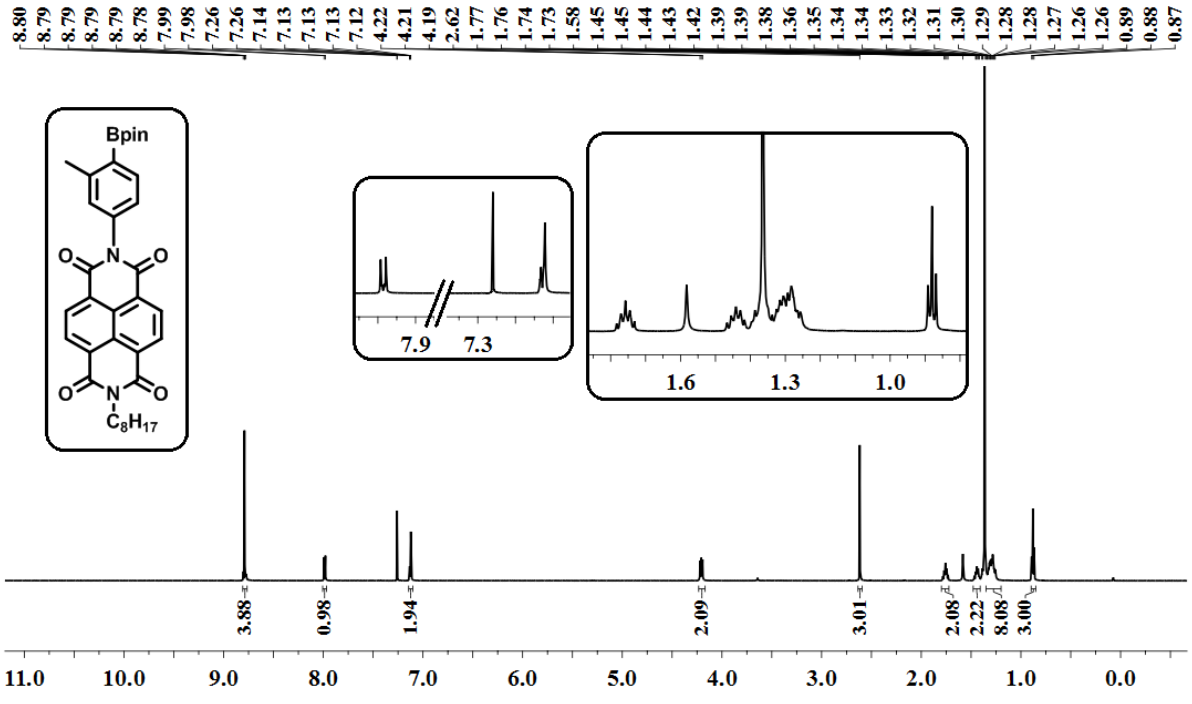

Fig. S30. ^{1}H-NMR spectrum of **10** in $CDCl_3$.

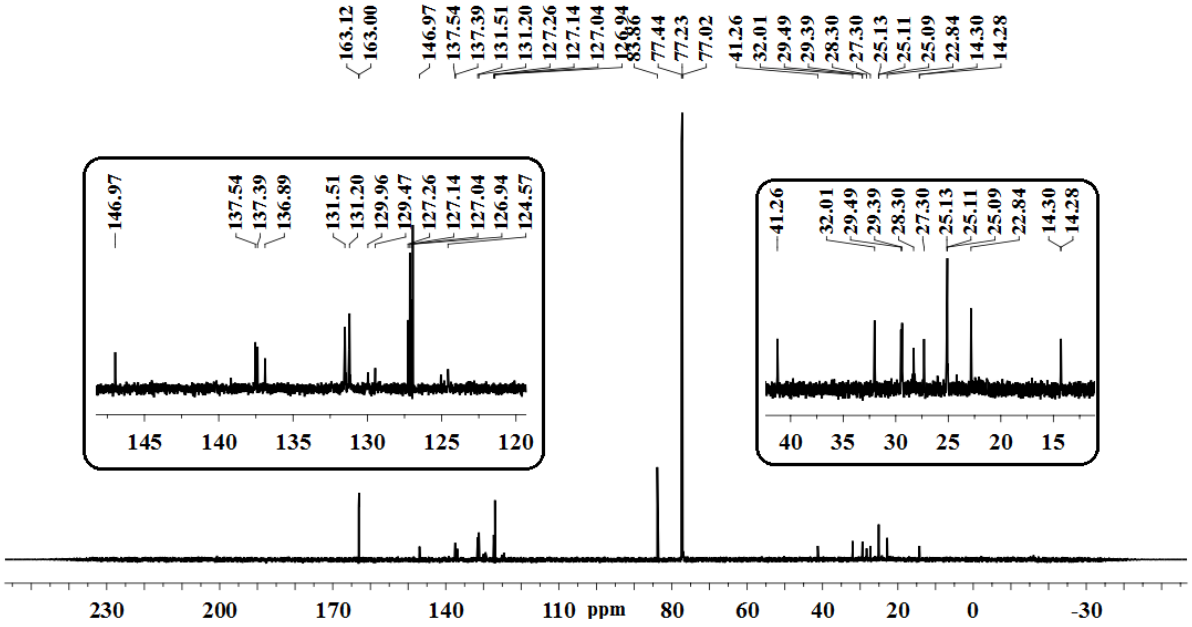

Fig. S31. ^{13}C-NMR spectrum of **10** in $CDCl_3$.

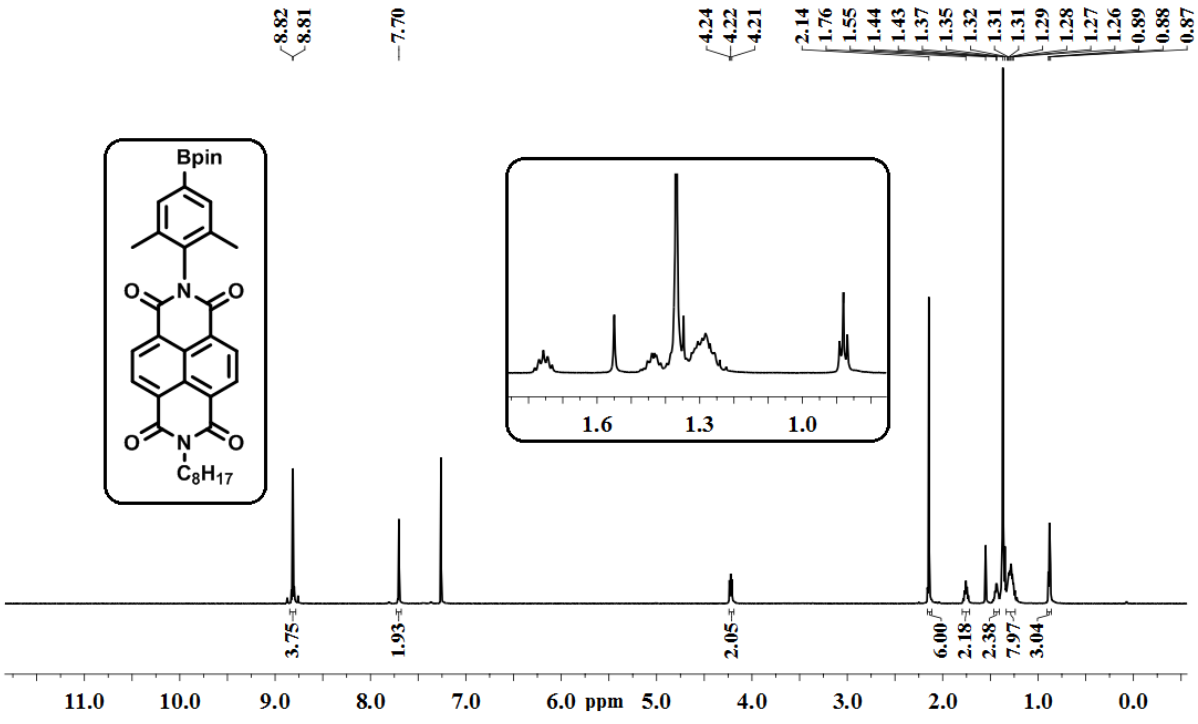

Fig. S32. ^{1}H-NMR spectrum of **11** in $CDCl_3$.

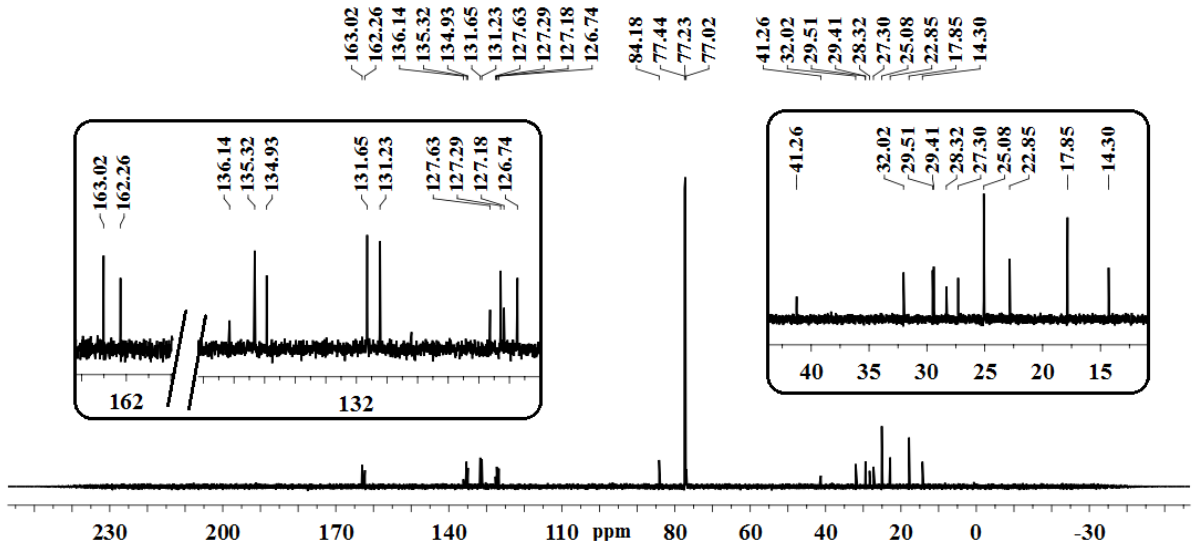

Fig. S33. ^{13}C-NMR spectrum of **11** in $CDCl_3$.

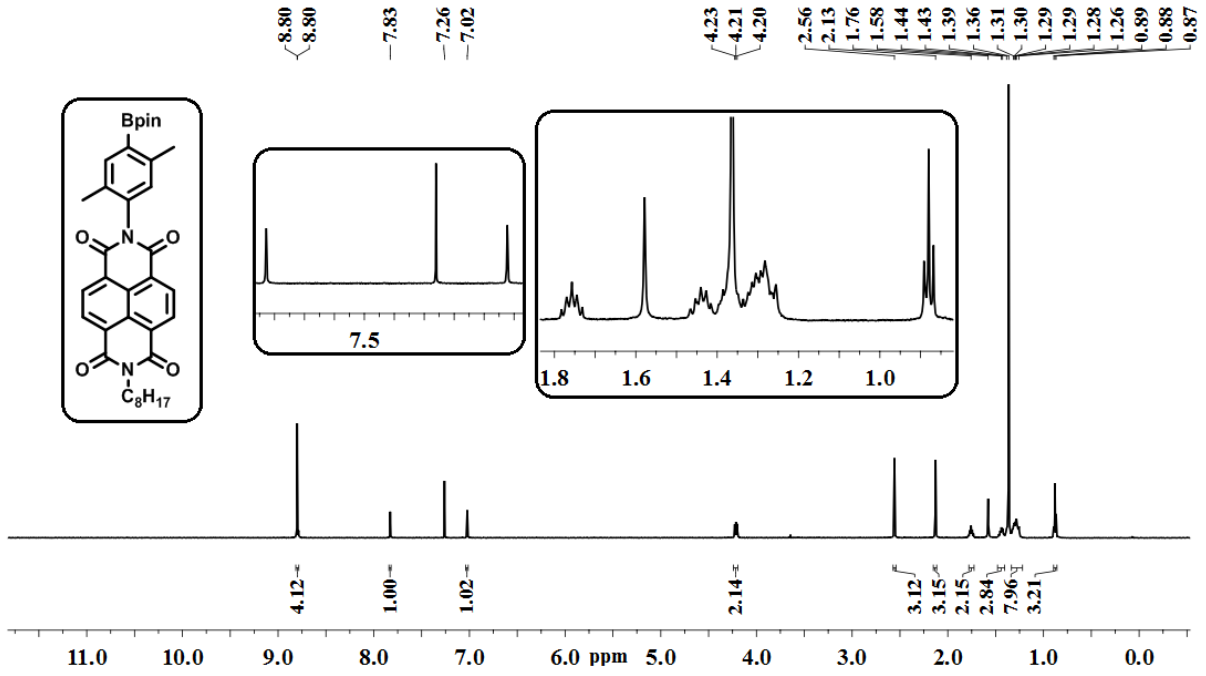

Fig. S34. ^{1}H-NMR spectrum of **12** in $CDCl_3$.

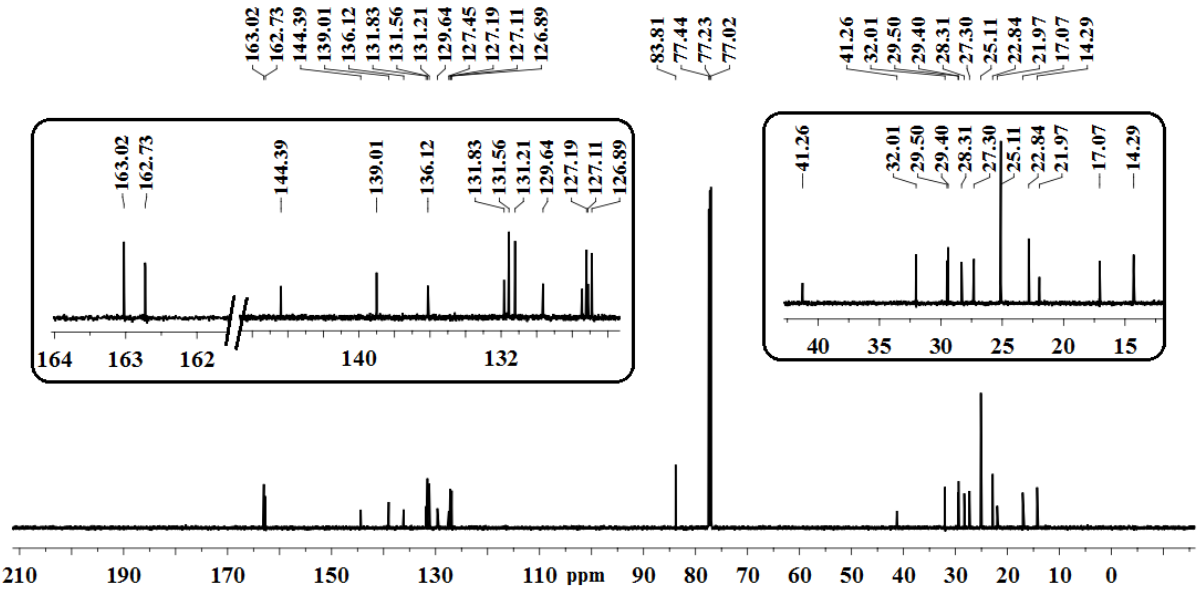

Fig. S35. ^{13}C-NMR spectrum of **12** in $CDCl_3$.

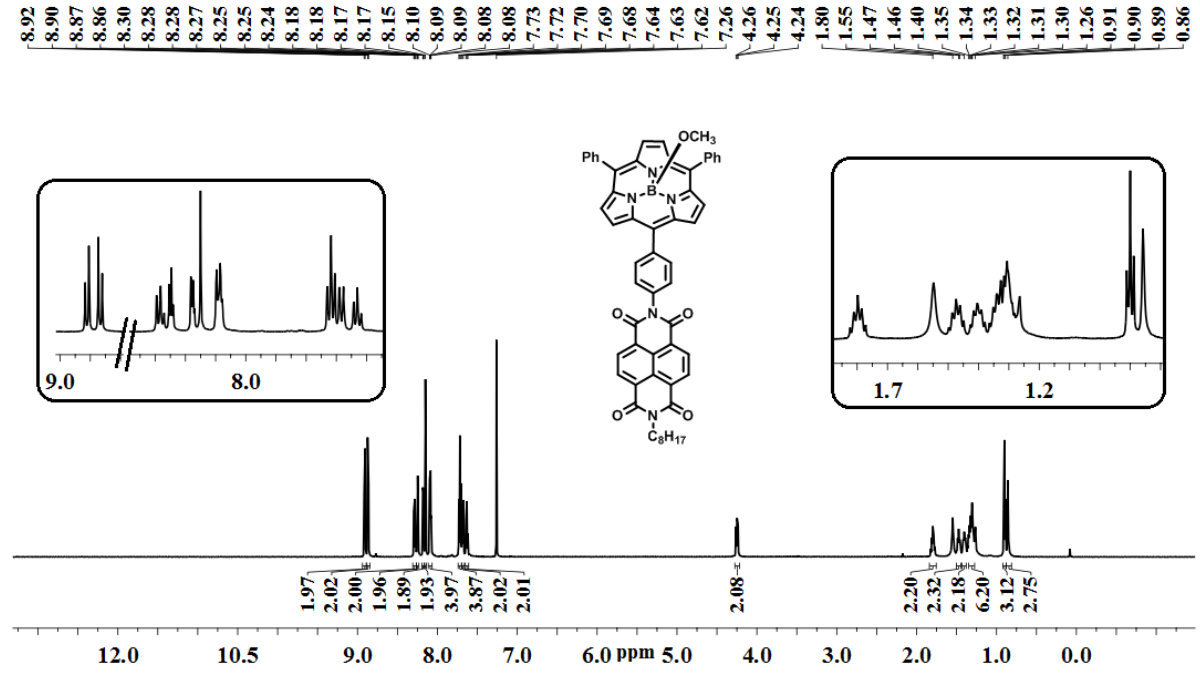

Fig. S36. ^{1}H-NMR spectrum of **SubP-NDI** in $CDCl_3$.

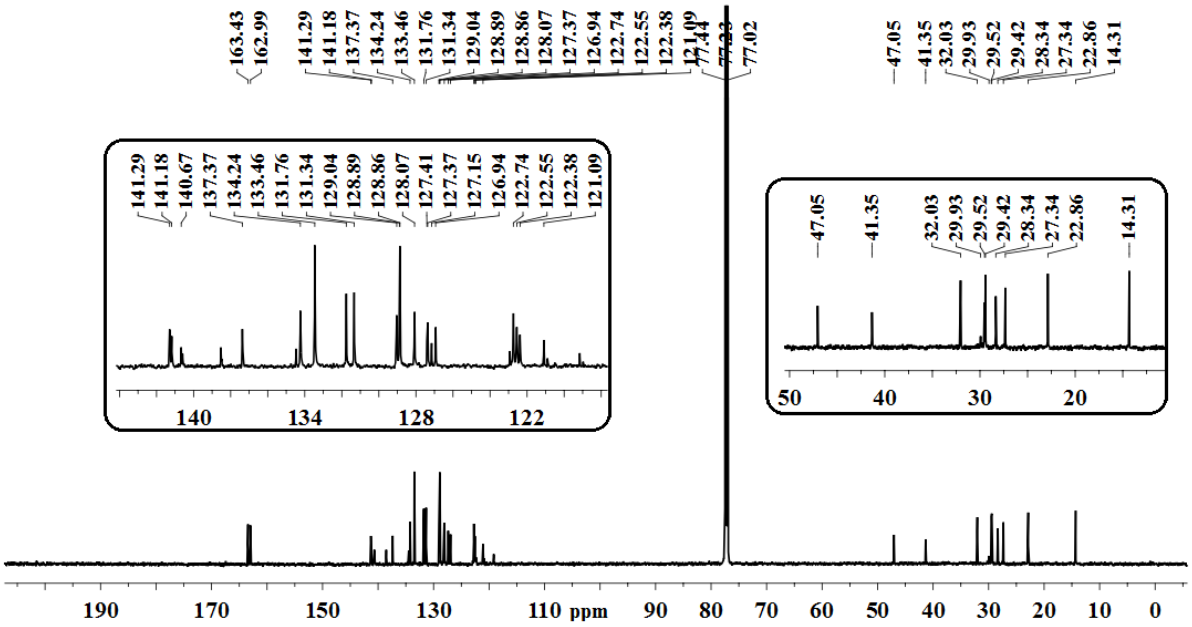

Fig. S37. ^{13}C-NMR spectrum of **SubP-NDI** in $CDCl_3$.

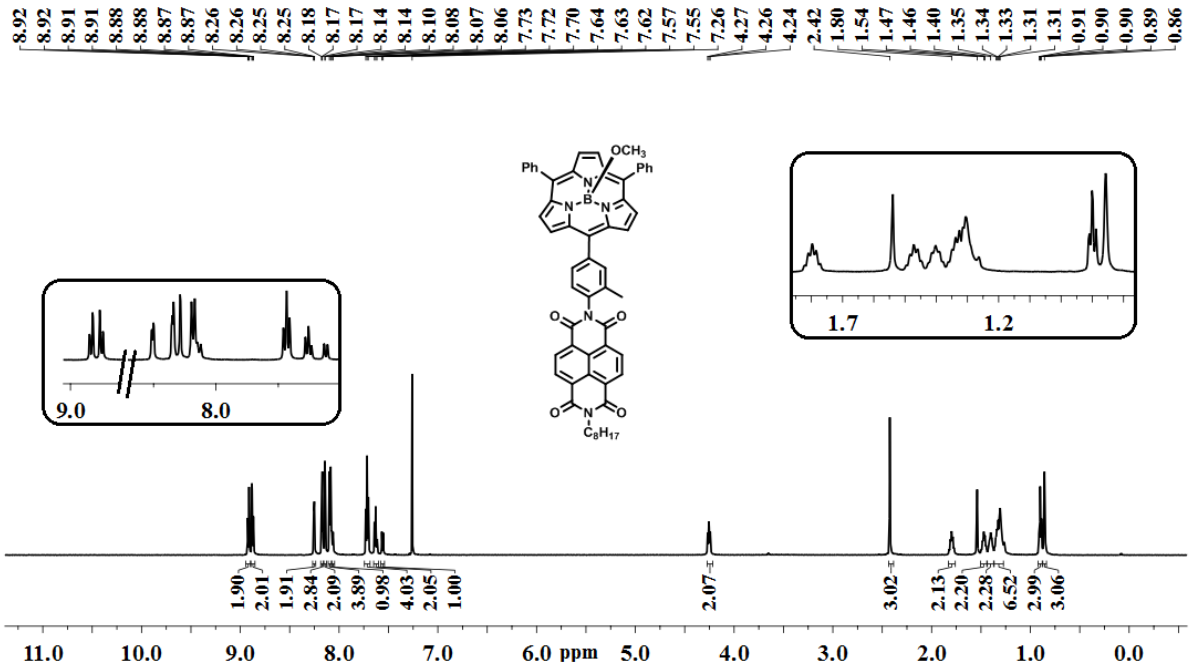

Fig. S38. ^{1}H-NMR spectrum of **SubP-2Me-NDI** in $CDCl_3$.

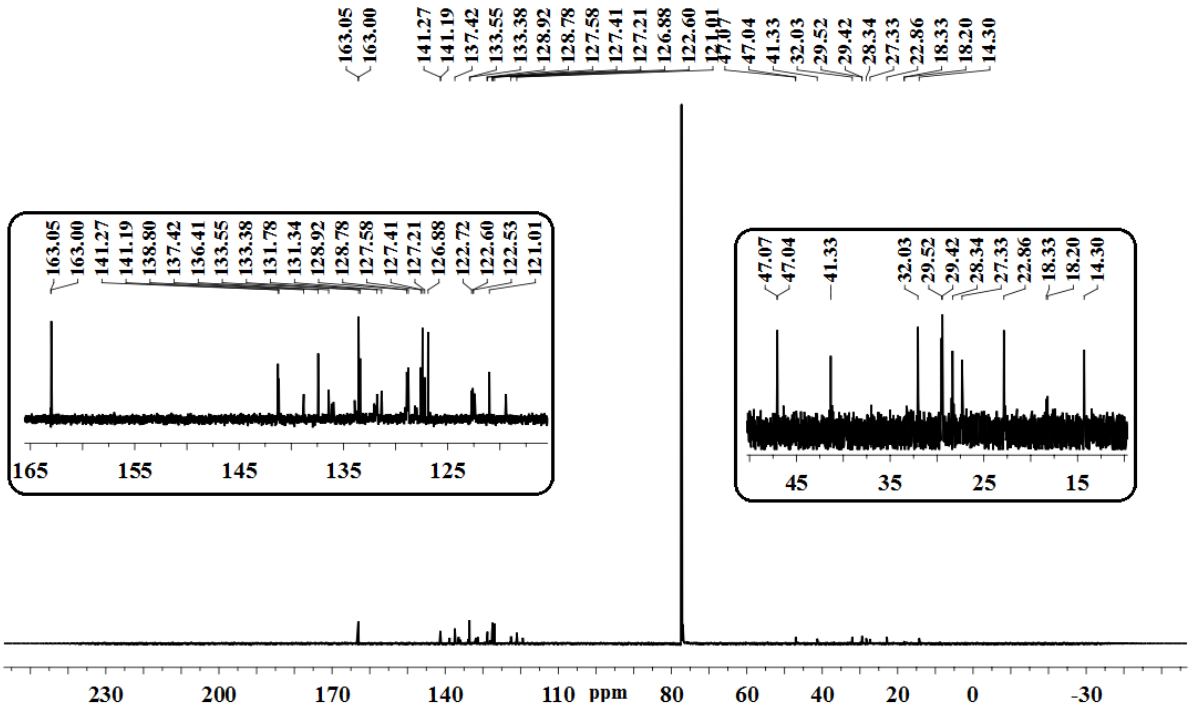

Fig. S39. ^{13}C-NMR spectrum of **SubP-2Me-NDI** in $CDCl_3$.

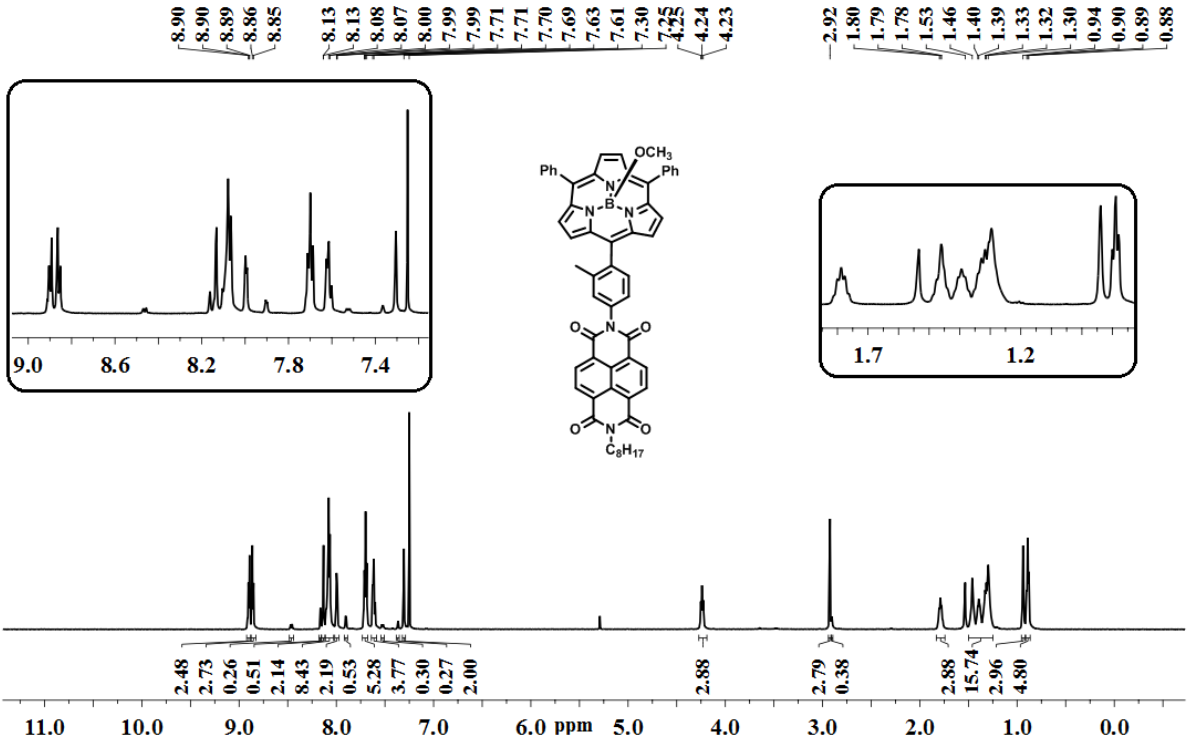

Fig. S40. ^{1}H-NMR spectrum of **SubP-3Me-NDI** in $CDCl_3$.

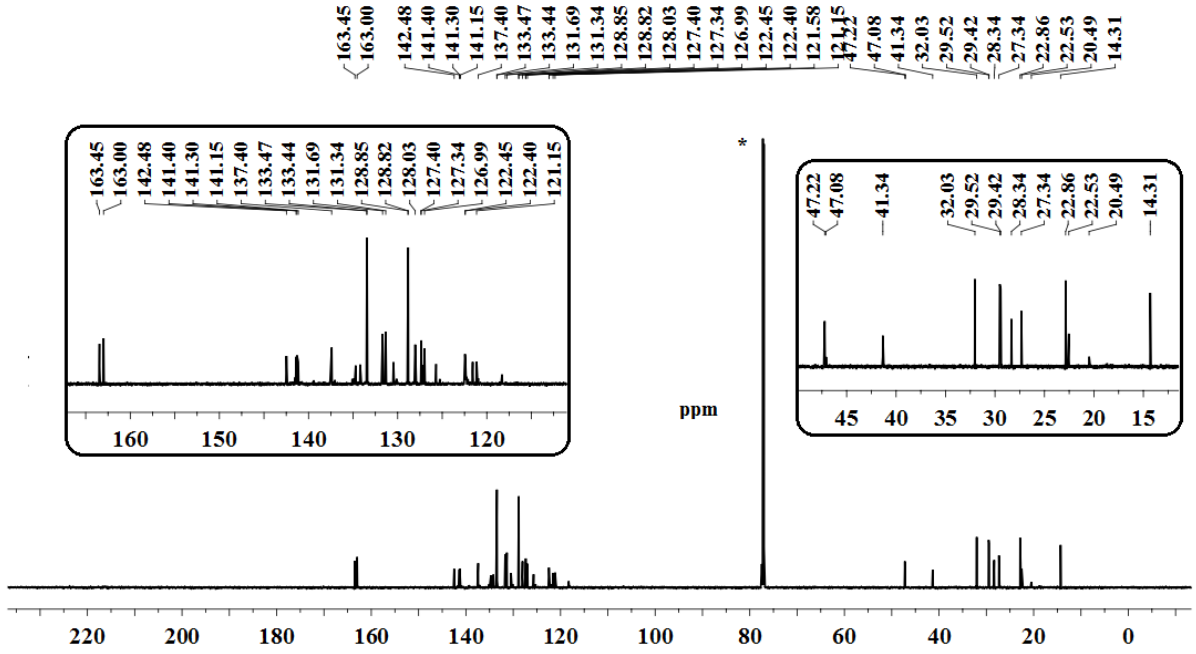

Fig. S41. ^{13}C-NMR spectrum of **SubP-3Me-NDI** in $CDCl_3$.

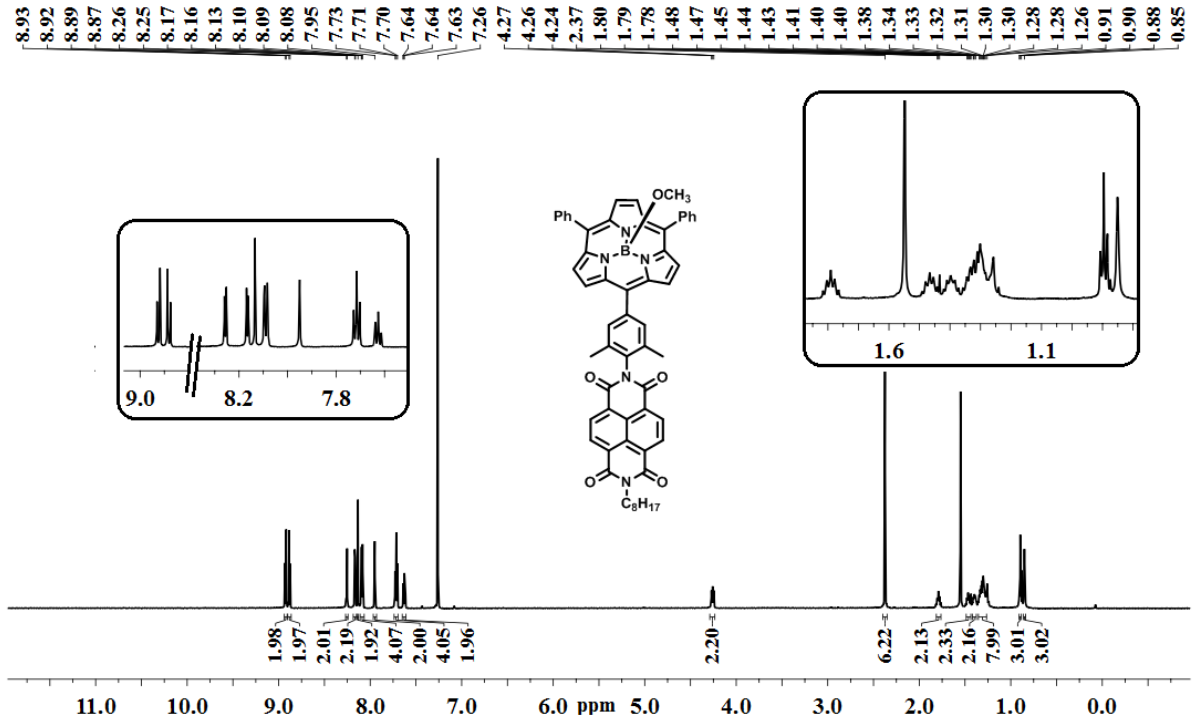

Fig. S42. ^{1}H-NMR spectrum of **SubP-2,6DiMe-NDI** in $CDCl_3$.

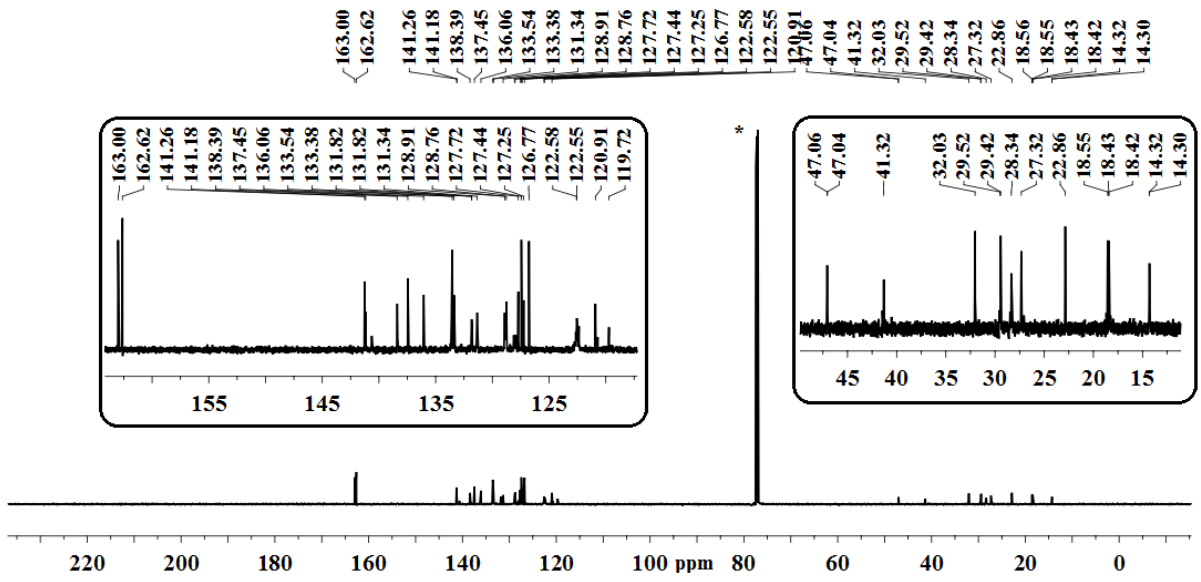

Fig. S43. ^{13}C-NMR spectrum of **SubP-2,6DiMe-NDI** in $CDCl_3$.

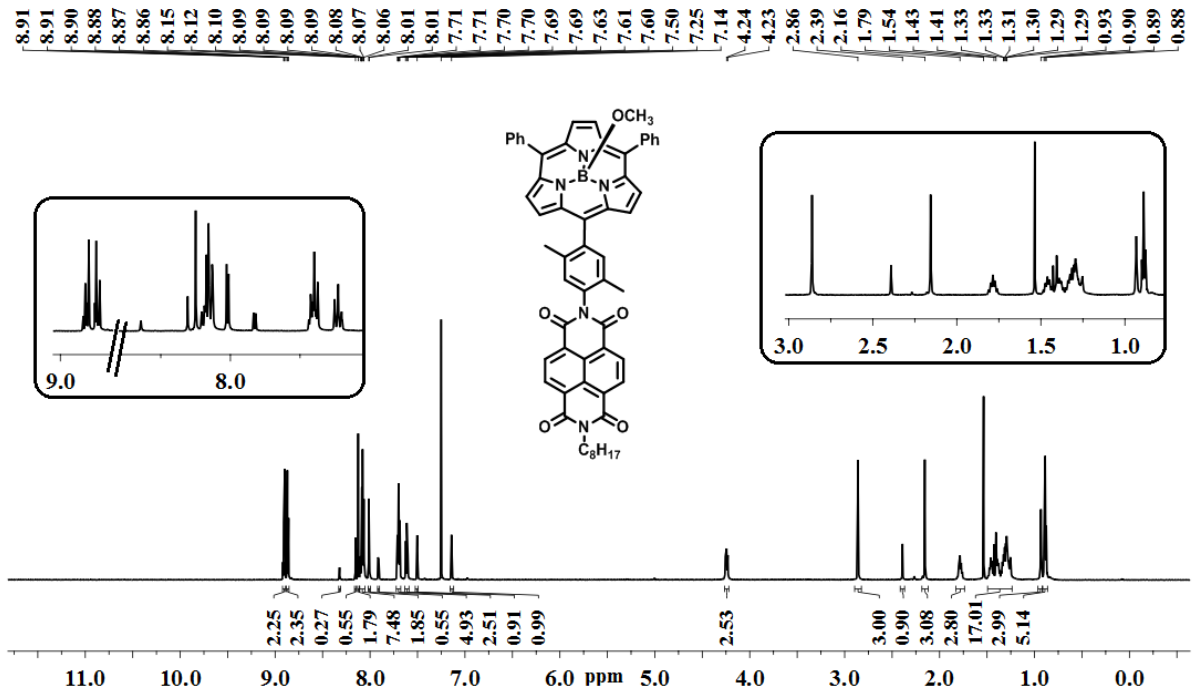

Fig. S44. ^{1}H-NMR spectrum of **SubP-3,6DiMe-NDI** in $CDCl_3$.

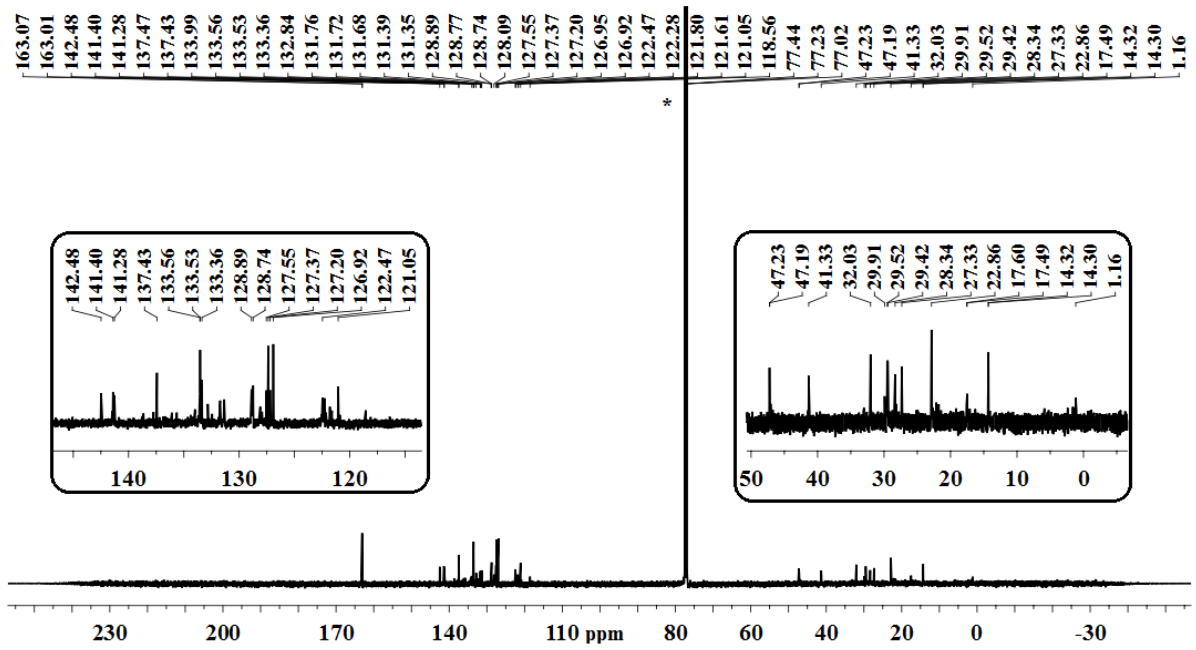

Fig. S45. ^{13}C-NMR spectrum of **SubP-3,6DiMe-NDI** in $CDCl_3$.

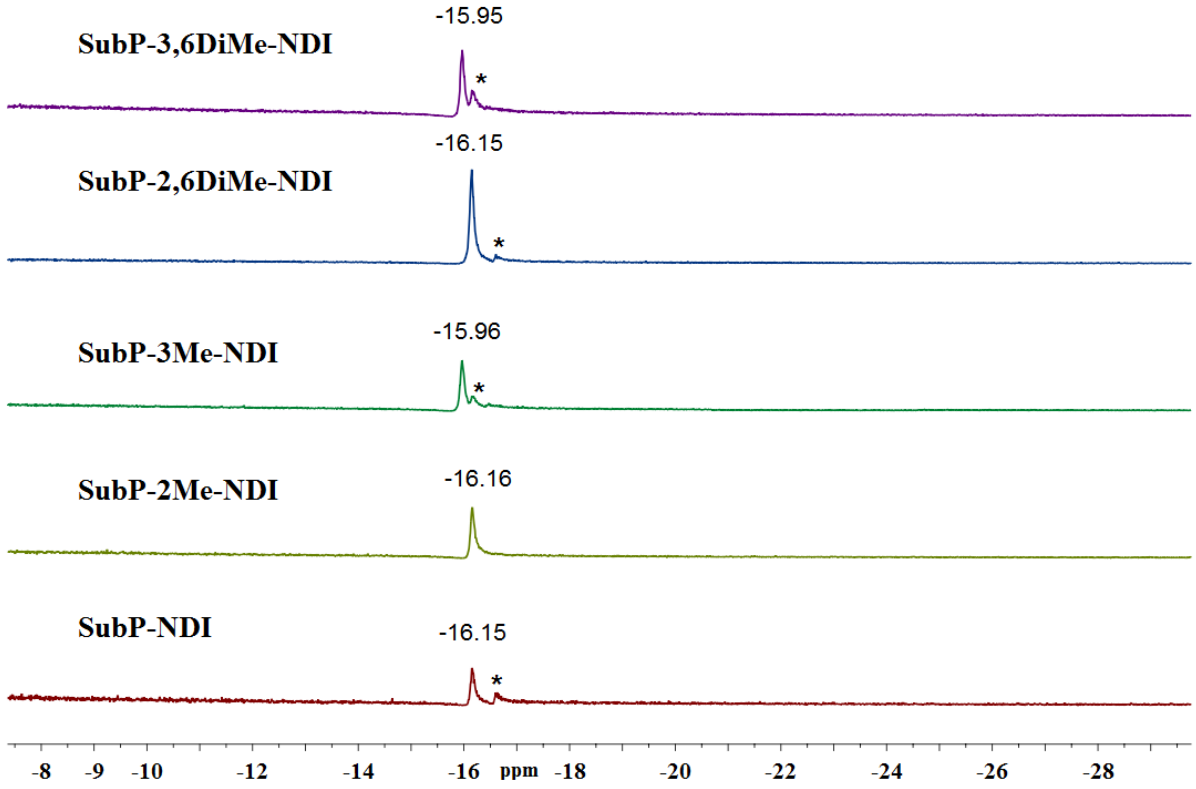

Fig. S46. ^{11}B-NMR spectrum of **SubP-XMe-NDI** dyads where X indicates the position of the methyl substituent(s) on the phenyl spacer (XMe = none; 2Me; 3Me; 2,6DiMe; 3,6DiMe). in $CDCl_3$. (* corresponding to the presence of B-OH species)

5. Single crystal X-ray structure and analysis of SubP-3Me-NDI:

Table S1: **Crystal data for SubP-3Me-NDI**:

Crystal parameters	**SubP-3Me-NDI**
Formula	$C_{57}H_{46}BN_5O_5$
M/g mol^{-1}	891.80
T/K	93
Crystal dimensions/mm^3	0.42 x 0.28 x 0.03
Crystal system	Monoclinic
Space group	$P2_1/n$
a/Å	10.4325(1)
b/Å	15.6205(2)
c/Å	54.3789(1)
α/°	90
β/°	93.124(1)
γ/°	90
V/Å^3	8848.5(2)
Z	8
ρ_{calcd}/mg m^{-3}	1.339
μ/mm^{-1}	0.685
F(000)	3744
Reflns. collected	61003
Indep.reflns. [R(int)]	16539 [0.0294]
Max/min transmission	1.000 and 0.918
Data/restraints /parameters	16539/ 2064 / 1306
GOF on F^2	1.052
Final R indices[$I > 2\sigma(I)$]	R_1 = 0.0982, wR_2 = 0.2880
R indices (all data)	R_1= 0.1064, wR_2 = 0.2959
Largest diff peak and hole [e Å^{-3}]	0.974 and -0.506
CCDC	1905324

6. Electronic absorption spectral analysis:

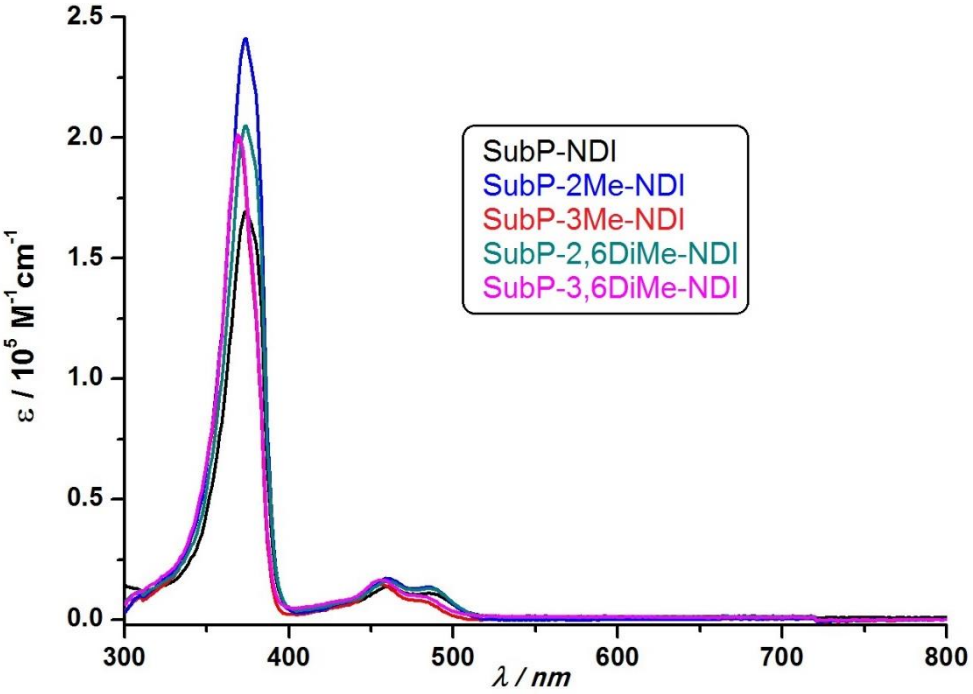

Fig. S47. Electronic absorption spectra of **Sub-NDI** derivatives (**14-18**) in DCM.

Table S2: **Electronic absorption parameters of 14-18 in DCM solution**

Compound	B band in (nm)	ε_0 values corresponding to B bands (in $M^{-1}cm^{-1}$)	Q band in (nm)	ε_0 values corresponding to Q bands (in $M^{-1}cm^{-1}$)	Concentration (in M^{-1})
SubP-NDI	374	$1.68x10^5$	460 486	$1.34x10^4$ $1.10x10^4$	$3.87x10^{-6}$
SubP-2Me-NDI	374	$2.41x10^5$	459 486	$1.72x10^4$ $1.35x10^4$	$2.78x10^{-6}$
SubP-3Me-NDI	369	$2.00x10^5$	457 480	$1.47x10^4$ $0.79x10^4$	$3.48x10^{-6}$
SubP-2,6DiMe-NDI	374	$2.05x10^5$	460 485	$1.59x10^4$ $1.29x10^4$	$3.64X10^{-6}$
SubP-3,6DiMe-NDI	369	$2.01x10^5$	457 480	$1.65x10^4$ $0.98x10^4$	$2.82x10^{-6}$
SubP	373	$1.66x10^5$	461 484		

7. Cyclic Voltammograms:

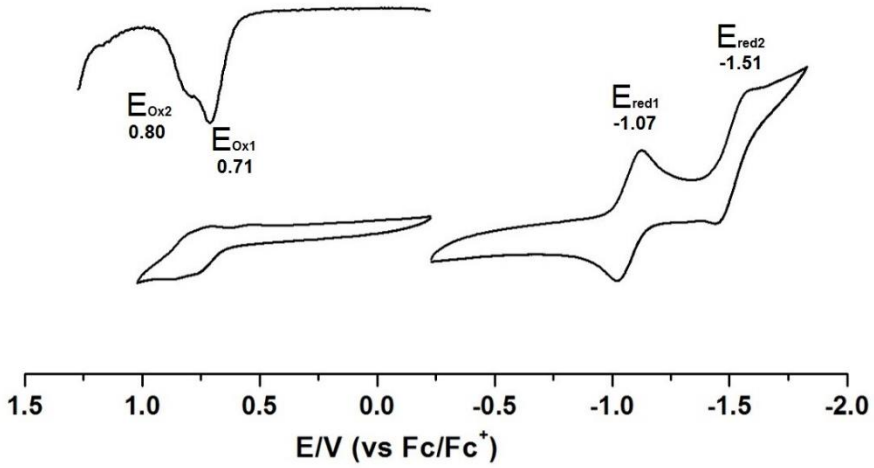

Fig. S48. Cyclic voltammogram of **SubP-NDI** in DCM (scan rate: 0.05 V/s, supporting electrolyte: 0.1 M $^{n}Bu_4NPF_6$, working electrode: Pt, counter electrode: Pt wire, reference electrode: Ag/0.01 M $AgClO_4$). Differential Pulse Voltammogram (left top) was used to confirm the oxidation potentials.

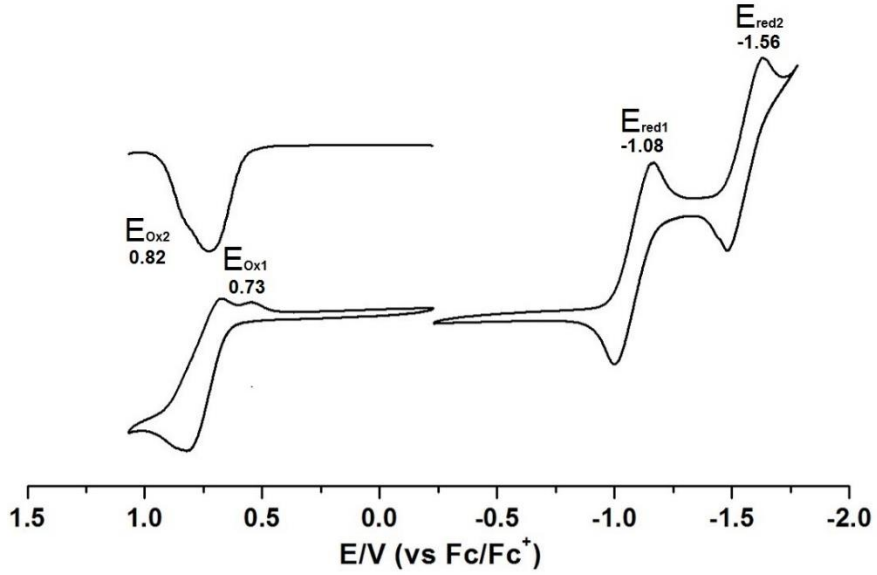

Fig. S49. Cyclic voltammogram of **SubP-2Me-NDI** in DCM (scan rate: 0.05 V/s, supporting electrolyte: 0.1 M $^{n}Bu_4NPF_6$, working electrode: Pt, counter electrode: Pt wire, reference electrode: Ag/0.01 M $AgClO_4$). Differential Pulse Voltammogram (left top) was used to confirm the oxidation potentials.

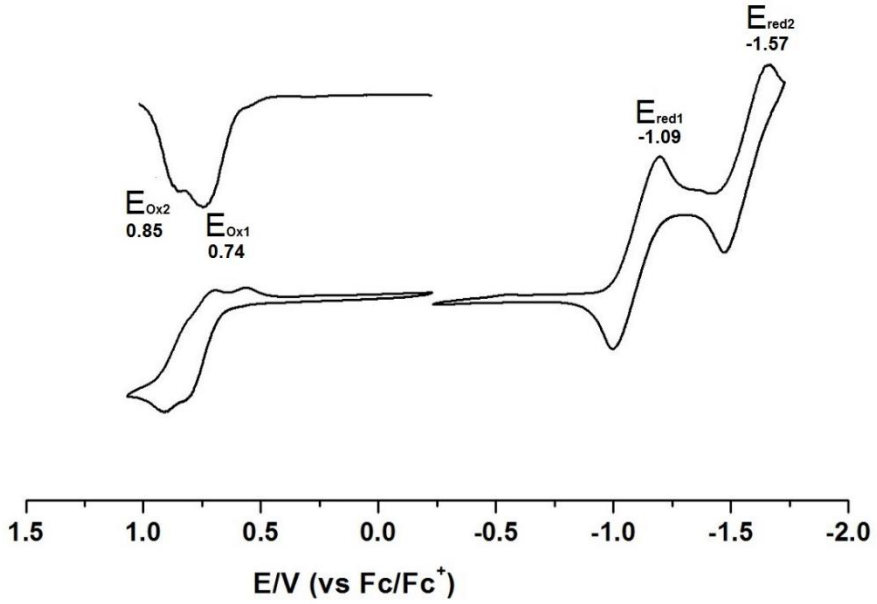

Fig. S50. Cyclic voltammogram of **SubP-3Me-NDI** in DCM (scan rate: 0.05 V/s, supporting electrolyte: 0.1 M $^{n}Bu_4NPF_6$, working electrode: Pt, counter electrode: Pt wire, reference electrode: Ag/0.01 M $AgClO_4$). Differential Pulse Voltammogram (left top) was used to confirm the oxidation potentials.

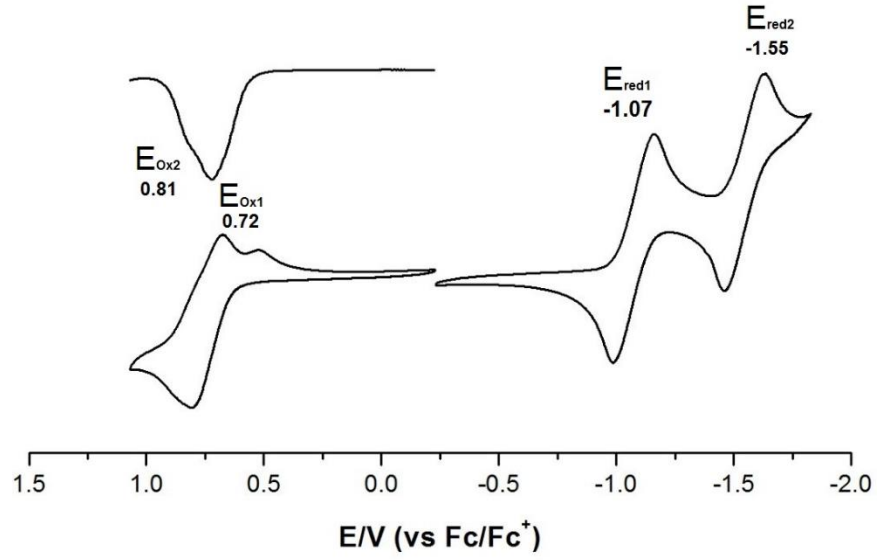

Fig. S51. Cyclic voltammogram of **SubP-2,6DiMe-NDI** in DCM (scan rate: 0.05 V/s, supporting electrolyte: 0.1 M $^{n}Bu_4NPF_6$, working electrode: Pt, counter electrode: Pt wire, reference electrode: Ag/0.01 M $AgClO_4$). Differential Pulse Voltammogram (left top) was used to confirm the oxidation potentials.

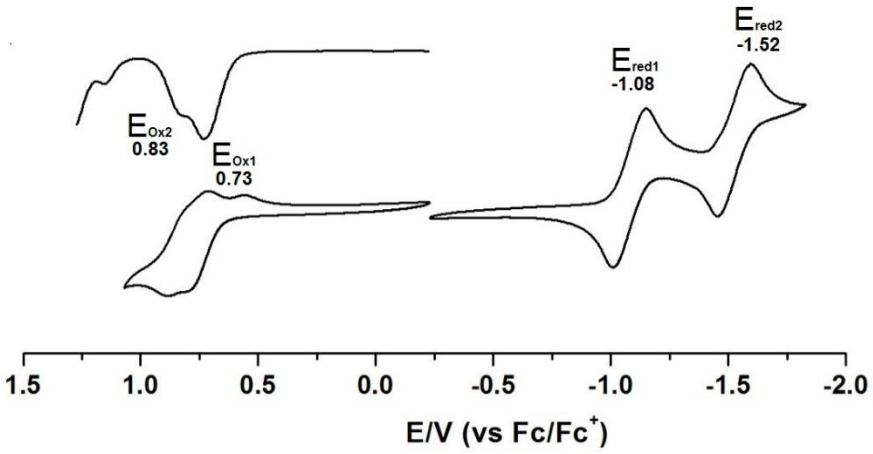

Fig. S52. Cyclic voltammogram of **SubP-3,6DiMe-NDI** in DCM (scan rate: 0.05 V/s, supporting electrolyte: 0.1 M $^{n}Bu_4NPF_6$, working electrode: Pt, counter electrode: Pt wire, reference electrode: Ag/0.01 M $AgClO_4$). Differential Pulse Voltammogram (left top) was used to confirm the oxidation potentials.

Table S3: **Redox potentials of SubP-XMe-NDI derivatives:**

Compd.	**E_{OX1}/V[a]**	**E_{OX2}/V[a]**	**$E^{1/2}_{RED1}$/V**	***$E^{1/2}_{RED2}$/V***
SubP-NDI	**0.71**	**0.80**	**-1.07**	**-1.51**
SubP-2Me-NDI	**0.73**	**0.82**	**-1.08**	**-1.56**
SubP-3Me-NDI	**0.74**	**0.85**	**-1.09**	**-1.57**
SubP-2,6DiMe-NDI	**0.72**	**0.81**	**-1.07**	**-1.55**
SubP-3,6DiMe-NDI	**0.73**	**0.83**	**-1.08**	**-1.52**

8. Quantum mechanical calculations

Density functional calculations (DFT) were performed using the Gaussian 16 and 9 software packages[S9] using the hybrid functional B3LYP and the basis set 6-311G**. Full optimization of the ground-state structures and dihedral scans were performed using the 6-31G** basis set. Excited state energies (20 lowest) were calculated using the time-dependent formulism (TDDFT) and vertical excitation energies for the lowest electronic transitions are given in Table S4 and compared to experiments. There is a consistent shift of 0.3-0.4 eV in all the calculated values compared to experiments which is not surprising since stabilizing solvent effects are neglected in the calculation. Fig. S53 shows the optimized geometry of the SubP-NDI compound and Fig. S54 shows the frontiers orbitals of the SubP-3Me-NDI compound. The potential energy surfaces displayed in Fig. 7 were calculated by scanning the dihedral angles α or β between -90° and 90° in steps of 10° while fully optimizing the remaining internal coordinates. To avoid hysteresis for the highest potential energy barriers, re-optimizations approaching the summit from both sides were performed.

Table S4. State energies for SubP in toluene as estimated from spectroscopic and electrochemical[S7-S8] measurements. Experimental results are compared to TDDFT calculated values.

	S1 / eV	S2 / eV	T1 / eV	CSS[a] / eV
Experiments	2.5	3.3	1.8	2.1
Theory[b]	2.9 (degenerate)	3.7 (degenerate)	2.1 (degenerate)	----

[a] Energy of the charge separated state is based on the oxidation and reduction potentials in DCM and corrected with the Weller equation (Eq. 1) to toluene conditions. Singlets calculated to be 0.4 eV higher in energy compared to experiments. If the calculated triplet energy is shifted by the same amount, agreement with the observed phosphorescence becomes excellent. [b]TDDFT/B3LYP/6-311G** calculations on DFT/B3LYP/6-31G** optimized structures.

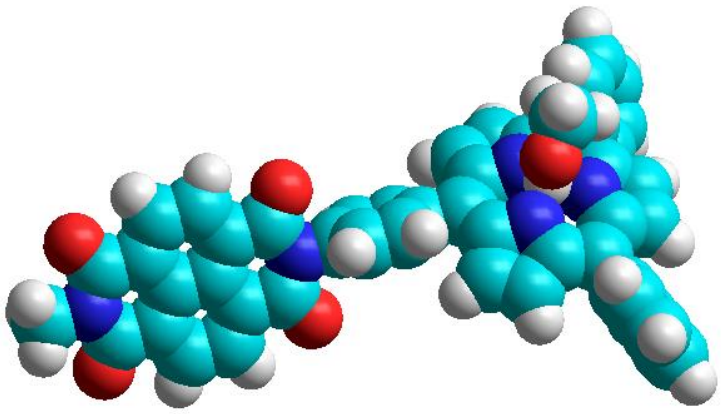

Fig. S53. Optimized geometry of the SubP-NDI, donor-acceptor compound. The donor-acceptor distance measured from the central boron to the middle of the NDI acceptor is 12.2 Å.

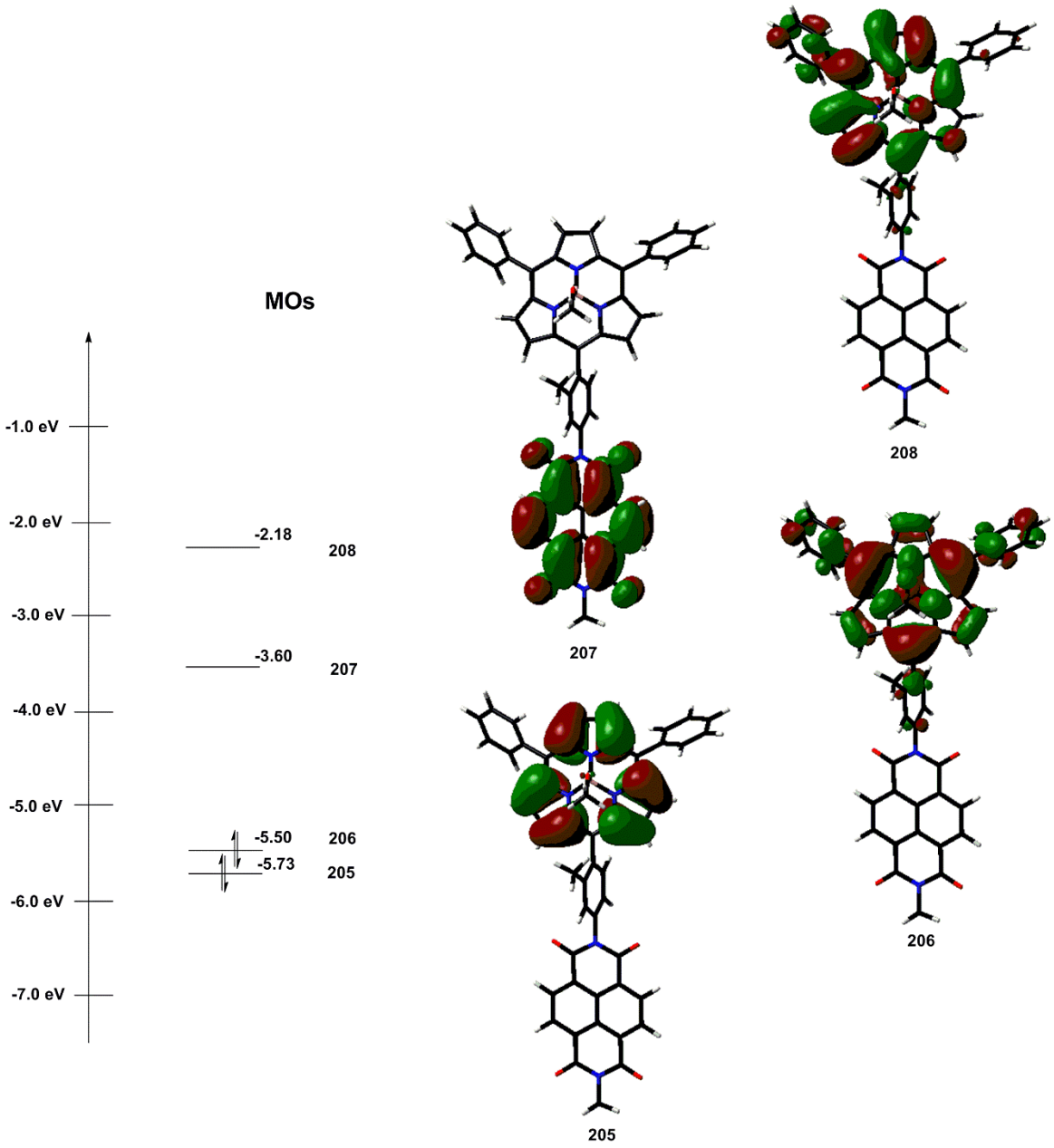

Fig. S54. Frontier orbitals for **SubP-3Me-NDI**.

9. Fluorescence Lifetime Measurement

Fluorescence lifetime of the SubP donor was determined with time-correlated single photon counting upon 483 nm excitation.

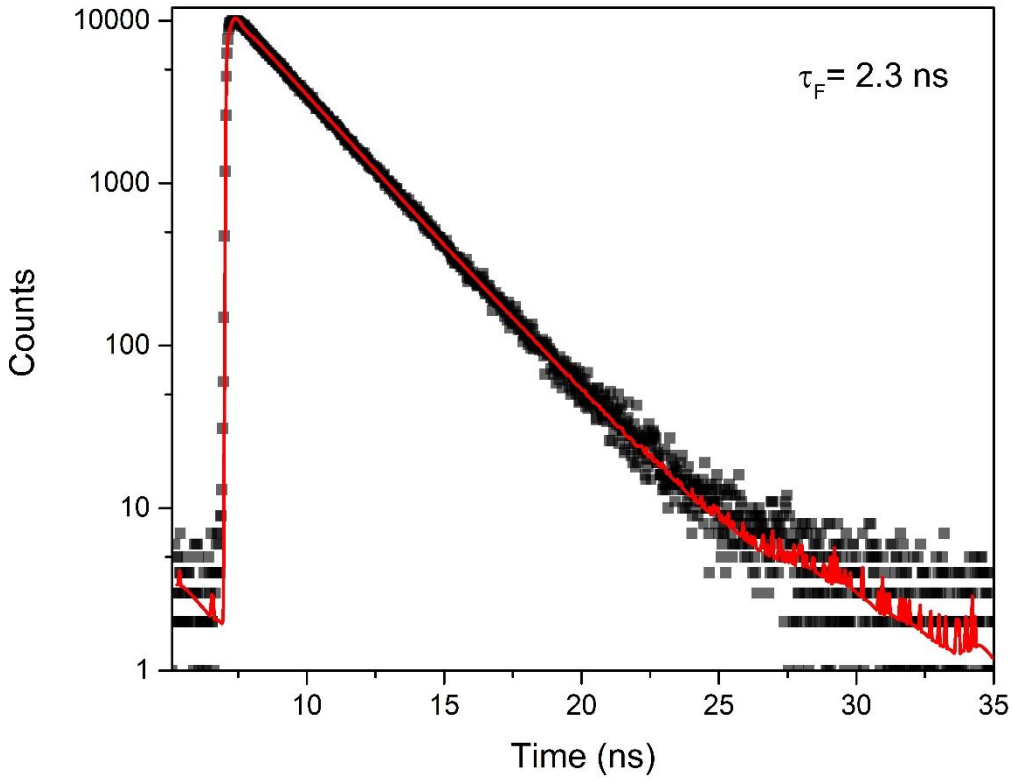

Fig. S55. Fluorescence decay of SubP donor in toluene upon 483 nm excitation

10. Transient Absorption Measurements

Fig. S5-S59 show that transient absorption signal of the Sub-X-NDI dyads have broad excited state absorption (ESA) signal over white light wavelength region. Characteristic radical anion ESA signal of the NDI (NDI$^{\cdot-}$) is seen around 475 nm and radical cation ESA signals of SubP (SubP$^{\cdot+}$) are located 540 nm and 700 nm which are well know from literature [S5, S6]. It is clearly seen that these radical cation and anion signals rising with time delay that indicates charge separation formation while exciting singlet state of subporphyrin. The transient characteristics are similar for all Sub-X-NDI compounds, but the charge separation rate is different since it depends on electronic coupling of donor (SubP) and acceptor (NDI) units. Further, transient absorption spectra for SubP has only singlet and triplet ESA signals without any radical characteristics (Fig. S60). In Fig. S61, it is shown that the charge separation rate is different for the the different dyads. Forming and decaying of the CSS slows down with increasing dihedral angle between donor and acceptor.

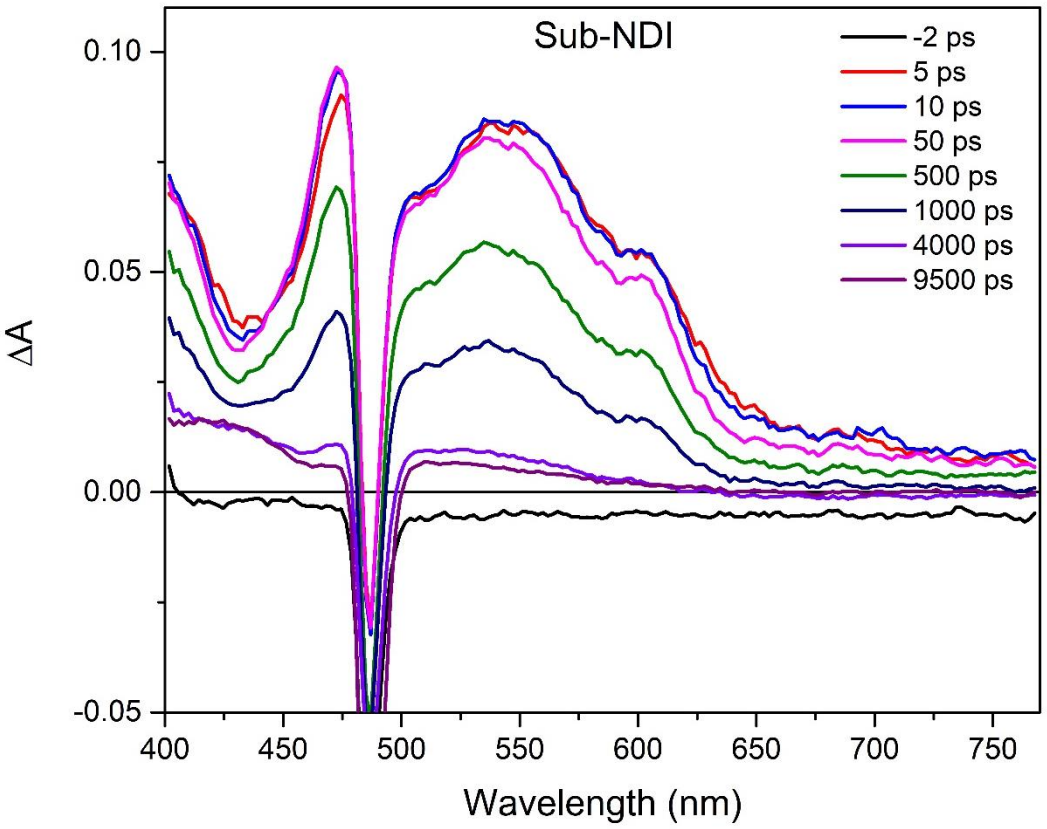

Fig. S56. Transient spectra of SubP-NDI in toluene with 490 nm excitation

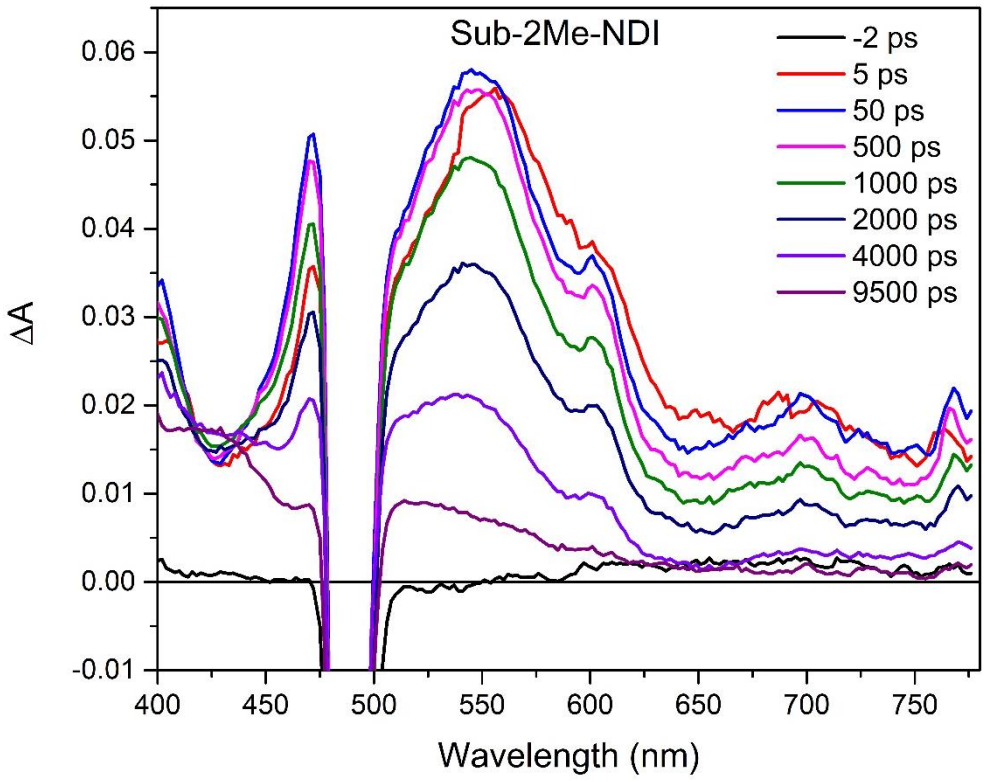

Fig. S57. Transient spectra of SubP-2Me-NDI in toluene with 490 nm excitation

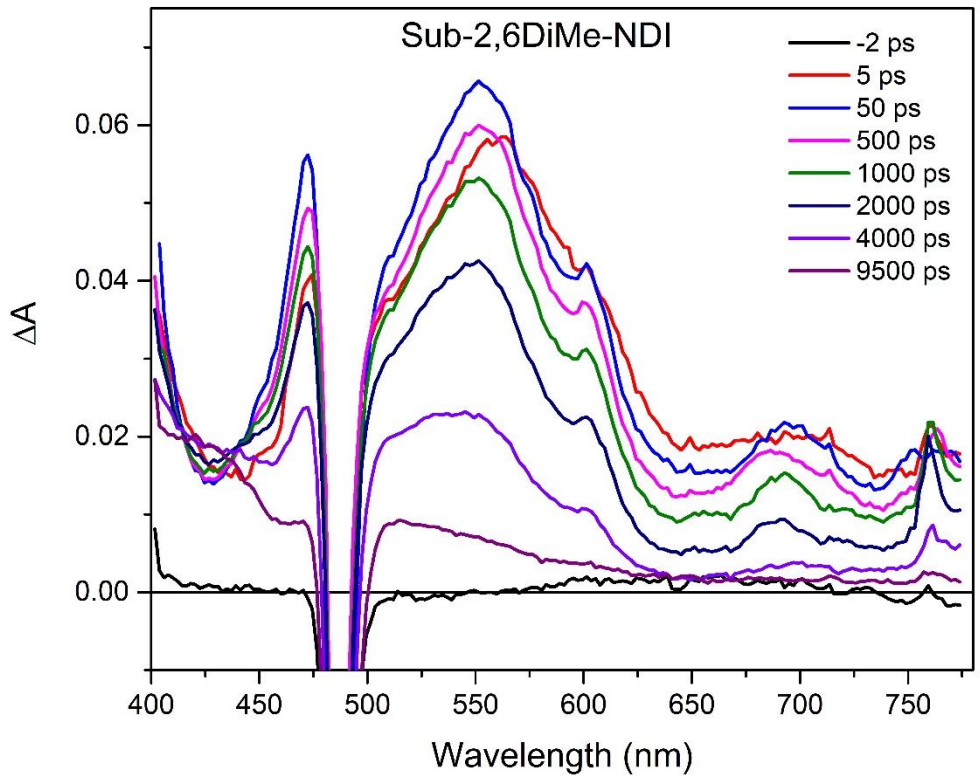

Fig. S58. Transient spectra of SubP-2,6DiMe-NDI in toluene with 490 nm excitation

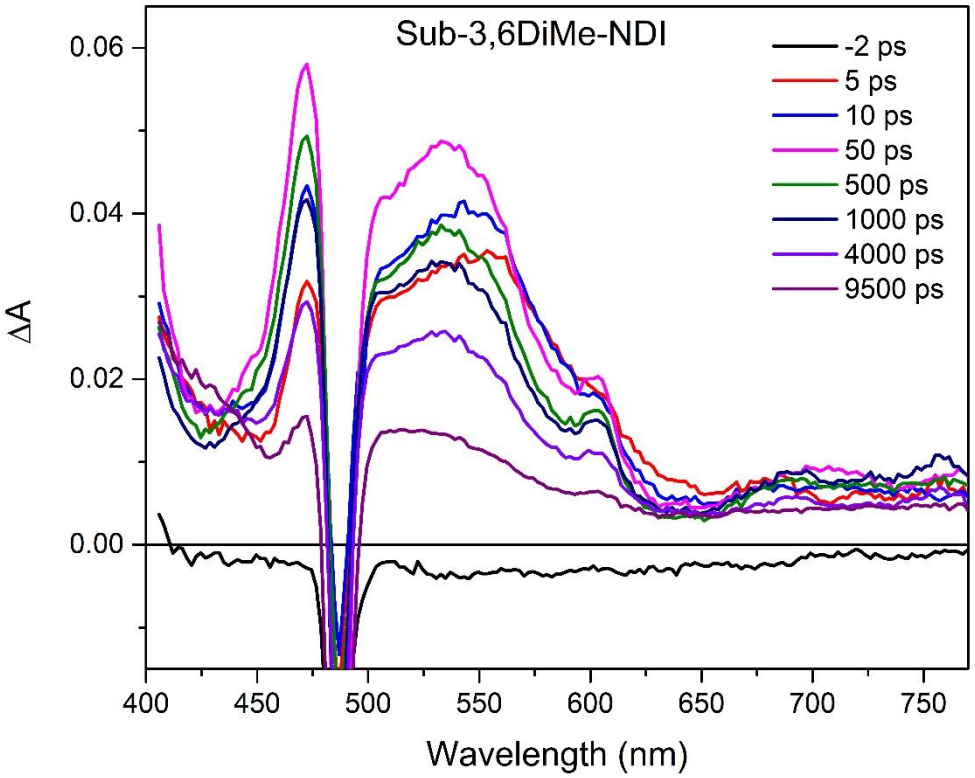

Fig. S59. Transient spectra of SubP-3,6DiMe-NDI in toluene with 490 nm excitation

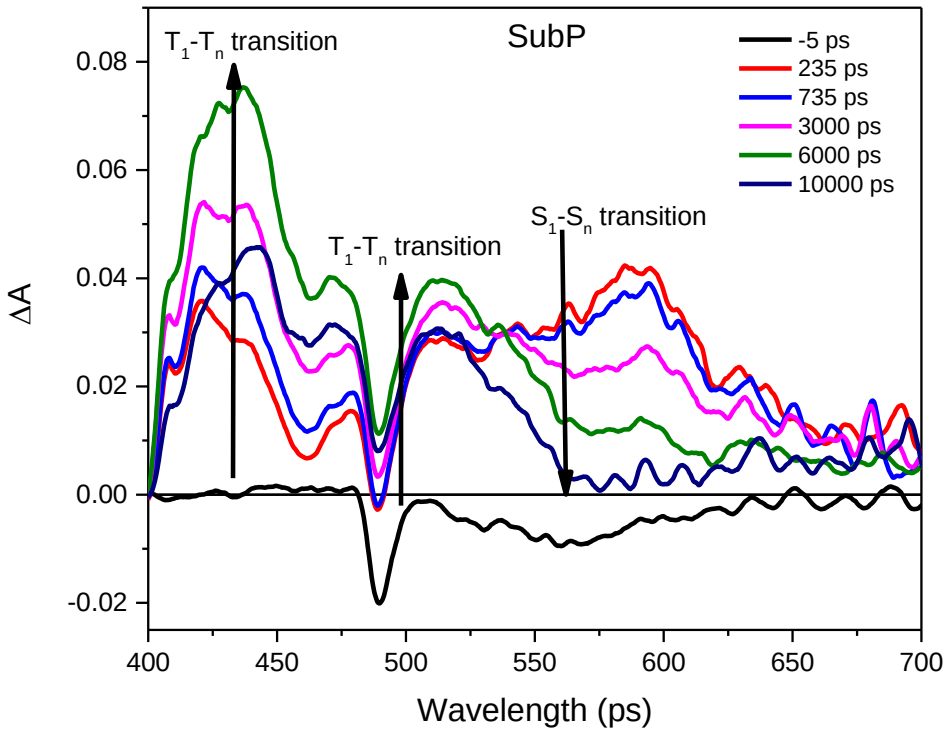

Fig. S60. Transient spectra of SubP in toluene with 490 nm excitation

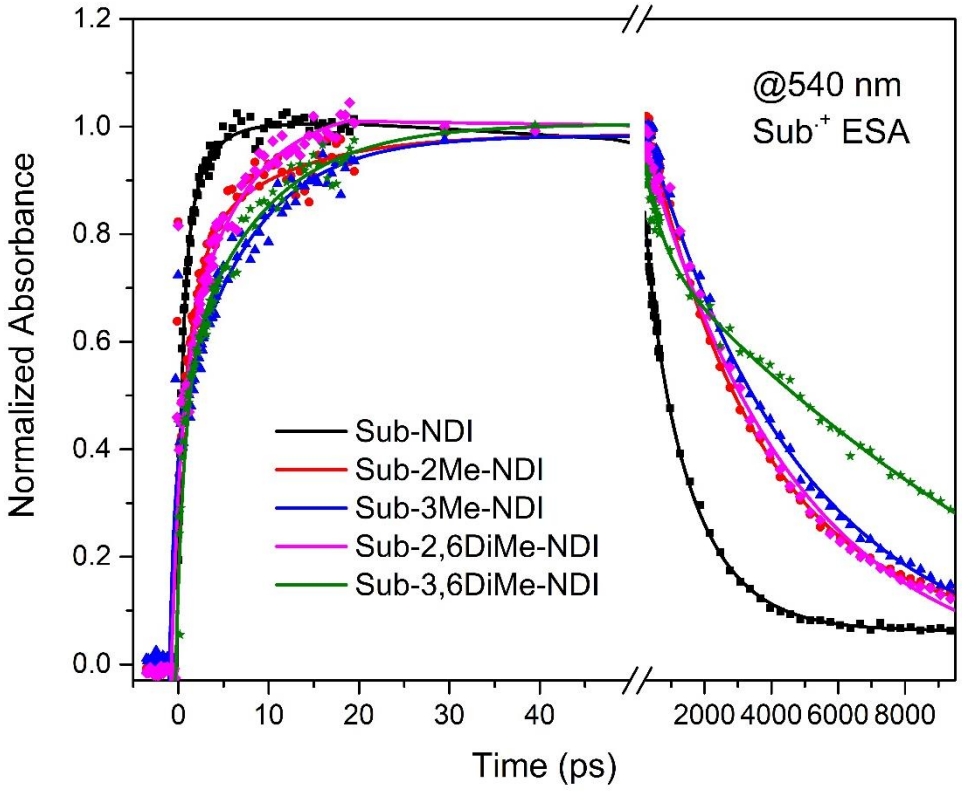

Fig. S61. Radical cation signal (SubP $^{\cdot+}$) grow and decay kinetics at 540 nm for all dyads (overlap with singlet ESA)

11. Temperature Dependent Emission Measurements

Emission intensity of the Sub-XMe-NDI compounds increase between 15 to 40 times upon lowering the temperature and phosphorescence is observed for all dyads at 85 K (Fig. S62-S66). For the SubP (donor alone), temperature dependency of the fluorescence is not pronounced, and very weak relative phosphorescence is also seen at 85 K (Fig. S67).

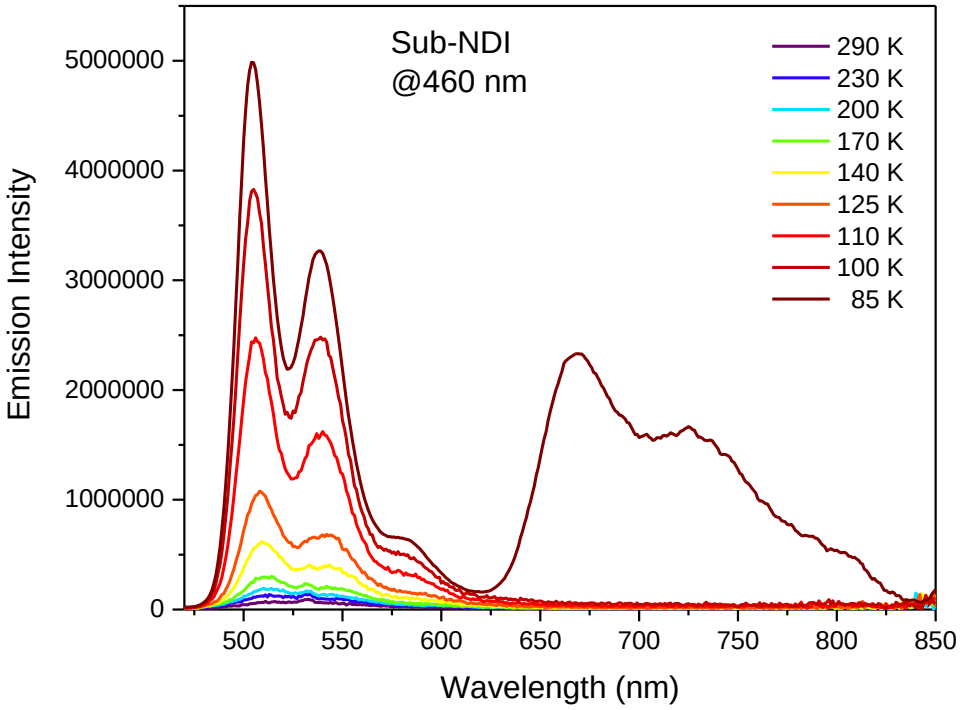

Fig. S62. Temperature dependent emission spectra of SubP-NDI (λ_{exc}=460 nm)

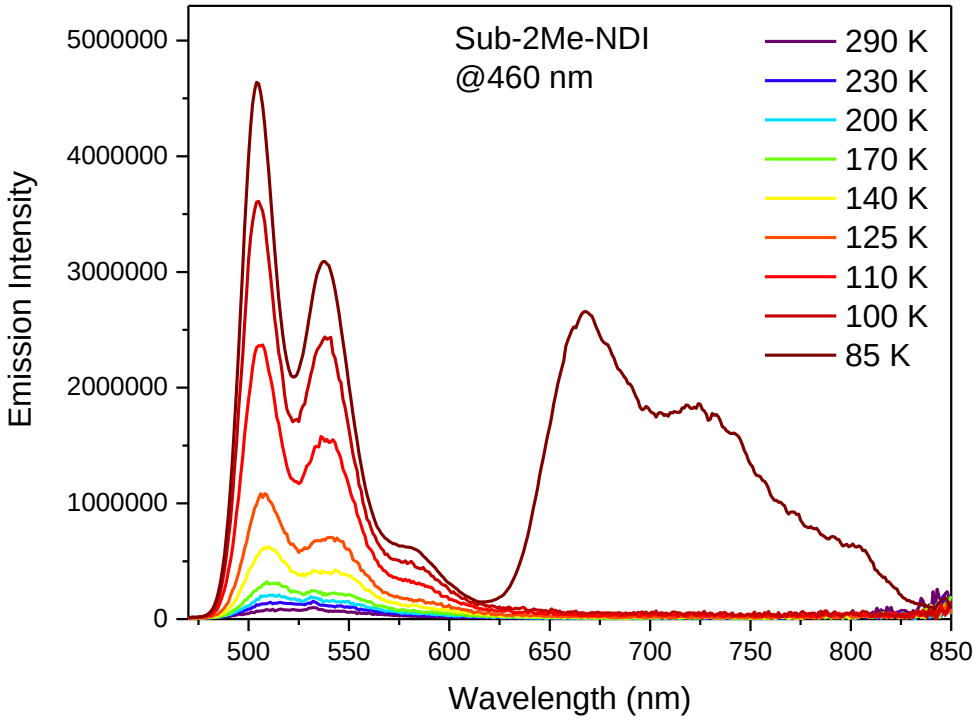

Fig. S63. Temperature dependent emission spectra of SubP-2Me-NDI (λ_{exc}=460 nm)

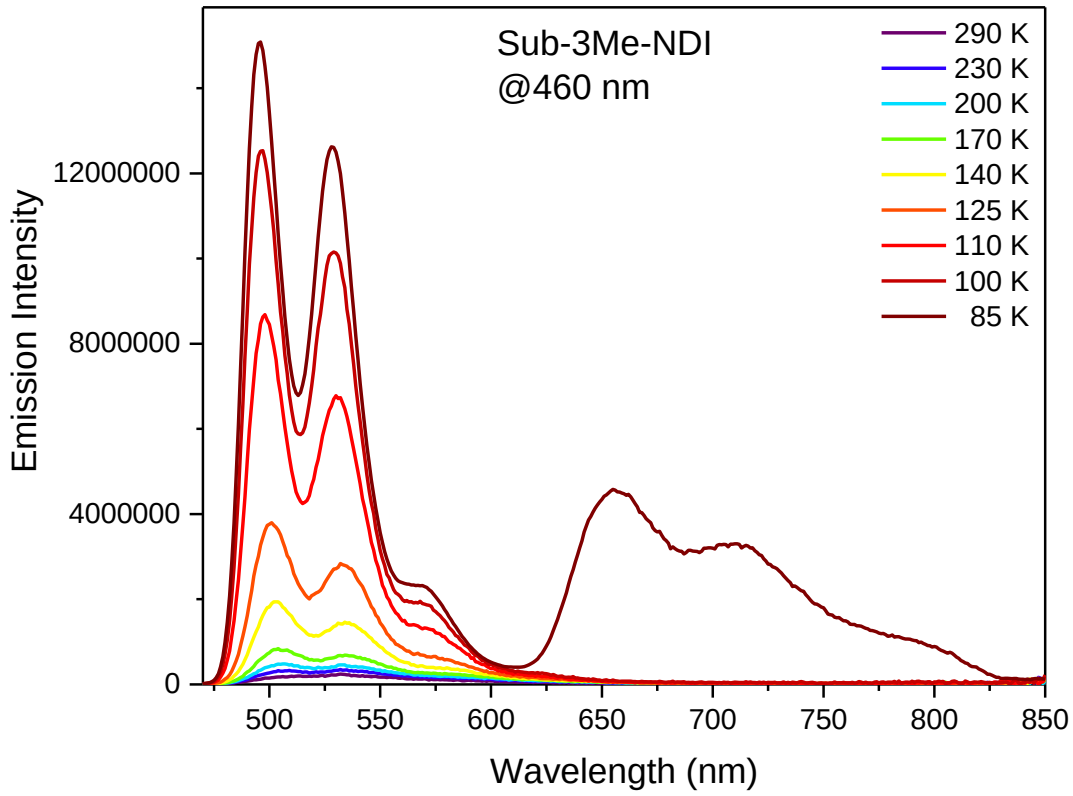

Fig. S64. Temperature dependent emission spectra of SubP-3Me-NDI (λ_{exc}=460 nm)

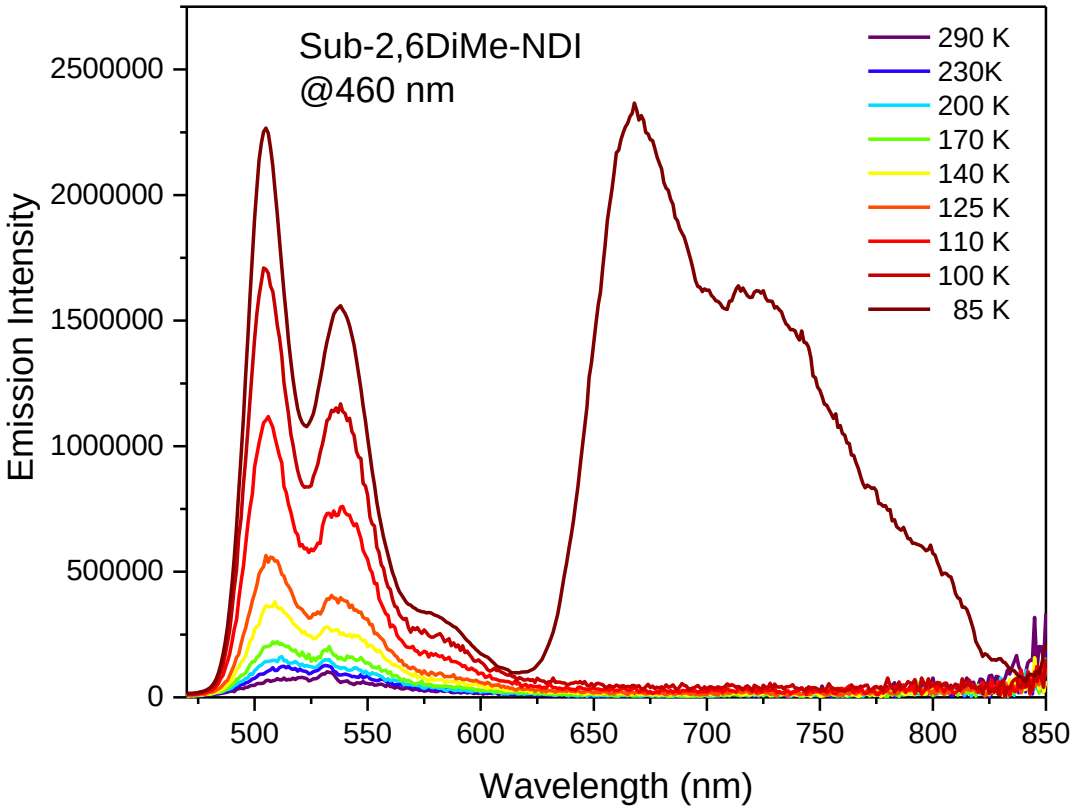

Fig. S65. Temperature dependent emission spectra of SubP-2,6DiMe-NDI (λ_{exc}=460 nm)

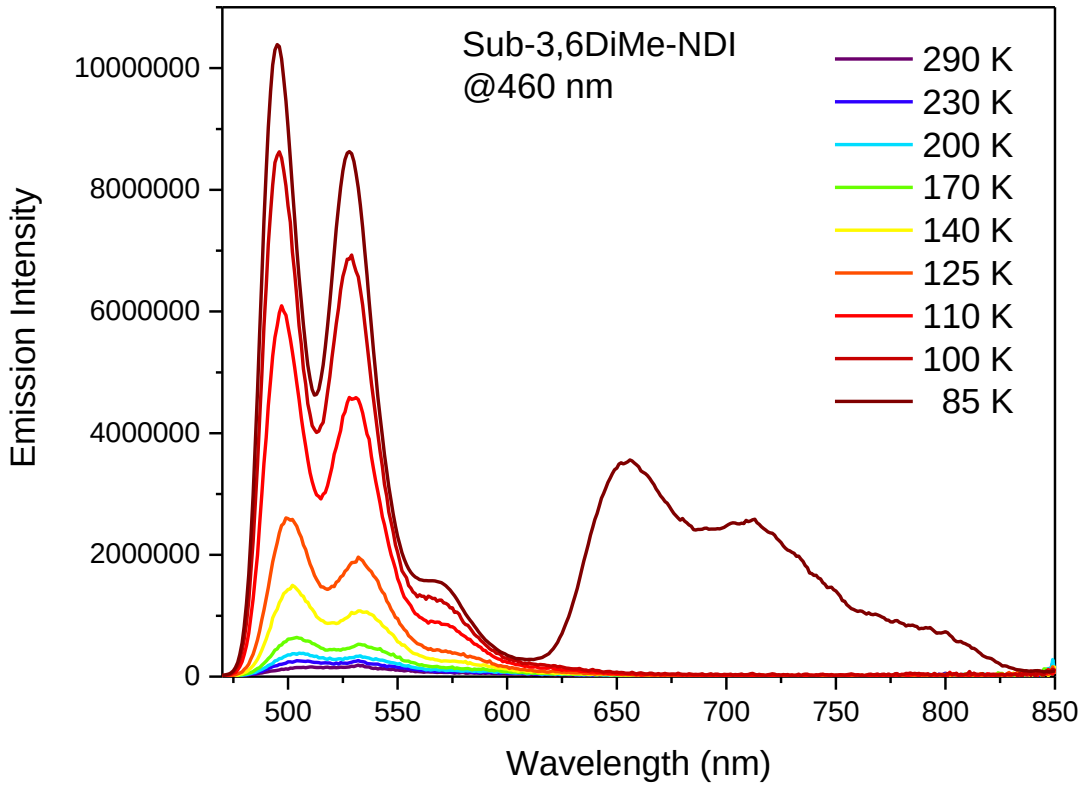

Fig. S66. Temperature dependent emission spectra of SubP-3,6DiMe-NDI (λ_{exc}=460 nm)

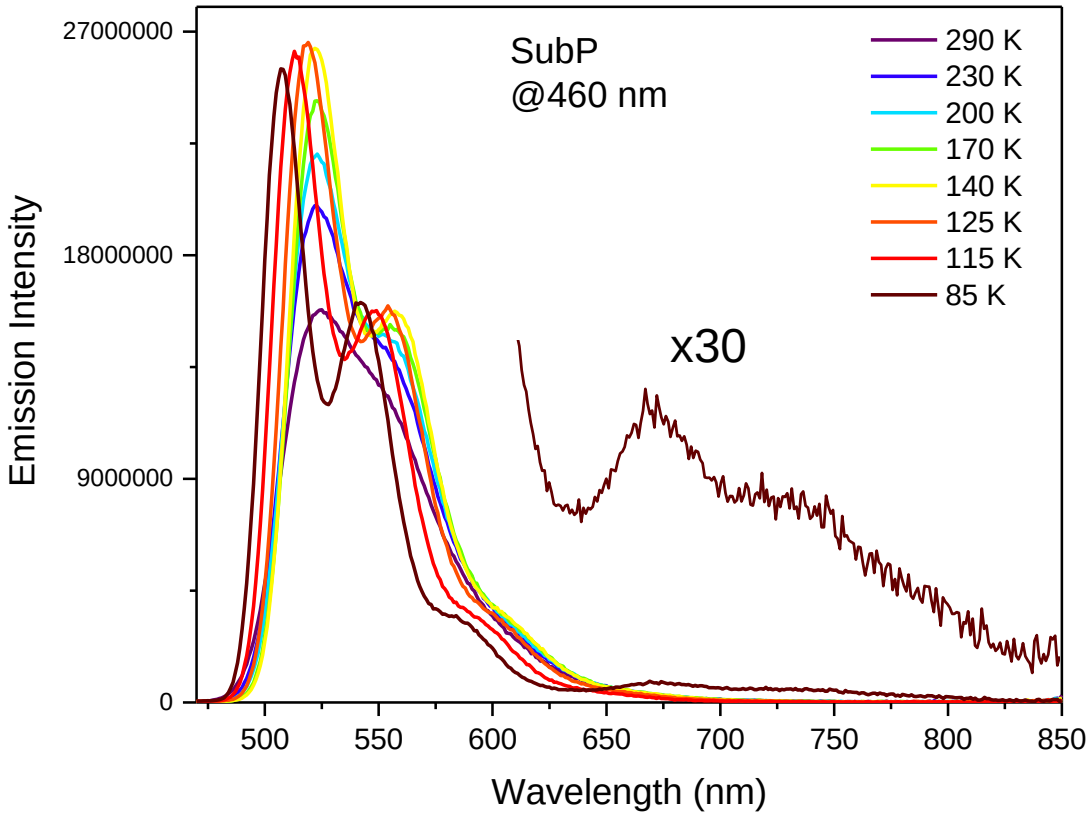

Fig. S67. Temperature dependent emission spectra of SubP (donor only) (λ_{exc} = 460 nm)

Table S5. Fluorescence and phosphorescence quantum yields as function of temperature. The quantum yields at room temperature were estimated from the know quantum yield for SubP and the relative lifetimes of the singlet excited state of SubP and the five donor-acceptor compounds. The relative changes in intensity, compensated for changes in solvent density and refractive index, were used to determine emission quantum yields

Φ_F (*10^{-3})	290 K	230 K	200 K	170 K	140 K	125 K	110 K	100 K	85 K	Phos. at 85 K
SubP-NDI	0.3	0.6	0.8	1.2	2.3	3.9	8.7	13.2	17.4	17.8
SubP-2Me-NDI	0.3	0.5	0.6	1.0	1.8	3.0	6.3	9.5	12.1	14.9
SubP-3Me-NDI	0.7	1.2	1.7	2.6	5.3	9.8	21.5	31	37.8	24.1
SubP-2,6DiMe-NDI	0.4	0.5	0.6	0.8	1.4	2.0	3.8	5.8	7.71	16.6
SubP-3,6DiMe-NDI	0.9	1.4	2.0	3.2	6.8	11.7	26.1	37.3	45.8	33.1
SubP	160.0[a]	200.4	218.5	235.1	252.6	253.5	237.9	235.7	229.9	15.2

[a] from ref S4

Table S6. Quantum yield for the charge separation as a function of temperature

	290 K	230 K	200 K	170 K	140 K	125 K	110 K	100 K	85 K
SubP-NDI	1.00	1.00	1.00	0.99	0.99	0.98	0.96	0.94	0.92
SubP-2Me-NDI	1.00	1.00	1.00	1.00	0.99	0.99	0.97	0.96	0.95
SubP-3Me-NDI	1.00	0.99	0.99	0.99	0.98	0.96	0.91	0.87	0.84
SubP-2,6DiMe-NDI	1.00	1.00	1.00	1.00	1.00	1.00	0.98	0.98	0.97
SubP-3,6DiMe-NDI	1.00	0.99	0.99	0.99	0.97	0.95	0.89	0.84	0.80

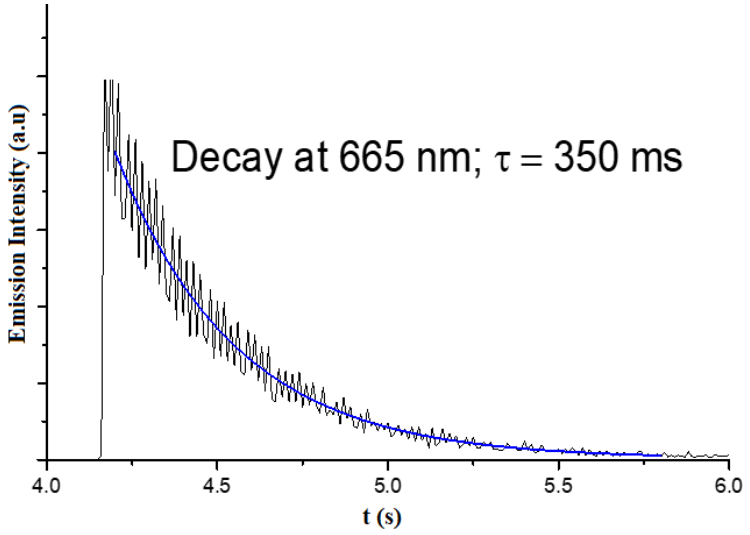

Fig. S68. Phosphorescence decay of SubP-NDI dyad at 85 K.

12. Phosphorescence Quantum Yield Calculation

For the derivation of equation 7 we combine measurements on the dyads and the SubP donor. All rate constants are defined in connection to Fig. 7 and below.

Formation of triplet in SubP.

The fluorescence quantum yield and lifetime in absence of acceptor are given by

$$\Phi_F^0 = \frac{k_F}{k_F+k_{IC}+k_{ISC}} \qquad \tau_F^0 = \frac{1}{k_F+k_{IC}+k_{ISC}} \tag{S1}$$

where k_F, k_{IC}, and k_{ISC} are the rate constants for fluorescence (radiative), internal conversion and intersystem crossing, respectively. The quantum yield of phosphorescence is

$$\Phi_P^0 = \frac{k_{ISC}}{k_F+k_{IC}+k_{ISC}} \frac{k_P}{k_P+k'_{ISC}} \tag{S2}$$

where k_P is the radiative rate constant for phosphorescence and k'_{ISC} the rate constant for intersystem crossing back to the ground state. The phosphorescence lifetime for both the SubP donor and the dyads is

$$\tau_P^0 = \tau_P = \frac{1}{k_P+k'_{ISC}} \tag{S3}$$

By combining Eqs. S1, S2 and S3 we get

$$\Phi_P^0 = k_{ISC}.\tau_F^0.k_P.\tau_P^0 \tag{S4}$$

Formation of triplet in the dyads.

The fluorescence quantum yield and lifetime for the dyads are given by

$$\Phi_F = \frac{k_F}{k_F+k_{IC}+k_{ISC}+k_{CS}} \qquad \tau_F = \frac{1}{k_F+k_{IC}+k_{ISC}+k_{CS}} \tag{S5}$$

where k_{CS} is the rate constant for charge separation. In the dyads the triplet is formed both from the direct intersystem crossing and through the charge separated state and the phosphorescence quantum yield is, thus, given by

$$\Phi_P = \frac{k_{ISC}}{k_F+k_{IC}+k_{ISC}+k_{CS}}.\frac{k_P}{k_P+k'_{ISC}} + \frac{k_{CS}}{k_F+k_{IC}+k_{ISC}+k_{CS}}.\frac{k_{CR1}}{k_{CR1}+k_{CR2}}.\frac{k_P}{k_P+k'_{ISC}} =$$

$$= k_P\tau_P^0\left(k_{ISC}\tau_F + \Phi_{CS}\frac{k_{CR1}}{k_{CR1}+k_{CR2}}\right) \tag{S6}$$

where k_{CR1} and k_{CR2} are the rate constants for recombination through the triplet state and directly to the ground state, respectively (cf. Fig. 7).

From Eq. S4 we have

$$k_P.k_{ISC} = \frac{\Phi_P^0}{\tau_F^0.\tau_P^0} \tag{S7}$$

which inserted into Eq. S6 gives

$$\Phi_P = \Phi_P^0.\frac{\tau_F}{\tau_F^0} + k_P.\tau_P^0.\Phi_{CS}.\frac{k_{CR1}}{k_{CR1}+k_{CR2}} \qquad \text{(Eq. 7 in main text)}$$

Supporting references:

[S1] N. M. Shavaleev, H. Adams, J. Best, J. A. Weinstein, *J. Organomet. Chem.* **2007**, *692*, 921-925.

[S2] M. Kitano, S.-y. Hayashi, T. Tanaka, H. Yorimitsu, N. Aratani, A. Osuka, *Angew. Chem., Int. Ed.* **2012**, *51*, 5593-5597.

[S3] Y. Inokuma, Z. S. Yoon, D. Kim, A. Osuka, *J. Am. Chem. Soc.* **2007**, *129*, 4747-4761.

[S4] G. Copley, J. Oh, K. Yoshida, D. Shimizu, D. Kim, A. Osuka, *Chem. Commun.* **2016**, *52*, 1424-1427.

[S5] W.Y. Cha, J.M. Lim, K.H. Park, M. Kitano, A. Osuka, D. Kim, *Chem Commun.* **2014**, *50*, 8491-8494.

[S6] M.E. El-Khouly, J.H. Kim, J.H. Kim, K.Y. Kay, S. Fukuzumi, *J Phys Chem C.* **2012**, *116*, 19709-19717.

[S7] Y. Inokuma, S. Easwaramoorthi, S. Y. Jang, K. S. Kim, D. Kim, A. Osuka, *Angewandte Chemie International Edition* **2008,** *47* (26), 4840-4843.

[S8] N. Zainalabdeen, B. Fitzpatrick, M. Kareem, V. Nandwana, G. Cooke, V. Rotello, *International Journal of Molecular Sciences* **2013,** *14* (4), 7468.

[S9] Frisch, M. J.; Trucks, G. W.; Schlegel, H. B.; Scuseria, G. E.; Robb, M. A.; Cheeseman, J. R.; Scalmani, G.; Barone, V.; Petersson, G. A.; Nakatsuji, H.; Li, X.; Caricato, M.; Marenich, A. V.; Bloino, J.; Janesko, B. G.; Gomperts, R.; Mennucci, B.; Hratchian, H. P.; Ortiz, J. V.; Izmaylov, A. F.; Sonnenberg, J. L.; Williams; Ding, F.; Lipparini, F.; Egidi, F.; Goings, J.; Peng, B.; Petrone, A.; Henderson, T.; Ranasinghe, D.; Zakrzewski, V. G.; Gao, J.; Rega, N.; Zheng, G.; Liang, W.; Hada, M.; Ehara, M.; Toyota, K.; Fukuda, R.; Hasegawa, J.; Ishida, M.; Nakajima, T.; Honda, Y.; Kitao, O.; Nakai, H.; Vreven, T.; Throssell, K.; Montgomery Jr., J. A.; Peralta, J. E.; Ogliaro, F.; Bearpark, M. J.; Heyd, J. J.; Brothers, E. N.; Kudin, K. N.; Staroverov, V. N.; Keith, T. A.; Kobayashi, R.; Normand, J.; Raghavachari, K.; Rendell, A. P.; Burant, J. C.; Iyengar, S. S.; Tomasi, J.; Cossi, M.; Millam, J. M.; Klene, M.; Adamo, C.; Cammi, R.; Ochterski, J. W.; Martin, R. L.; Morokuma, K.; Farkas, O.; Foresman, J. B.; Fox, D. J. *Gaussian 16 Rev. B.01*, Wallingford, CT, 2016.